

**RESERVOIR CHARACTERIZATION AND RESERVOIR MODELING
IN THE NORTHWESTERN PART OF HASSI MESSAOUD FIELD
ALGERIA**

A Thesis

Submitted to the Graduate Institut
In fulfillment of requirements for the
Degree of

PhD

At the Departement of Earth Sciences
of the University of Hamburg

By
FADILA BESSA

Hamburg, Germany
2004

Als Dissertation angenommen von Fachbereich Geowissenschaften
Der Universität Hamburg
Auf Grund der Gutachten von
Und

Prof. Dr. C. Betzler
Dr. E. Martin

Prof. Dr. H. Schleicher
Dekan
Des Fachbereiches Geowissenschaften

Executive summary

This study was undertaken at the request of Sonatrach petroleum engineering and development division in order to provide petrographic support, pore-level description, petrophysical interpretation, reservoir characterization and reservoir modeling for the best exploitation of the faulted, fractured Cambrian sandstone reservoir in the northwestern part of the Hassi Messaoud Field, Algeria.

The principal goals were to assess pore level controls on reservoir quality and wireline log response, and to investigate relationships between composition, pore geometry and reservoir quality. This study is based on the detailed core description and petrographic examination of available cores of about 41 wells and over 1200 thin-sections, and integration of this information with geological, petrophysical and engineering data.

Table of contents

Executive summary and goals	i
Chapter 1. Introduction to the Hassi Messaoud field	1
1. Introduction	1
2. The geographical situation	1
3. Structural and stratigraphical aspect	3
4. The major problems of the field	3
5. Objectives of the study	6
Chapter 2. Sedimentology	8
1. Introduction	8
2. Core description	9
2.1. Sedimentary structures	9
2.1.1. Inclined strata	9
2.1.2. Trace fossils	9
2.2. The Silts	9
3. Core Analysis and environments interpretation	14
3.1. Lower sequence	14
3.2. Upper sequence	14
3.3. Cross sections	14
4. Conclusion	22
Chapter 3. Petrography and Pore level characteristics	25
1. Introduction and goal	25
2. Pore-level characteristics	25
2.1. General attributes	25
2.2. Texture and fabric	25
2.3. Detrital components	25
2.4. Authigenic Components	31
2.5. Minor component	39
3. Diagenesis	39
3.1. Textural maturity of sandstone	39
3.2. Authigenic kaolin and illitic minerals during burial diagenesis of sandstone	43
3.3. Kaolin in sandstones diagenesis	43
3.4. Differential illitization of kaolin polytypes in sandstones	43
3.5. The HMD diagenetic sequence reconstitution	45
4. Pore Types	52
Intercristalline macropores	52
Interparticle macropores	52
Moldic macropores	52
Interparticle micropores and Intercristalline micropores	52
5. Rock Types	55
Rock Type D (Dickite –rich microporous sandstones)	55
Rock Type I (Intercristalline macroporous quartz sandstone)	55
Rock Type B (Bioturbated sandstone)	55
Rock Type P (Pseudomatrix-rich sandstone)	58
Rock Type M (Moldic macroporous quartzose sandstone)	58

6. Reservoir Quality and Heterogeneity	58
7. Comparison among the	60
Chapter 4. Hydraulic Units (HU)	65
1. Concept of Hydraulic Units (HU)	65
2. Methodology	65
3. Comparison between flow units and rock types	67
4. Conclusion	67
Chapter 5. Modeling	72
1. Procedure and methods	72
2. Structural Modeling	74
3. Facies and Petrophysical models	74
3.1. Introduction	74
3.2. Facies Modeling	78
3.2.1. Facies model of geological facies (Object Modeling)	78
3.2.2. Facies model of flow units (Sequential Indicator)	81
3.3. Petrophysical Modeling process	85
Chapter 6. General Conclusions	88
Key References	90

1. Introduction

The Saharan platform is located to the south of an Algerian alpine system and belongs to the North African craton. It includes a Precambrian basement which is unconformably overlain by the Phanerozoic. The Paleozoic succession has been structured during the Hercynian and Prehercynian stage. They are separated into provinces by structural highs: an occidental province is separated from an oriental, and a central Triassic (Fig. 1).

The occidental province consists of the Bechar, Tindouf, Regan , l'Ahnet Mouydir, Timmimoun and Sebaa basins. The oriental province consists of the basins of Illizi and Ghadames, which are limited by the mole of Dahar. The Triassic central province is a large E-W oriented anticlinorium, and contains the following major elements:

- Vault of Tilrhemt and the Talemzane high;
- The structural system of Djemaa- Tougourt;
- The dislocation system of El Agreb – Messaoud;
- The Dahar high.
- The Hassi Messaoud high belongs to this province and is located in the oriental Erg.

The Hassi Messaoud Field, a very thick sandstone reservoir of Cambrian age covering an area of 2000 km² is a multi-billion barrel oil field in the Triassic Basin of Algeria (Fig. 2). This oil field was discovered in 1956.

The producing layer, which occurs at an average depth of 3400 m, is characterized by largely variable petrophysical properties. The properties impacting productivity (including porosity , shaliness and permeability) remain unpredictable, despite the knowledge accumulated from more than 1216 vertical and horizontal wells continuously cored over the past 48 years.

Note that most of the documents used in this study concerning the Hassi Messaoud field and the Saharan platform are Sonatrach internal documents; because of this, the references are sometimes not indicated.

2. The geographical situation

Hassi Messaoud is located 800 km southeast of Algiers, between the meridians 5°30' 6°00' and the parallels 31°00' and 32°00'N (Fig. 2). It is 350km from the Algero-Tunisian frontier and 80 km east of Ourgla. It is considered to be one of the largest oil deposits in the world and the more prospected of the Saharan platform.

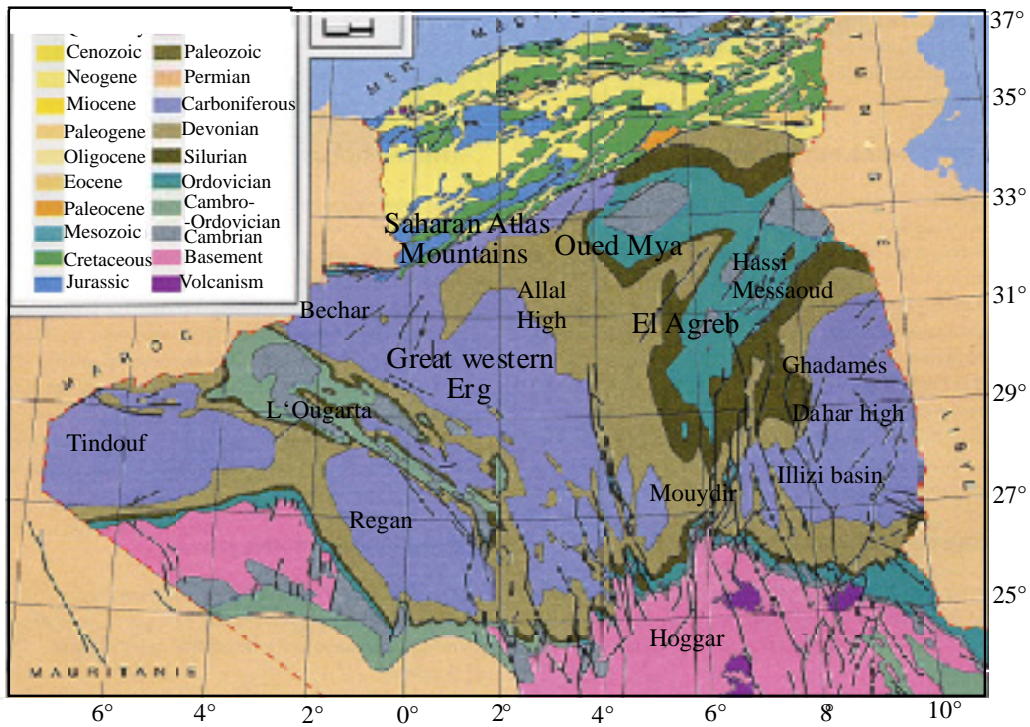


Figure 1: Geological and structural map of Algeria (Sonatrach, 1995)



Figure 2: Location map of the Hassi Messaoud field, Algeria (Mc Gowen et al., 1996)

3. Structure and stratigraphy

The Saharan desert within the so-called Triassic Basin (Oued Mya Basin) is part of the North African stable craton. The basin has had a long history from Cambrian times onwards, and has a sedimentary column of about 5,000 m (Fig. 3). The **Cambrian** sediments are a thick series of fluvial and shallow marine sandstones, deposited on a peneplained surface composed, in the Hassi Messaoud area, of Early Cambrian granites. The Algerian Sahara was invaded by a relatively deep anoxic sea during the **Ordovician**, but this was followed by a regional regression and a period of coarse clastic, continental and glacial sedimentation.

During the **Late Silurian**, deep marine conditions once again occurred over a wide area in North Africa, but the **Caledonian orogeny** led to the creation of a number of gentle, regional uplifts. **Devonian** sandstones and shales were deposited extensively in fluvial and shallow marine environments over much of North Africa, including Algeria, and lie unconformably on tilted and eroded Lower Palaeozoic sediments. They were followed by deltaic and marine sandstones and shales of **Carboniferous** age. It is not known for certain whether these Upper Palaeozoic sediments were deposited over the Hassi Messaoud high because they have not been preserved there. They may have been deposited with a reduced thickness, but in any case would have been subsequently removed as a result of the tectonic upheavals related to the **Hercynian orogeny** of Late Carboniferous to Permian times. The grain of the Hercynian orogeny in the Hassi Messaoud area is oriented mostly NE-SW, as is typically seen in the trend of the Messaoud - El Agreb (Sonarach, WEC, 1995).

The productive formation of Hassi Messaoud is a series of Cambrian sandstones, with an average thickness of 300 m and 4 productive zones denominated R3, R2, Ra, Ri (from bottom to top). The Ra represents the best reservoir qualities. The Paleozoic of Hassi Messaoud has been eroded by the Hercynian unconformity which reaches the R2 in places. This erosion is increasingly important from the periphery to the center where the Ra is locally absent (Fig. 4). Structurally, only the top of R2 allows us to correctly define the geometry of the Cambrian of Hassi Messaoud (Fig. 5). The Hassi Messaoud structure appears as a large SSW-NNE oriented anticline, affected by the major faults SSW-NNE.

The major problems of the field

The definition of facies of the Cambro-Ordovician of Hassi Messaoud field is the result of the summary of many research works:

- Geological studies early in 1960 by SN Repal et CFPA with scientific help of IFP;
- Outcrop and subsurface work by Charpal and Riché in 1975;
- Outcrop and subsurface work by Beicip and Sonatrach from 1990 to present.

The objective of the first outcrop studies was to improve the knowledge of the petroleum series of the basins. The Beicip studies (outcrop and subsurface, including the data of 900 wells), is essentially concentrated on the aspect of fracturation and petrophysical characterization of the reservoir. This model, proposed by Beicip Franlab to Sonatrach, has been in use since 1995 for well positioning. The aim of the previous studies was to define the exploitable representation of the reservoir characteristics evolution, and to help decide where new horizontal and vertical wells should be drilled. Nevertheless, we realized that the previous reservoir characterization studies of the Hassi Messaoud field, based on the classical model in use, do not eliminate the problems of the field which still subsist due to the high horizontal and vertical heterogeneity of the reservoir.

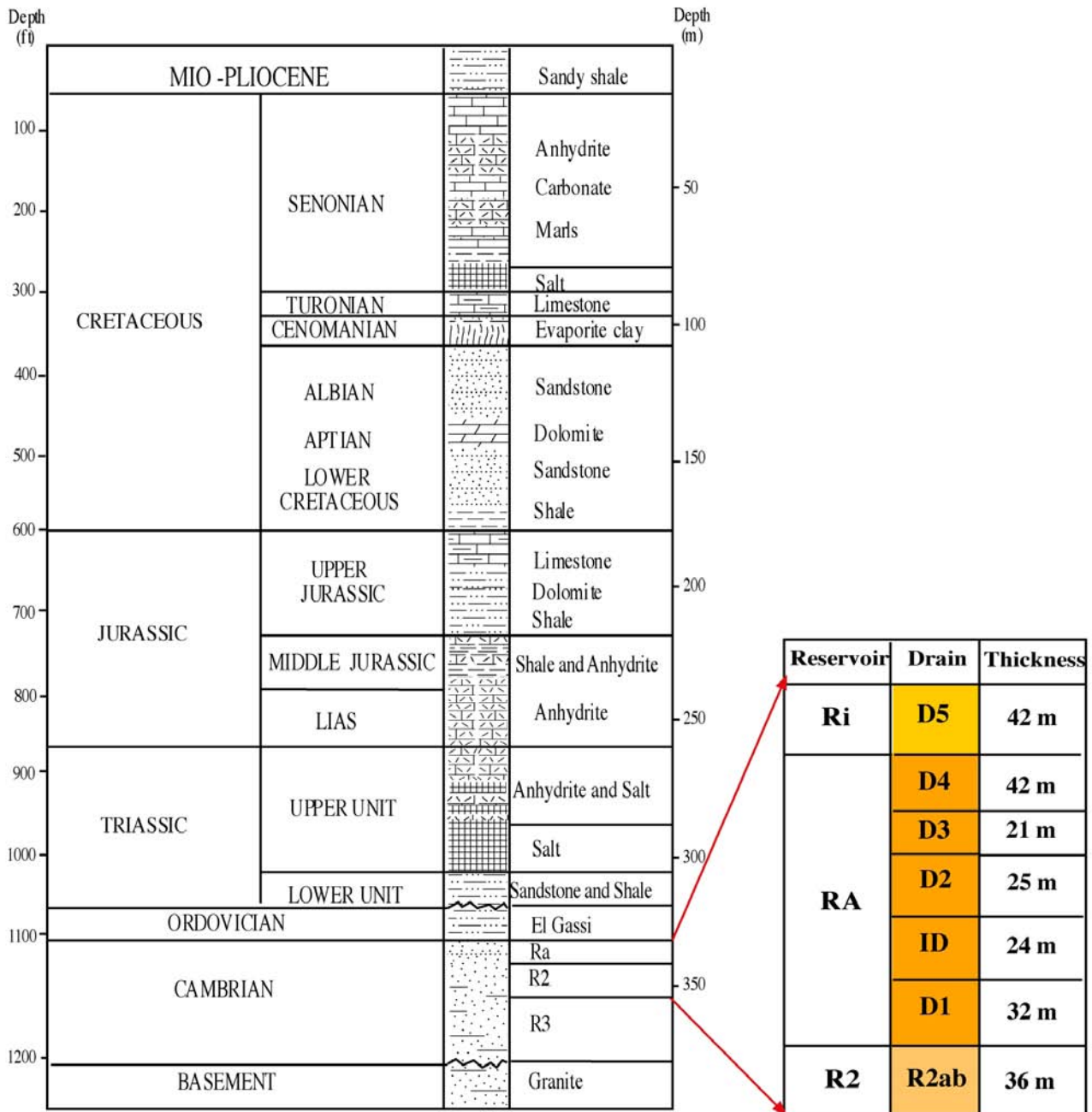


Figure 3: Left handside: Summarized stratigraphy for the Hassi Messaoud field (Balducchi and Pommier, 1971). Right handside: Detailed column of the four productive zones R3, R2, Ra, Ri of the Cambrian of Hassi Messaoud field.

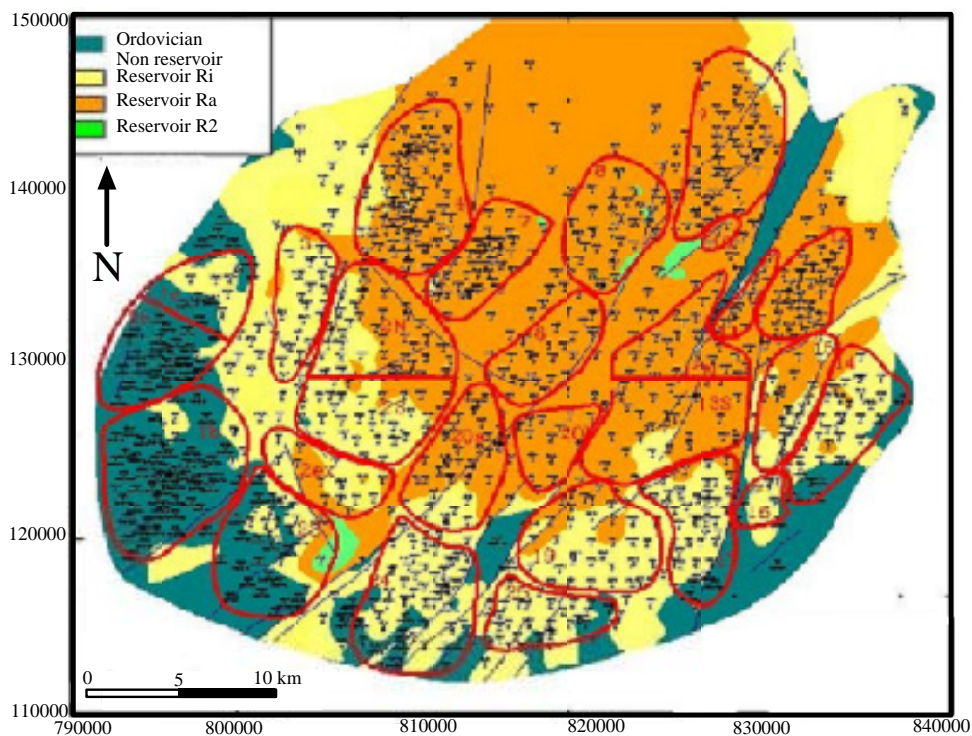


Figure 4: Peel Map of Hassi Messaoud Field: Reconstruction of the hercynian unconformity distribution of underlying formations by « peeling off » the overlying formations. The red zones are the production zones of the field.

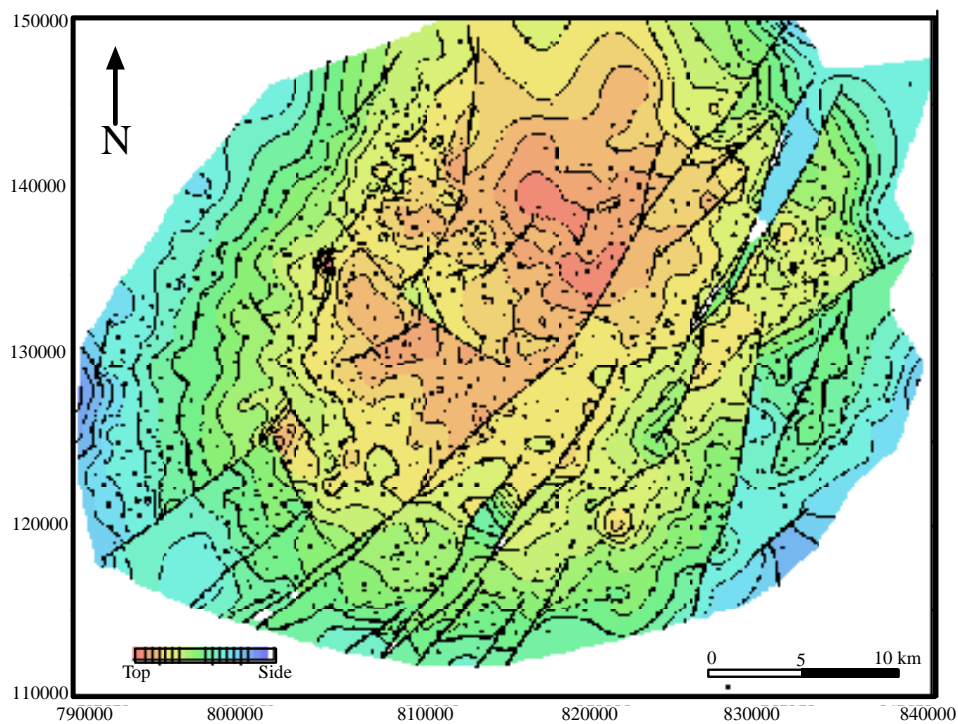


Figure 5: Hassi Messaoud Field. Isobaths of the top of the Cambrian R2 showing an anticline feature with low dipping faults.

The heterogeneity of Hassi Messaoud field (HMD) is tied to two important factors:

- A. faulting and the erosion cause the local complications;
- B. Diagenesis is tied to tectonics and caused the deterioration of the reservoir qualities.

The drains

In different sectors of the Hassi Messaoud field (HMD), different drains participate in the production. In the central zone it is D2, ID, D1. In the west periphery of the field it is D4 and D5 (fig. 3).

The production zones

The pressure evolution of wells according to the production has been interpreted with the help of numerical simulators. This brought out 25 producer zones parted by the unproductive zones (Fig. 6). This subdivision of the field (this zoning) is not based on geological criteria. Some producer zones are limited by the major faults which can play a major role as permeability barriers. However, the limits for other zones are inexplicable.

Gas injector

Within the producer zones, gas injections reveal an apparent anisotropy of fluid movement. The gas injected can reach neighboring wells in differing lengths of time reaching up to 10 years.

Dry wells

The plantation of 106 dry wells in the field is considered to be one of the negative points inexplicable by the present geological and reservoir models.

Intracambrian intrusion

Intrusive phenomena characterize the Cambrian of the southwest part of the field. The type, the mode of placement, and the vertical and horizontal extension have been little known until now. Intracambrian intrusions occur in the southwest of the field (Fig. 6). The intrusions are unfavorable to production, because in some cases the laccoliths can reach thicknesses of 67 m; in this case, the reservoir thickness is reduced. Intrusions can cause problems for the horizontal wells when their lateral extension and thickness are unknown. Allocation of the intrusions is accompanied by silicification, which also deteriorates reservoir quality.

The following intrusions occur in the Hassi Messaoud (HMD) field:

Dykes, which are associated with faults, and occur especially in zones which are characterized by the major faults. Laccoliths occur in the southwestern zone of HMD and are associated with a domed structure. Sills occur practically in the same stratigraphical level.

5. Objectives of the study

This study was undertaken at the request of P.E.D (Petroleum Engineering and Development):

1. To describe the geological context of the Cambrian sandstone reservoir;
2. To provide petrographic and pore-level reservoir characterization of the Zones D5, D4, D3, D2, ID, D1 of the reservoir Ra of the North west part of Hassi Messaoud field;
3. To define the different rock types of the sandstone reservoir Ra according to their reservoir properties;
4. To analyze the petrophysical data of the wells studied and to determine the flow units;

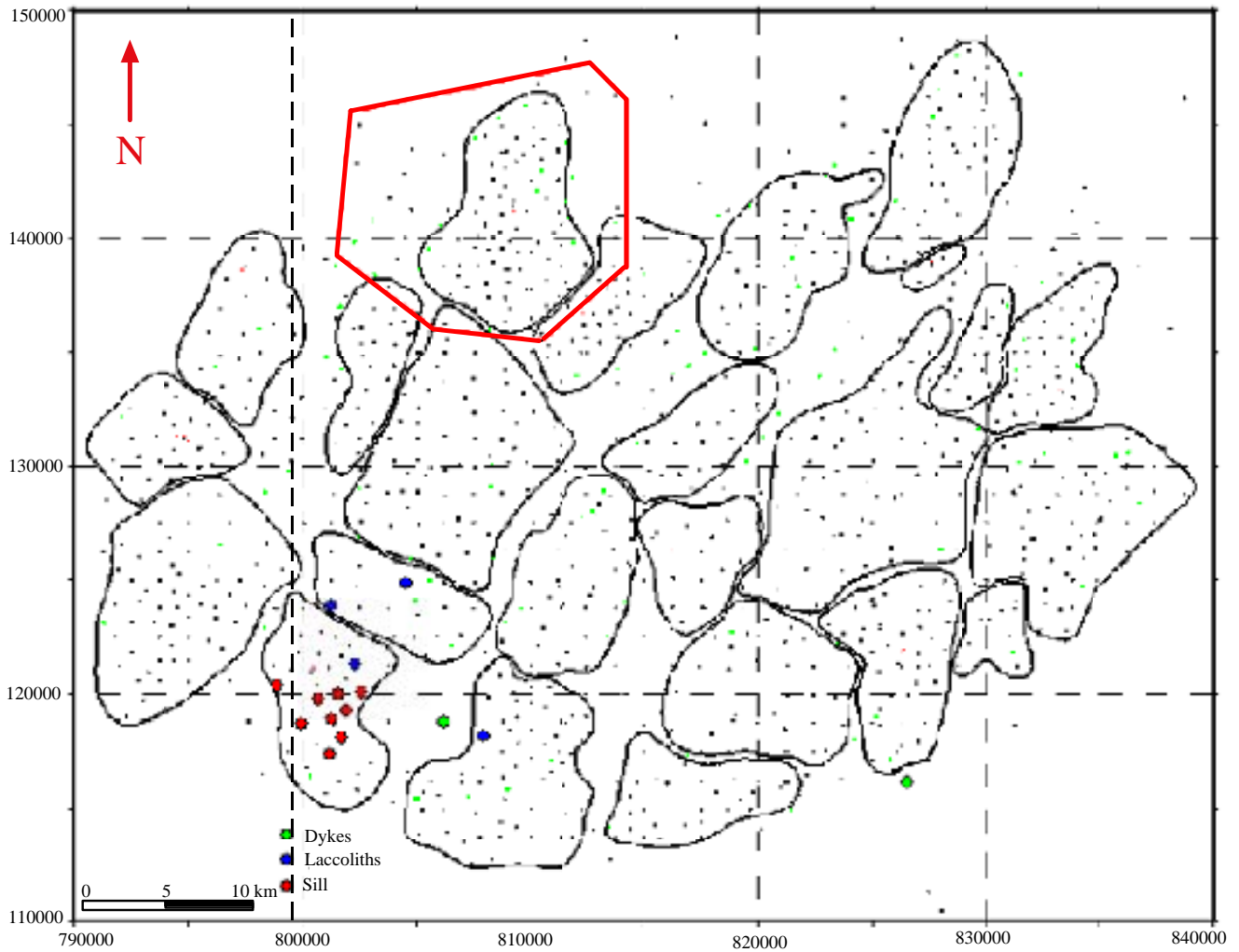


Figure 6: Some examples of Intracambrian intrusions in the Southwest part of the Hassi Messaoud Field. Red frame enclose the area of interest. A system of 25 isolated zones having different petrophysical and pressure characteristics, can be identified within the reservoir.

1. Introduction

In the area of Hassi Messaoud field (HMD), there is a Paleozoic series including a thin Ordovician succession in the upper section. The lower part of the Paleozoic sediment is Cambro-Ordovician in age. This Paleozoic sediment rests unconformably on an Infracambrian series. The Cambrian of Hassi Messaoud field is composed entirely of azoic sandstones. These deposits cannot be dated. An age assignment of the Cambrian relies on the stratigraphic position between the marine Ordovician and the Infracambrian.

The Cambrian of Hassi Messaoud field is subdivided into 4 zones which are, from top to bottom: Ri (D5), Ra, R2, R3. These four zones have been defined and assembled by Beuf et al. (1971) for all the Saharan platform and they are known as Unit II with Ra +R2 and Unit I for R3.

The criteria used to differentiate these zones are essentially petrographic and particularly rely on the cement types of the sandstone, as well as the maximal and medium grain size. Many geologists have been interested in the Cambrian subsurface study of the Saharan platform in Algeria firstly to understand the depositional mode, to then reconstruct the paleoenvironment with the aim to exploit the hydrocarbon reserves which it contains; secondly, to try to create a correlative model at the Saharan platform scale. These efforts are still in progress. All subsurface Cambrian studies to this day are based on the outcrop studies of the Cambrian by Beuf and al. (1971) in the Tassili.

In other words, the geologists and sedimentologist refer to the outcrop to study the subsurface by using logs, cores, and all well data. It should be noted that understanding the depositional mode and reconstitution of the paleoenvironment is very important, but the most important focus for us, as reservoir geologists, is to combine the geological, petrophysical and reservoir study methods for the best exploitation of the reservoir richness. The petroleum interest is the objective of the subsurface studies. Because of the lack of this kind of study in the Hassi Messaoud field, it was necessary to consult as many available studies as possible concerning the similar reservoir of the neighboring fields (Fig. 1-2). Most of the studies used were on the Baguel field, El Gassi, El Agreb and Illizi basin, and some PhD theses (see key references).

2. Core description

To describe sedimentary structures visible in the cores, the works realized by Petit, (1949-1957), Potter, (1961), Gubler, (1966), Bouma, (1962), and others (see key references) were used.

41 wells have been the subject of a detailed core description in the area of interest (Fig.7).

2.1. Structures

2.1.1. Inclined strata

Three types of inclined strata have been defined in the Cambrian reservoir Ra of Hassi Messaoud field in the area of interest:

simple inclined strata (Fig. 8)

- inclined strata with gentle slopes $<12^\circ$
- inclined strata with relatively steep slopes $12^\circ-25^\circ$
- trough cross-beds $12^\circ-25^\circ$

Flaser bedding (Fig. 8)

Flaser bedding occurs in fine grained sandstones interbedded with clay laminations. This stratification is generally present in the D5 top at the reservoir.

Diastems (Fig. 9)

These represent an interruption of the sedimentation, manifested by the discontinuity surfaces, corresponding to a temporary sedimentation failure. The vertical distance between this kind of discontinuity is 1-25 cm. Diastems have been defined in the upper part of the reservoir, and especially on the top.

2.1.2 Trace fossils

The marine Cambro-Ordovician of the Saharan platform is rich in Scolithos traces (Fig. 9). These traces are vertical pipes crossing sands, silts, and clays, although some works proposed an organic origin of the traces (Seilacher, 1967 and Selly, 1976). The ichnofacies (Scolithos) correspond to an intertidal to nearshore environment (Seilacher, 1967, and Beuf, et al. 1971). The appearance of Scolithos from the upper part of the Cambrian indicates an environment propitious for their growth (Fig. 10-11).

It should be noted that the Scolithos are commonly known as tigillites in the Saharan platform in North Africa.

2.2. The Siltstones

The siltstone and clay distribution in the sandstone beds depends on the sedimentation conditions. The core analysis of wells in the area of interest indicates that the silt beds are very common and thick in the upper part of the Ra reservoir (Fig. 9). The silt deposits likely correspond to the lagoon regime of a marshland (waterlogged area).

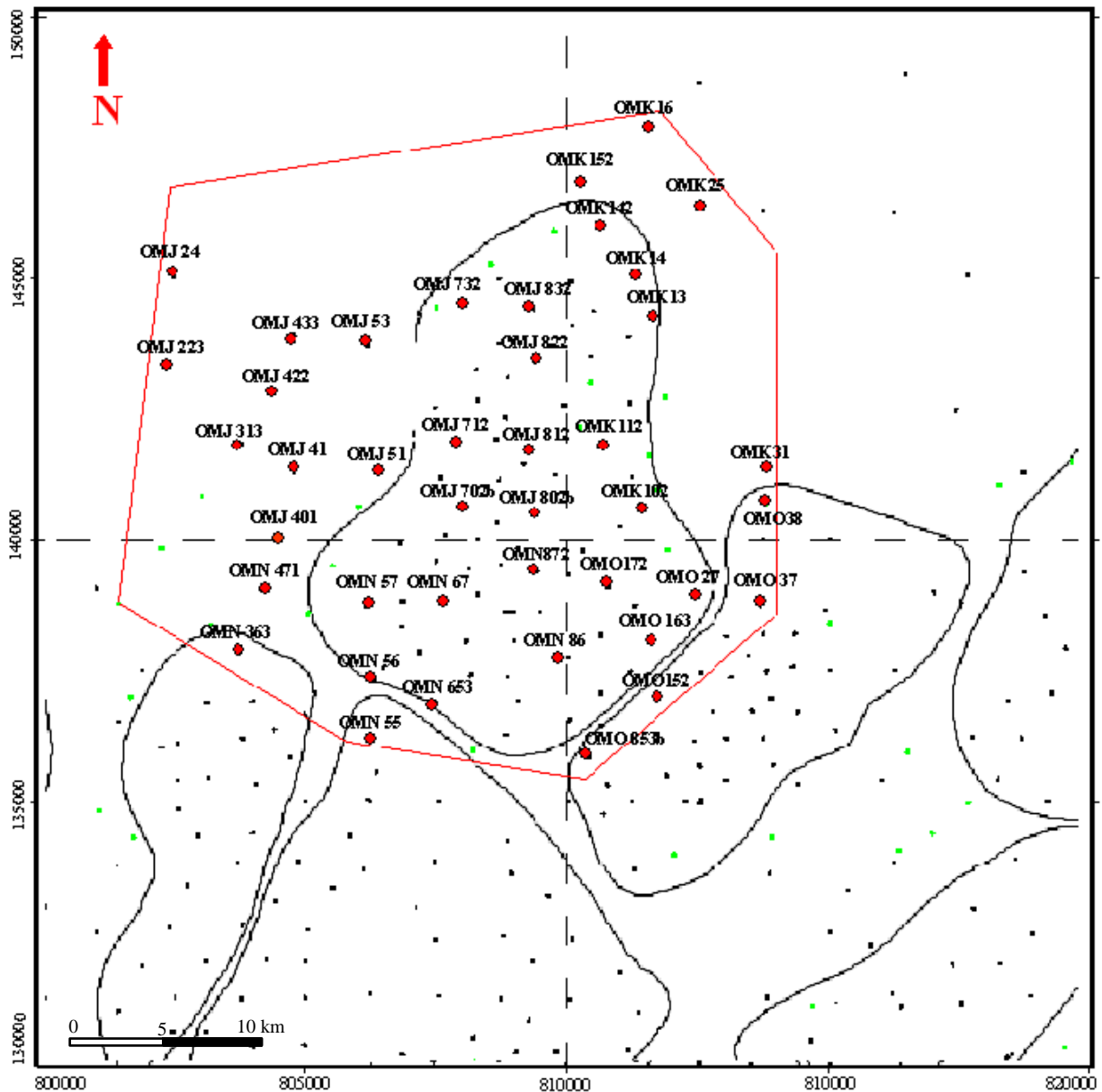
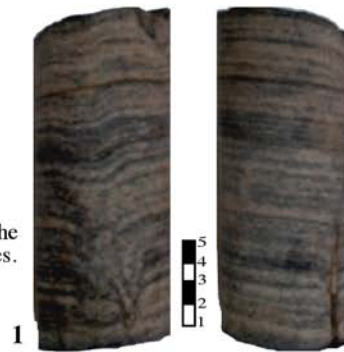


Figure 7: The position of the 41 cored and described wells which were used for the sedimentological interpretation and the palaeo-environment reconstruction.

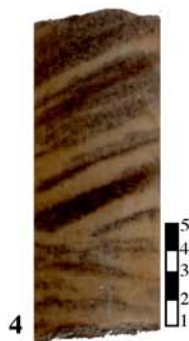
1. Inclined strata: Fine-grained and argillaceous sandstone. The stratifications are gently inclined. Scolithos appear in places. OMJ223b, 3421.90 m, D5, tidal deposits.



2. Inclined strata: Coarse grained sandstone characterized by trough cross bedding. OMN872, 3347.5 m, D1, fluvial deposits.



3. Inclined strata: Bituminous coarse grained sandstone and conglomerate with cross bedding highly inclined and underlined in places by coarse grained quartz and mud clast. OMK142, 3406.6 m, D2, fluvial deposits .



4. Inclined strata: Coarse grained sandstone with medium scale cross bedding OMJ822, 3345 m, D3, fluvial deposits.



5. Inclined strata: Coarse grained silicified sandstone with small scale trough cross bedding OMJ223b, 3490,30 m, D3, fluvial deposits.

6. Flaser bedding : Elongated lenticular structures of light grey isometric sandstones alternating a black clay. This kind of rock is typical for the tidal deposits. Sediment is bioturbated by Scolithos. OMJ223b, 3409.20 m, D5, tidal deposits.

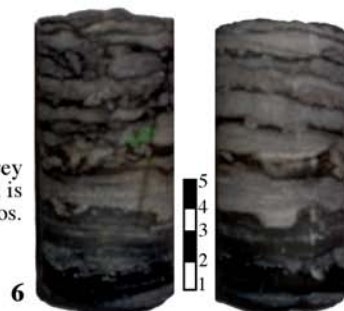
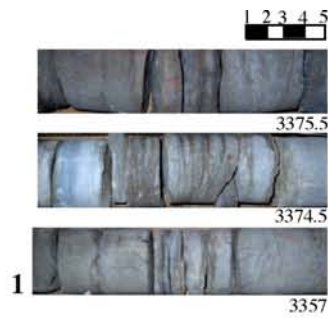


Figure 8



1. Diastem : Brief interruption in sedimentation indicated by stylolitic clay seams. OMK 142, 3375.5 m, 3374.5 m, 3357 m, ID, fluvial deposits.



Scolithus: Three main types of vertical burrow can be recognized based on the distribution of clay in the fillings and linings:

2. Muddy sand-filled, lined: Fine to medium highly silicified sandstone. Bioturbation cross-cuts the gently inclined stratification. OMJ702, 3340 m, D2, tidal deposits.

3. Muddy sand filled, unlined: Silicified sandstone rich in Scolithos. Left : transverse section. OMJ223b, 3432.5 m, D4, tidal deposits.

4. Clean(mud-poor) sand filled ,muddy sand-lined. OMJ223, 3409.20 m, D4, tidal deposits.



5.Silt: Photomicrograph illustrating mud balls (nodular shale) and stylolitic seams due to sediment compaction. The alternation of fine grained sandstones and silty clay is common in the upper part of the reservoir. OMJ812, 3337 m, D3, tidal deposits.



6. Silt: Stylolitic contact between highly silicified sandstones with inclined stratifications and silt. OMJ223b, 3466.80 m, D4, tidal deposits.

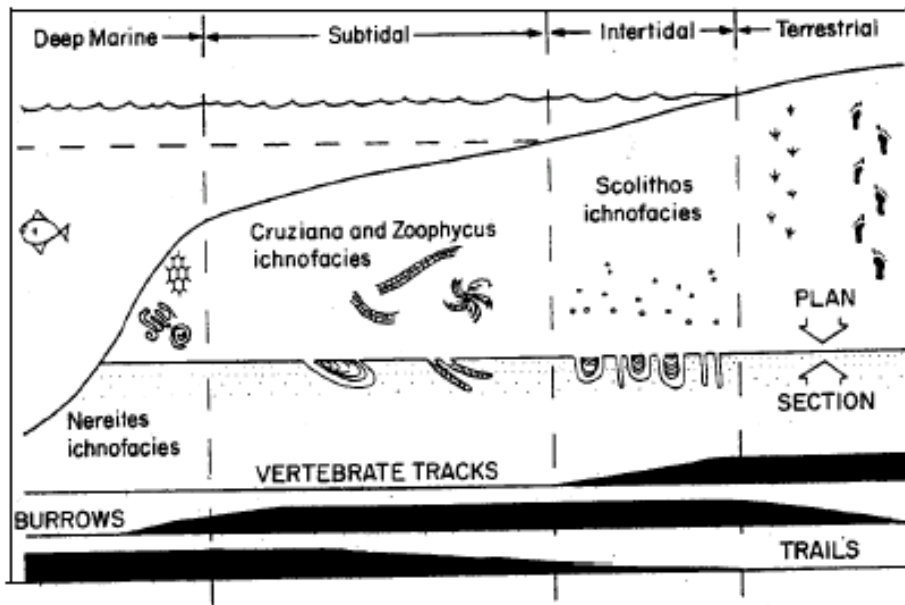


Figure 10: Characteristic ichnofacies for various environments . From Selly (1976).

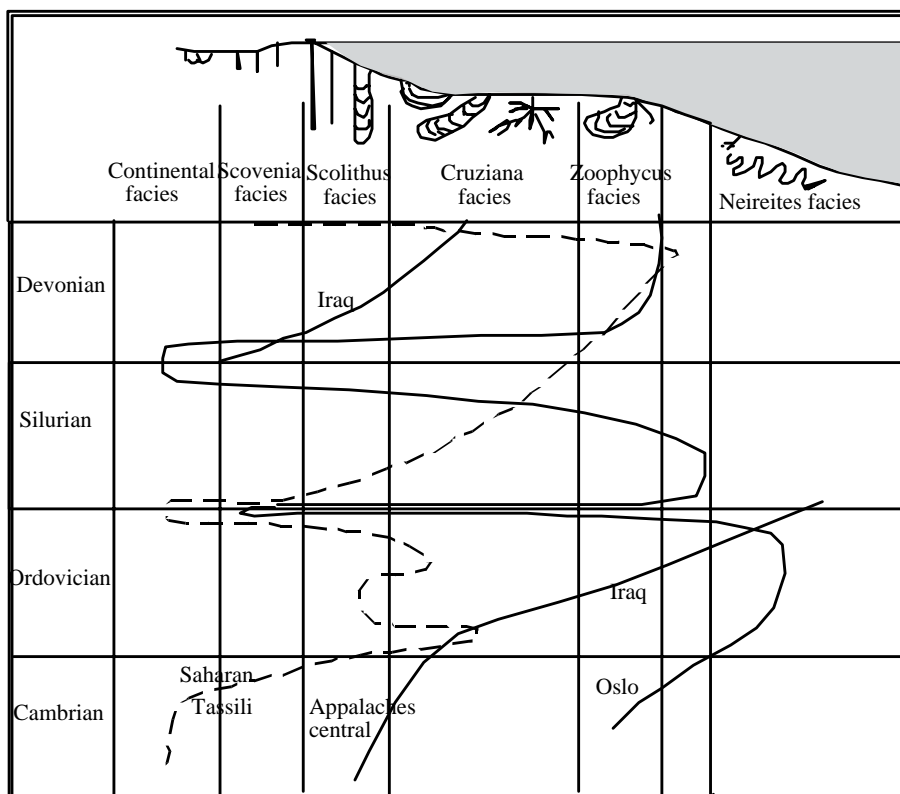


Figure 11: Zones and relative bathymetry of organism tracks. Reconstitution of a vertical bathymetric evolution of diverse regions completed as function of Paleozoic Saharan data (according to Seilacher, A., 1967). Scolithos is a synonym of Tigillites .

3. Core Analysis and environmental interpretation

Based on the detailed core analysis, grain size descriptions, and occurrence of *Scolithos* as geological criteria, the succession is subdivided into 2 sequences (Fig.12a-b):

3.1. Lower sequence (Fig. 13).

The lower sequence of Ra consists of coarse to upper-medium sandstones, according to the grains size scale, characterized by simple inclined strata and/or trough sedimentary structures with a relatively steep slope of 12°- 25°. This part of the reservoir Ra corresponds to braided channel deposits characterized by a low sinuosity and an absence of bioturbation. According to Mial, A.D., (2000) and Biju Duval, B., (1997), such deposits form in an instable current system with an irregular sinuosity. Grain size of deposits ranges from pebble to fine sandstone. Even if the channels are fitted together, a fining-upwards grain size is sometimes evident at channel scale.

3.2. Upper sequence (Fig. 14).

The upper sequence is composed of medium- to fine-grained sandstone with intercalations of coarse-grained sandstone. This part of the reservoir Ra is characterized by simple inclined strata with gentle-dipping (<12°) to sub-horizontal strata. The sediments are tidal channel deposits, especially with the appearance of the *Scolithus*, which indicate an intertidal environment as previously described. Coarsening-upwards elementary sequences are observed few meters around the *Scolithos* occurrence. The successions of the braided coarsening-upwards sequences confirm the alternating movement of the water slick, and suspect an earlier marine transgression. These observations lead to a definition of the environment of the Cambrian Ra in the area of interest: the sandstone deposit environments are then supratidal and intertidal to nearshore.

According to Beuf et al. (1971), the Cambrian channels of the Saharan platform are oriented SSW – NNE, and the major sources of the sediments were located in the SSW part of the Saharan platform. Beuf et al. (1971), proposed a summary bloc diagram based on sedimentological interpretations of the marine, lacustrine and fluvial systems of the Ordovician, Cambrian and Cambro- Ordovician of the Saharan platform. This interpretation is the result of the outcrop studies combined with the subsurface data from wells.

The results of the interpretation of Hassi Messaoud in the area of interest suggest that the Cambrian deposits of Hassi Messaoud correspond to the bloc diagram (A) for the lower fluvial deposits and (B) for the upper tidal-nearshore deposits (Fig. 15).

3.3. Cross sections

Beuf et al., 1971, propose that the silicoclastic input was from the SSW towards NNE in the Saharan platform. Two cross sections following this direction have been realized, these cross sections are flattened on the Hercynian unconformity. The cross sections show the vertical variation of grain size which indicates the transition from fluvial to tidal environment.

Laterally, the appearance of the *Scolithos* varies from well to well in many directions which can indicate a hesitant transgression (Fig. 16-17).

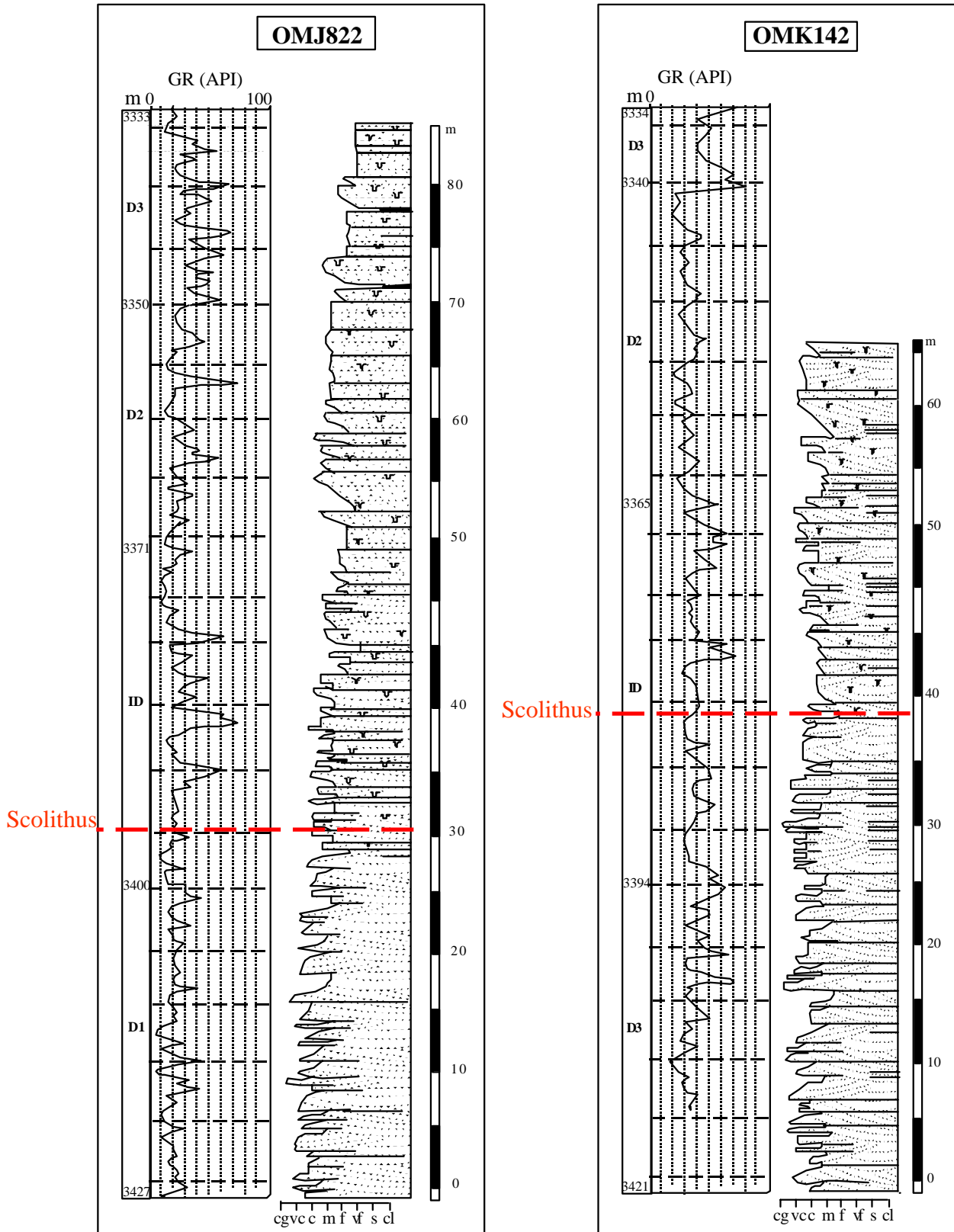


Figure 12a: Geological sections with Gamma Ray logs showing the lower and the upper parts of Ra Cambrian sandstones which are limited by the first appearance level of *Scolithos* traces.

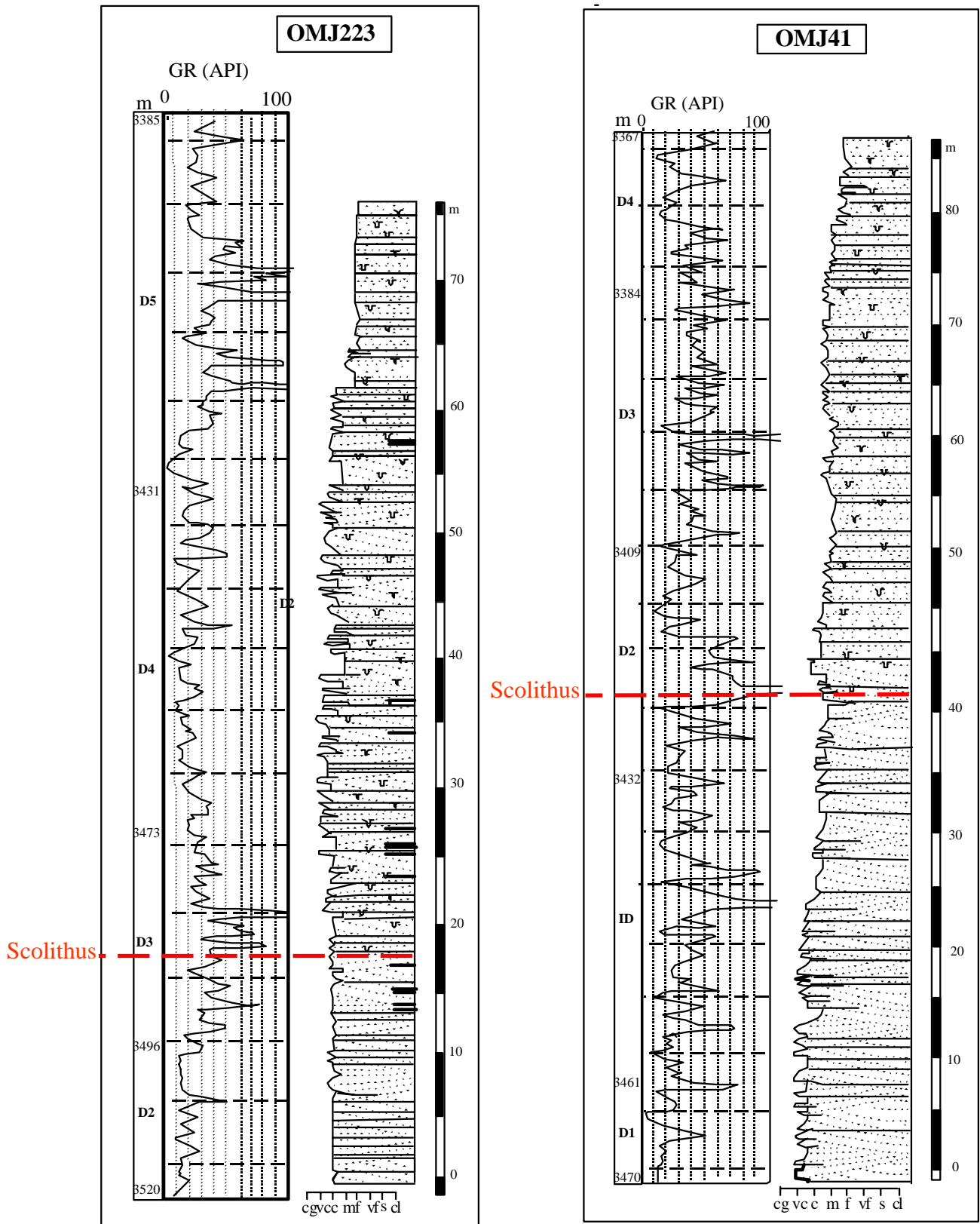
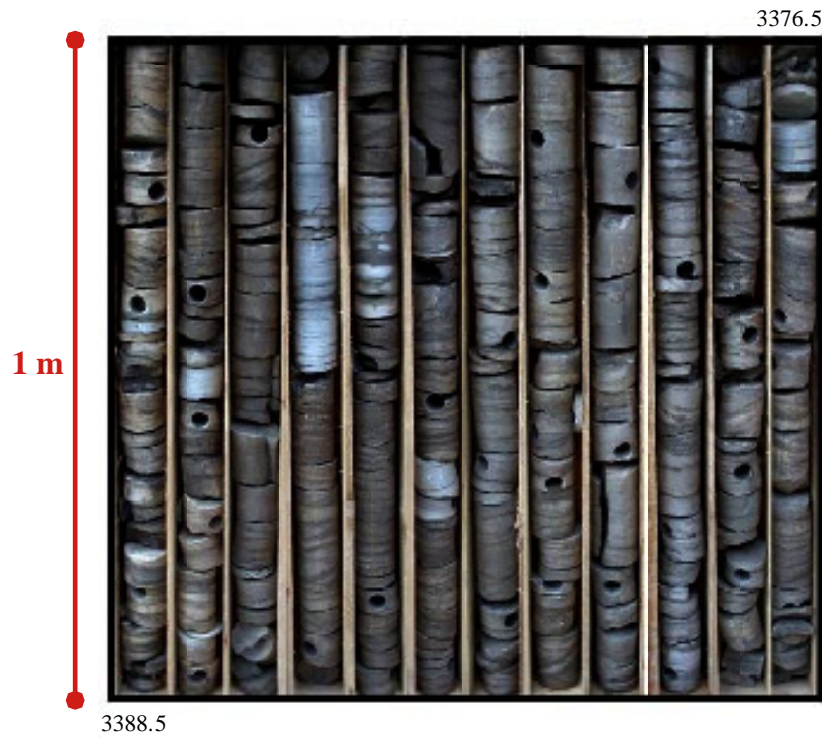
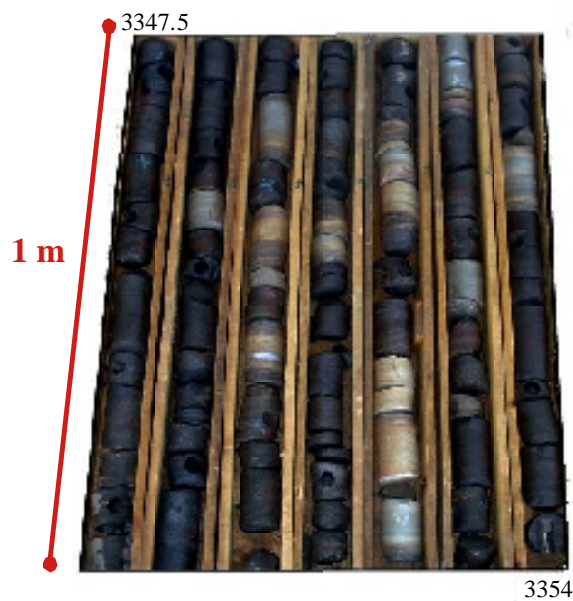


Figure 12b: Geological sections with Gamma Ray logs showing the lower and the upper parts of Ra Cambrian sandstones which are limited by the first appearance level of Scolithus traces.

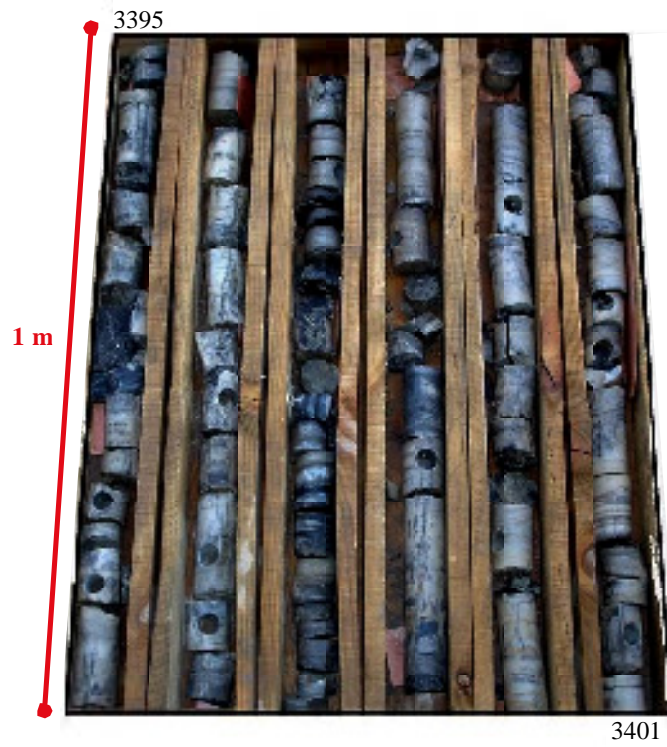


Example from the fluvial part of the reservoir with coarse to medium sandstones with steeply dipping inclined stratification. Siltstone intercalations between sandstone beds are several centimeters to a half a meter thick. OMJ732, D2, fluvial deposits.



Example from the fluvial deposits with coarse grained bituminous sandstone of braided channels. Siltstones intercalations between sandstone beds are several centimeters to a half a meter thick. OMN 86, D1, fluvial deposits .

Figure13



Example of fine to medium grained, silicified, argillaceous and bioturbated sandstone. OMJ223, D5, tidal deposits .



Fault breccia with argillaceous and cherty (siliceous) matrix and subangular rock fragments of sandstones and Quartzite. OMJ702b, D2, fluvial deposits.

Figure14

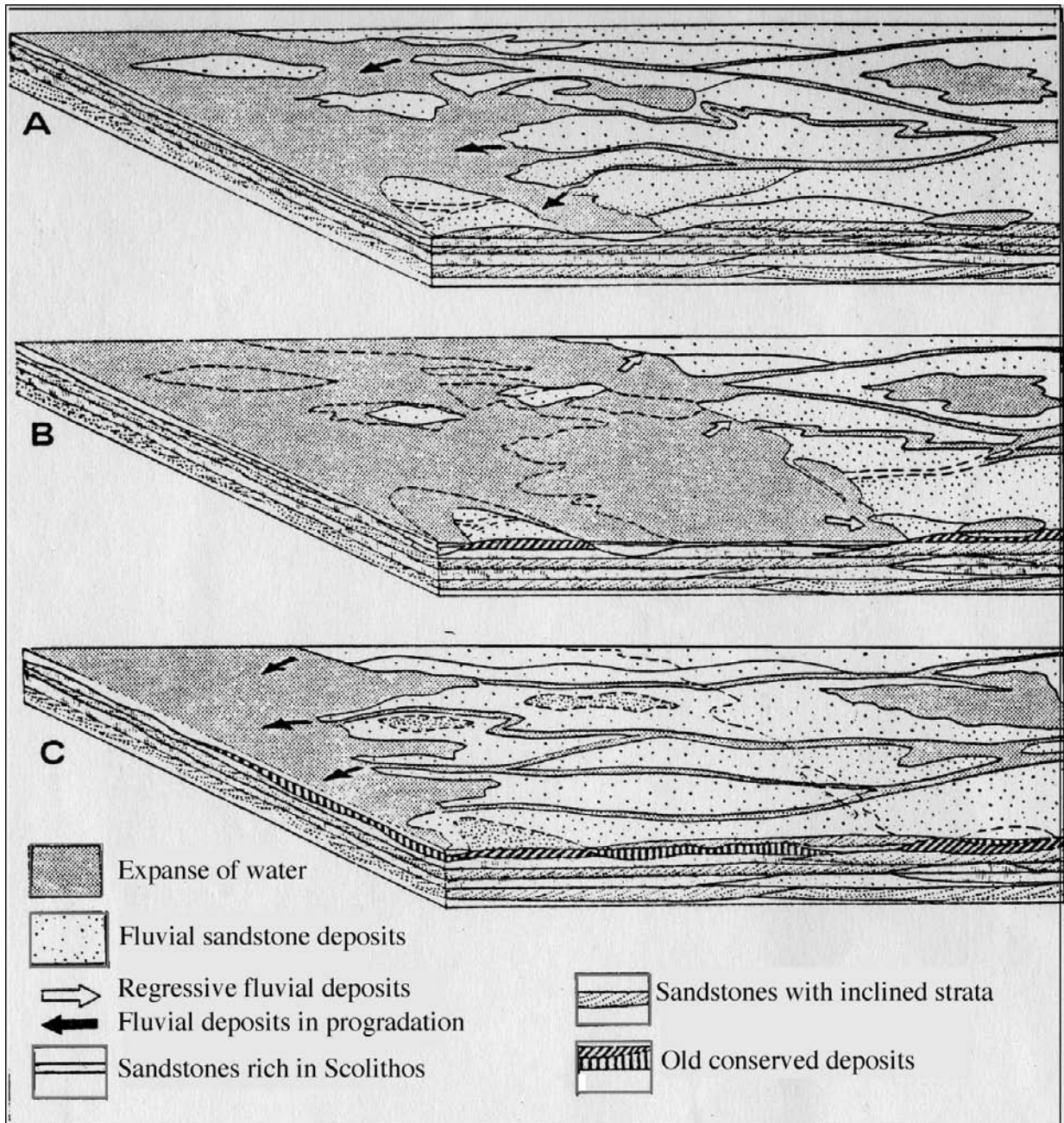


Figure 15: Interpretation of the evolution of the cambrian depositional sequences by Beuf et al. (1971). A: Period of a significant continental progradation. B: Transgressive episode. C: New continental progradation.

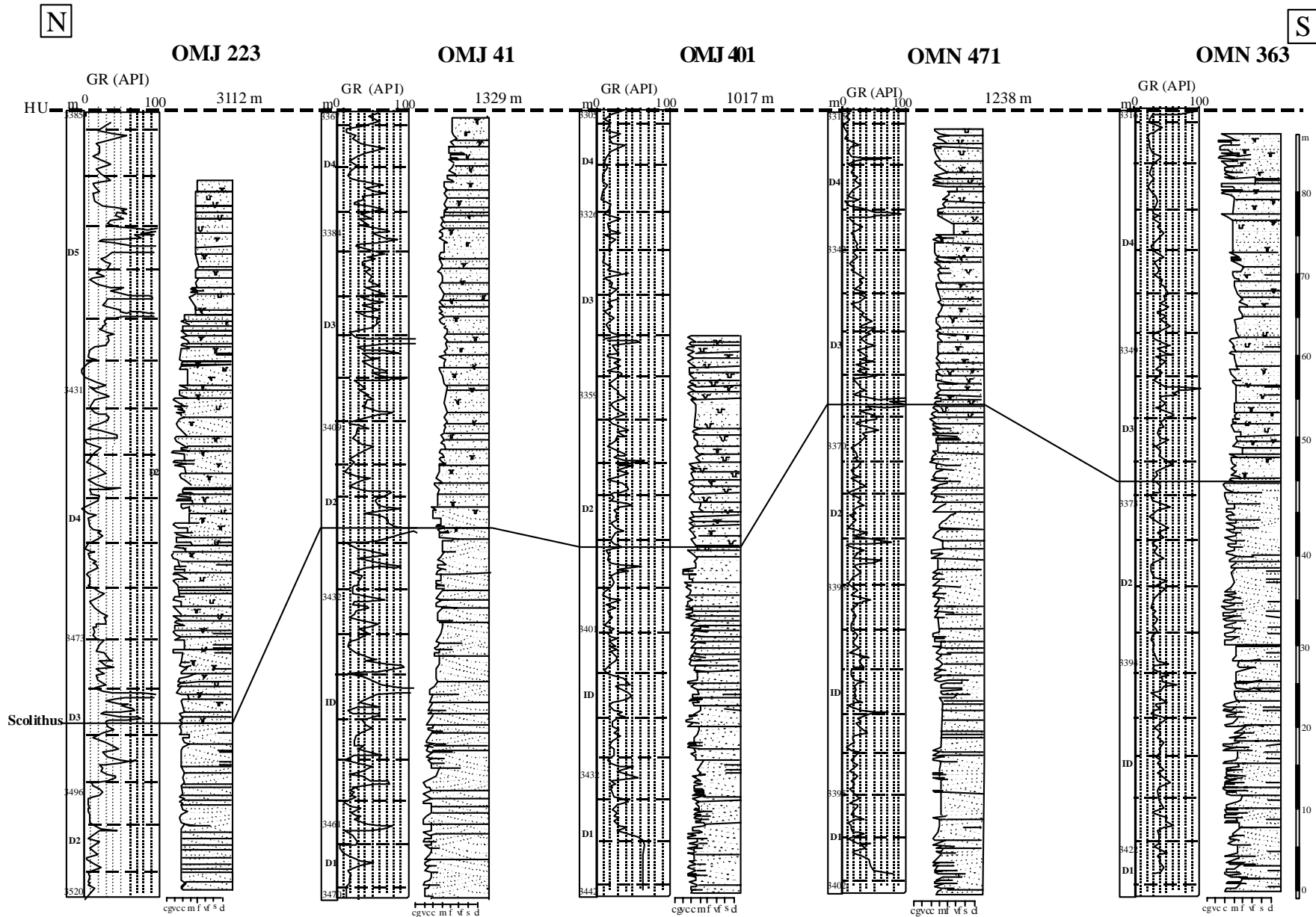


Fig. 16: N-S Geological cross section flattened on the Hercynian unconformity showing that the first appearance level of *Scolithus* traces vary in this direction which indicate an alternative marine and continental regime before the general transgression. This environment is designated as nearshore (domaine mixte) by Seilacher, A., (1967)., and Beuf, S., (1971).

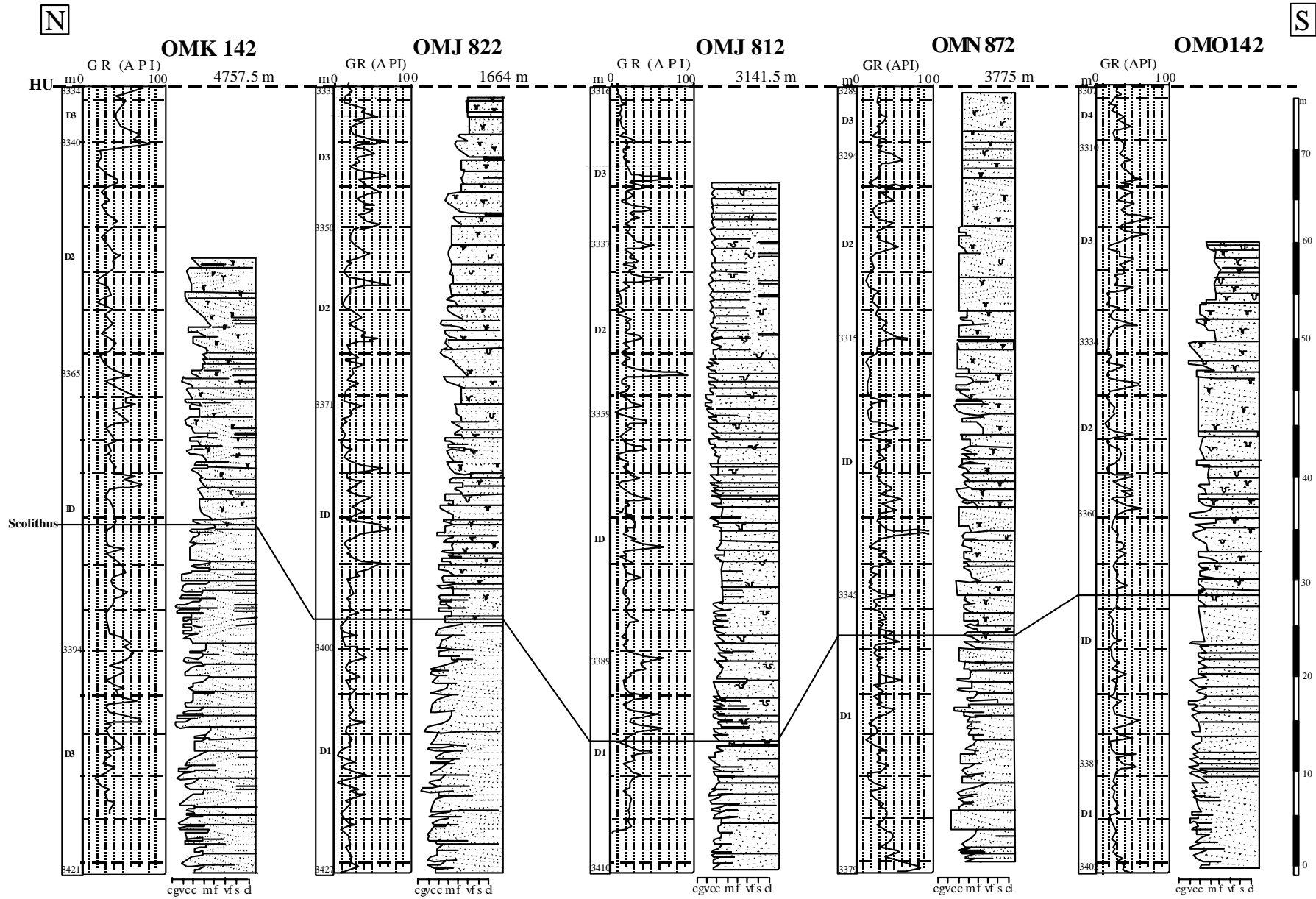


Fig. 17: N-S Geological cross section flattened on the Hercynian unconformity showing that the first appearance level of *Scolithus* traces vary in this direction which indicate an alternative marine and continental regime before the general transgression. This environment is designated as nearshore (domaine mixte) by Seilacher, A., (1967)., and Beuf, S., (1971).

4. Conclusion

The core description and sequence analysis of the Ra deposits allow for the following conclusions :

1. The Cambrian Ra consists of a supratidal to deeper intertidal environment.
2. The lower part of the Ra is represented by fluvial braided channels; the upper part is composed of tidal channels.
3. The fluvial part is characterized by fining-upwards stacked sequences of coarse- to medium-grain sized sandstone. The tidal part consists of coarsening upwards sequences; the grain size is medium to fine.
4. The base of the tidal deposits coincide with the lowermost occurrence of *Scolithus*.
5. By analogy to Zaitin et al. (1994), a model of simple piedmont incised system (incised valley sequence) showing its evolution over one complete sea-level cycle is proposed (Fig. 18). Robertson (2000) proposed an idealized model of different modes of the four deposits of the Illizi basin on the outcrop in the Algerian Sahara, which is used as a reference for the Cambrian of Hassi Messaoud field in this study. The fluvial deposits of the Cambrian Ra correspond to the lowstand system tract (LST) and the tidal deposits corresponds to the earlier transgressive system tract (TST) Fig. 19.

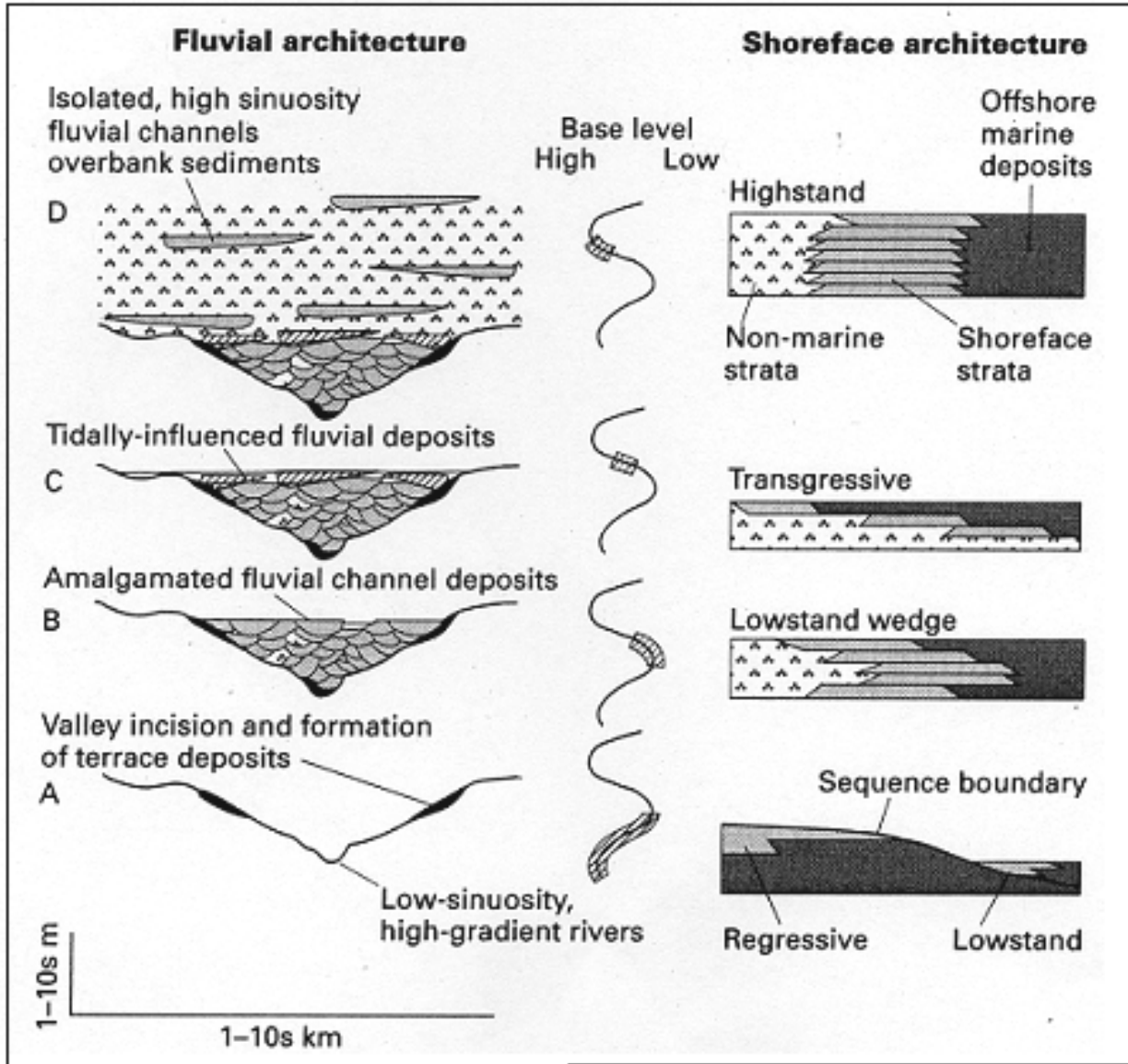


Figure 18: Model of evolution of an incised valley and its subsequent filling. Coeval changes in nearshore stacking patterns are also shown. Note the incidence of tidal influence and the low channel/overbank ratio once the rim of the paleovalley has been overtopped (after Shanley & McCabe, 1993).

AGE	SEA LEVEL CODE	SYSTEMS TRACTS	ENVIRONMENT OF DEPOSITION	LITHOLOGY	SUMMARY CORE LOG	SYNTHETIC GR PROFILE
Liand-overly	SS1	Mid TST Rapid rise in relative sea level	Drowned estuary to open shelf	Graptolitic shaly mudstone		
Ahegill	IV-4	Early TST Gradual deepening leads to flooding of braidplain	Drowned braidplain (estuarine to tidal flat conditions) (Ti, Tc, Wss, Wsl, Smh)	Fine, poorly sorted argillaceous sandstone locally burrowed		
	IV-3	LST Local incision followed by onset of fluvial braidplain and sand prone delta front	Braidplain, delta front and minor distributary channels (Ac, Ao, Wsm)	Very fine and medium grain clean pebbly sandstone with planar cross lamination and cross-bedding		
	III-2	TST to HST Incision, followed by rapid sea level rise, then progradation of delta systems as accommodation space is infilled	Unstable delta front (mouth bar) and prodelta (Sst, Ssp, Wsm)	Very fine and fine grain, clean or argillaceous sandstones. Common slumping and soft sediment deformation where most argillaceous. Interbedded with silty to sandy mudstones.		
	III-1	Late LST to early TST Incision followed by establishment of fluvial braidplain and, with increasing relative sea level, a shallow shelf	Braidplain to shallow marine storm-wave dominated shelf (Ac, Ao, Wss, Ws)	Coarse to medium or fine, generally clean sandstones		
	III-2	Mid to late TST OGlacial incision followed by rapid flooding	Deepwater distal prodelta possibly associated with floating ice, infills erosive relief (SSp)	Uncored in study area, schistose sandy to pebbly mudstones		
Uanv'm-Caradoc	III-3	Late TST to HST Progressive reduction in accommodation space relative to sand supply leads to repeated episodes of progradation and preservation of parasequences. Major period of condensation marks top of preserved sequence	Submerged protected shoals or attached shorefaces to inner shelf and offshore (storm-wave dominated) (Smh, Wsl, Wss, S uc)	Stacked coarsening and, less commonly, fining upwards parasequences. Comprising silty heterolithic mudstones associated with often intensely burrowed, moderately argillaceous sandstones. Burrows dominated by <i>Siphonichnus</i> . Locally on highs thin limestone caps sequence.		
	III-2	TST Rising sea level reduces sediment input	Mixed tide/wave-dominated shelf (Wss, Wsl)	Interbedding of heterolithics and burrowed sandstones		
	III-1	LST to early TST Relative sea level fall followed by drowning and tidal reworking of fluvial braidplain	Extensive shallow marine platform swept by tidal and/or semi-permanent wind drift currents (Ssb)	Fine to medium grain, generally clean sandstones with Oolite rock texture. Few if any sedimentary structures are preserved		
Tremadoc	III-1	HST Rising sea level reduces sediment input	Submerged shoals, protected shoreface to inner shelf and offshore (storm-wave dominated) (Smh, Wsl, Wss)	Stacked coarsening and, less commonly, fining upwards parasequences. Comprising heterolithic mudstones associated with burrowed, argillaceous sandstones. Burrows dominated by <i>Siphonichnus</i> .		
Upper Cambrian	I	LST to early TST Prolonged marine peneplanation followed by establishment of a sand prone proximal tidal sand sheet. Rising relative sea level results in a gradual offshore shift in facies	Proximal tide-dominated shelf (possibly with subordinate braidplain deposits) becoming progressively wave/storm-influenced (SSc)	Arkosic and micaceous to increasingly clean pebbly to quartz sandstones with thin heterolithic interbeds		
Pre to Infracambrian	Basement	NA	NA	Igneous and metamorphic rocks (Pharusian) with Infracambrian slates		

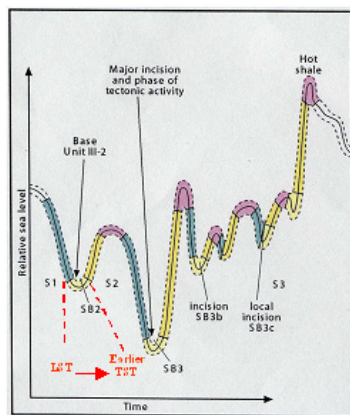
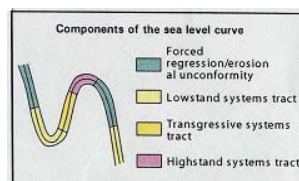


Figure 19: Sequence stratigraphic model of the El Gassi Field and the Illizi Basin (Robertson, 2000). This succession is subdivided by a series of sea-level controlled unconformities.



1. Introduction and goal

18 wells have been the subject of a detailed petrographic analysis and an interpretation of diagenetic phenomena (Fig. 20): OMK25, OMK16, OMK142, OMJ822, OMK112, OMJ812, OMJ802b, OMJ872, OMN86, OMO27, OMN67, OMN56, OMJ712, OMJ24, OMJ223, OMJ422, OMJ41, OMN471.

Five wells among the eighteen have been chosen to identify different rock types. These wells are: OMK25, OMK142, OMJ812, OMJ41, OMJ223.

2. Pore-level characteristics

2.1. General attributes

The Hassi Messaoud reservoir is dominated by quartzose sandstone with thin drapes of mudstone. Sandstone in the D5 and sometimes further down is bioturbated.

2.2. Texture and fabric

Hassi Messaoud sandstones are fine- to very coarse-grained. Most examined samples are moderately sorted. Accurate determination of grain size and sorting is complicated by abundant syntaxial quartz overgrowths that obscure original grain boundaries, especially in the upper portion of the reservoir where quartz cement is abundant. Some of the well sorted quartzose sandstones contain trace amounts of detrital clay. The clay can be found along the bottom of pores (on tops of grains), creating a geopetal fabric. The reservoir Ra is formed by pale beige quartzose sandstone, coloured when it is not impregnated with bitumen. The quartz cement, which can exceed 15% of the components, is accompanied by 5 to 10% of clay cement. The clay cement is more abundant in the lower part of the reservoir, whereas quartz cement is more abundant in the upper part.

2.3. Detrital components

Detrital component include quartz grains, rock fragments, clay matrix, mica and heavy minerals.

2.3.1 Quartz grains

Quartz grain are the most common detrital grain type in all examined samples (Fig. 21), and typically make up 60 to 70 percent of the sandstone. The abundance of quartzose grains increases upwards throughout the reservoir. This trend is accompanied by an increase in the proportion of monocrystalline quartz at the expense of polycrystalline quartzose grains.

These changes probably reflect a combination of maturing provenance and increased reworking and winnowing as the depositional environment evolved from channelized fluvial to tidal.

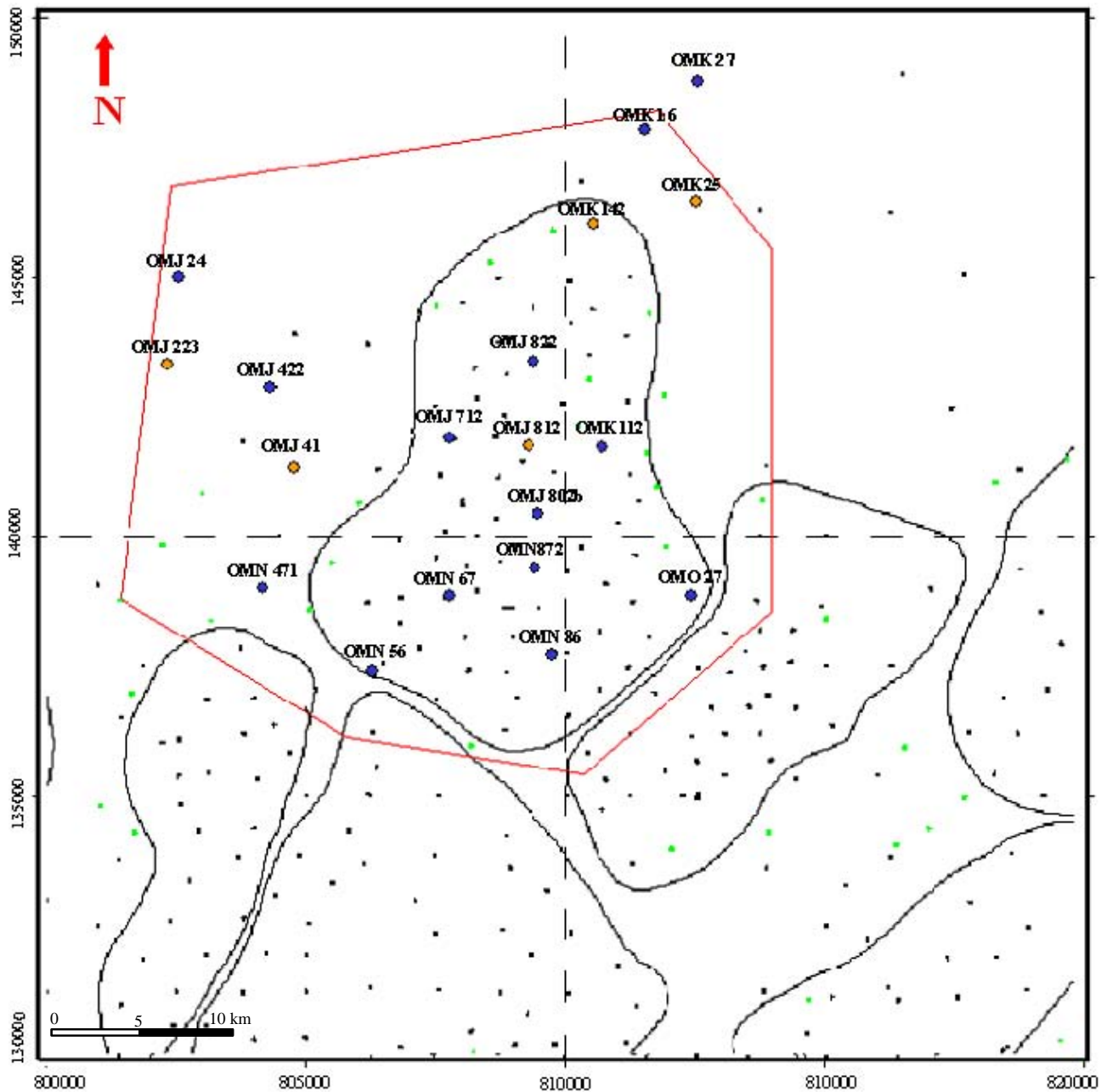


Fig20: The eighteen wells which were the subject of petrographic analysis, diagenetic interpretation, pore level characteristics and reservoir characterization .Yellow dots indicate the five wells which were analyzed in detail the for defining the Ra reservoir rock types. Red frame encloses the area of interest .

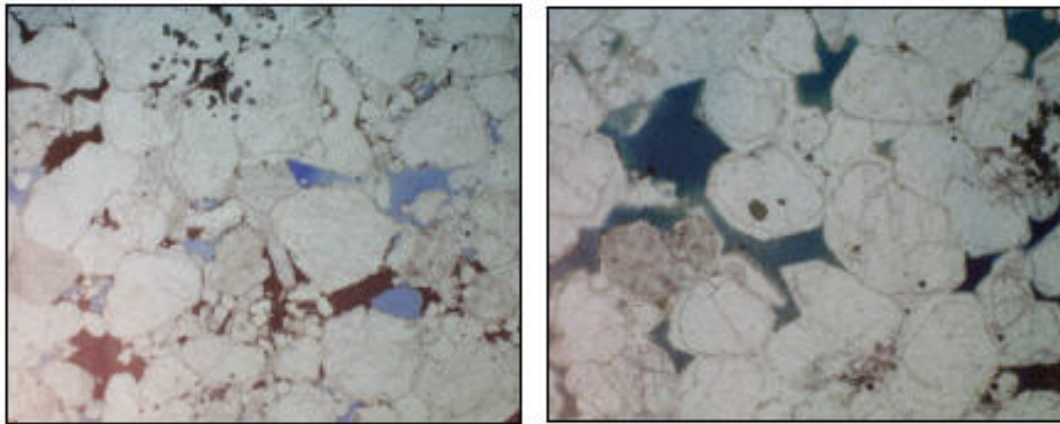


Figure 21: Left handside: Subangular to subrounded monocrystalline and polycrystalline quartz. This sediment compositions typical for OMJ822, 3424.50 m, LN_x4, D1. Right handside: Very well rounded monocrystalline quartz. OMJ812, 3359.00 m, LN_x2, ID.

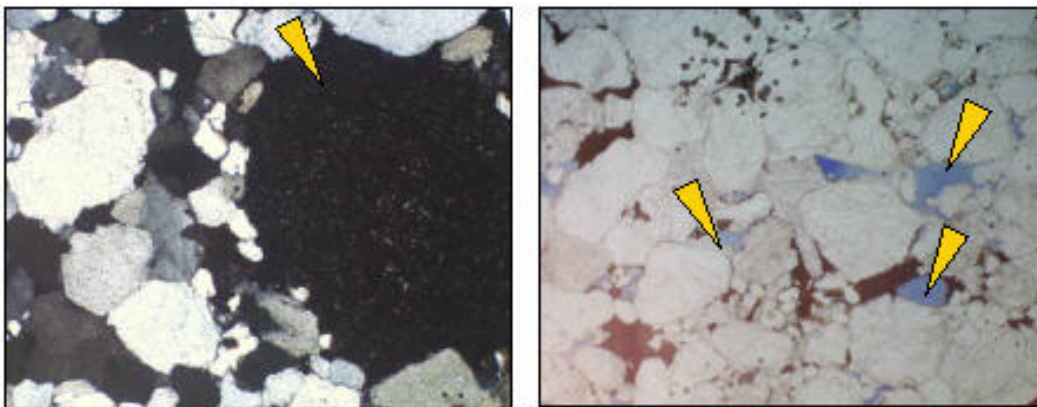


Figure 22: Left handside: Photomicrographs illustrating detrital grains (yellow arrows) of indeterminate origin completely altered to kaolinite. OMK142, 3459.00 m, LN_x40, D1. Right handside: Abundant moldic porosity (yellow arrows) resulting from complete grain dissolution, this grains were probably feldspars or lithic fragments. OMJ812, 3359.00 m, LP_x2, ID.

2.3.2. Detrital grains of indeterminate origin

Zone D1 to D4 sandstones contain detrital grains of indeterminate origin. These grains are common in zone D1 to D3, but present in a very low percentage in D4. This grain type is completely absent from zone D5. All original mineral material of this grain type has been altered to illite or dickite, or has been completely dissolved. Internal fabric and texture of the grains have been obliterated consequently (Fig. 22). It is not possible to determine whether these grains represent highly altered feldspar or rock fragments. Regardless of the specific identity of individual grains, the lower zones in HMD field clearly contain a higher proportion of these grains at the time of deposition (Fig. 23). The distribution of these grains, or more specifically, their diagenetic by-products, is responsible for the significant change in pore type and, therefore, reservoir properties between the lower and upper zones in the HMD.

2.3.3. Feldspar

In the zones D1 to D5, all samples examined in the wells are devoid of feldspar, but contain abundant products of feldspar alteration. The distribution of the feldspar alteration products strongly suggests that feldspar content was appreciably greater at the time of grain deposition, but that the feldspar was altered or dissolved during diagenesis. Feldspar diagenetic by-products (moldic pores and dickite or illite grain replacements) are absent from D5, suggesting that these sandstones were essentially devoid of feldspar at deposition.

Lithic fragments

The abundance of rock fragments and their alteration products (Fig. 23-24) decreases upward in the formation; they are common in zone D1 to D3 and rare in the D4.

Pseudomatrix

Pseudomatrix is a continuous interstitial paste formed by the compaction and dispersal of mechanically weak rock fragments into surrounding pore space (fig. 25).

Detrital clay

Detrital clay is a trace to minor component in most examined samples, and from less than five percent of the volume of clay. Detrital clay can be found as dispersed matrix associated with burrows and mud drapes and as geopetal clay.

A. Matrix: Detrital clay matrix is common to abundant within mudstone to argillaceous sandstone drapes. These drapes consist of silt- to coarse sand-sized grains floating in a recrystallized clay matrix. Grain types include quartz, mica and rock fragments. Incipient stylolites are common.

B. Geopetal clay: Detrital clay mineral occurs in trace (<1%) amounts as discontinuous clay rims with geopetal texture. These clays are especially common in well-sorted, very coarse- to coarse-grained laminations of quartz sandstone. Geopetal clays are common in the cross-bedded intervals (in the heavily oil-stained intervals) (Fig. 26).

C. Mica and heavy minerals: Mica (muscovite) occurs in minor amounts in most Hassi Messaoud (HMD) sandstones. Mica is common in the mud drapes/argillaceous sandstones. The presence of fresh and highly altered muscovite co-existing in some samples, suggests that mica originated from at least two sources (one fresh, one altered) (Fig. 27).

In the Hassi Messaoud sandstones, heavy minerals occur in trace amounts as dispersed grains.

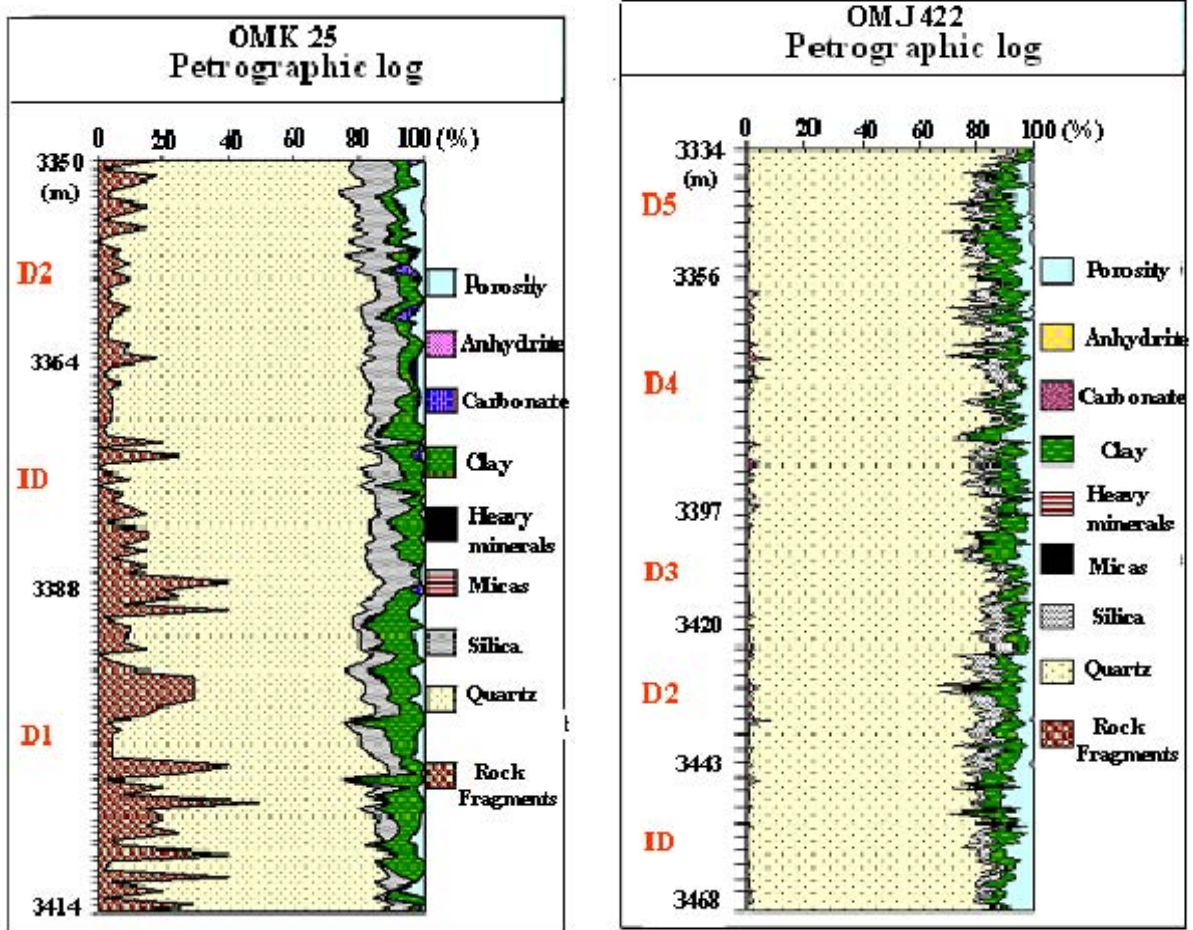


Figure 23: Two examples showing mineral components within the reservoir rocks in drill holes OMKJ422 and OMK25 (see map Fig. 20 for geographic location). The clay cement is more abundant in the low part of the reservoir. Quartz cement is more important towards the top. The percentage of rock fragments decrease from the bottom to the top of the Ra reservoir before their complete disappearance higher up in the D5.

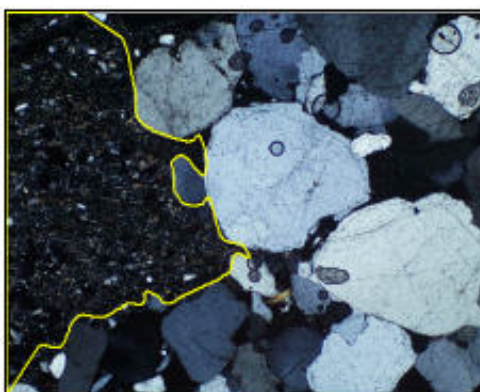


Figure 24 - Photomicrographs illustrating an example of lithic fragments: altered mudstone fragment with common mica. OMJ41, 3387.50 m, LN \times 40, D3.

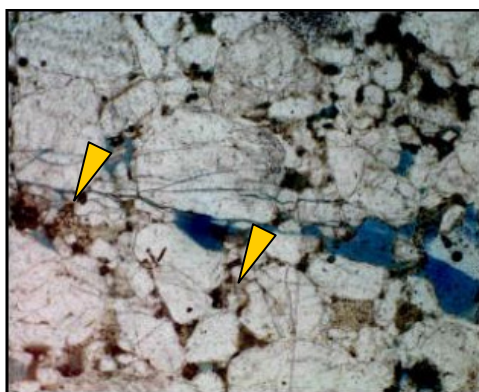


Figure 25 - Photomicrograph showing pseudomatrix, formed by the alteration and plastic deformation of rock fragments into interparticle pore space. OMJ422, 3413.5 m, LN \times 40, D3.

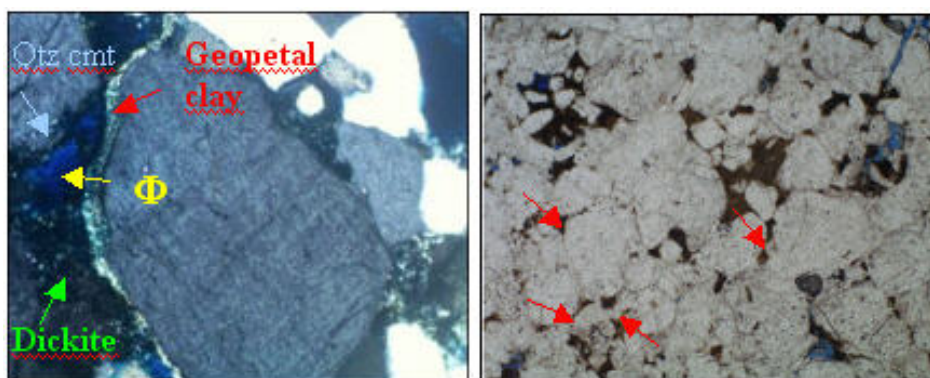


Figure 26 - Geopetal clay sandstone in HMD sandstones : geopetal clay (red arrows), which inhibited the formation of quartz cement . In some pores containing Dickite cement , there is a complex geopetal sequence of geopetal clay, dickite, remnant porosity and quartz cement results. Left handside: OMJ422, 3464.5 m, LN \times 100, ID. Right handside: OMN-56, 3401.5 m, LN \times 40, D1.

The preserved heavy mineral suite is restricted to the ultra-stable assemblage of zircon, tourmaline, pyrite and a lesser quantity of rutile as inclusions in some quartz grains (Fig. 28).

2.4. Authigenic Components

2.4.1 Quartz cements

Quartz cement is the dominant authigenic component in virtually all HMD sandstones (Fig. 29). Quartz occurs most commonly as syntaxial overgrowths. Quartz cement also commonly occurs as euhedral crystals that project into secondary pores formed by grain dissolution. Quartz is the principal cement lining and filling in fractures and veins. In some cases, dust rims and fluid inclusions delineate the boundary between host grains and cement overgrowth, or between grain and vein-fill. However, in many cases it is difficult to distinguish cement from grains using standard optical methods. Consequently, estimates of quartz cement abundance are subject to error. At the microscopic-scale, the distribution and abundance of quartz cement is controlled by a combination of the nature of the substrate grains, their surface area, and the presence of clay cements.

Finely grained and poorly sorted sandstones have high surface areas and, therefore, abundant cement nucleation sites. These rock types are therefore more susceptible to quartz overgrowth formation. Once overgrowth formation is initiated, the crystal growth will continue until it is physically blocked or until geochemical conditions no longer favor quartz cementation (fig. 30).

Monocrystalline quartz and polycrystalline quartz

There is a strong relationship between the thickness of quartz overgrowths and the character of the substrate grain. Monocrystalline quartz grains have thick, well developed overgrowths, whereas polycrystalline quartz grains have poorly developed overgrowths.

The abundance of quartz cement is inversely related to the abundance of clay cements.

Drain D1 to D5 sandstones display variation in quartz cementation that reflects variations in initial sediment composition. Compositionally less-mature sandstone contained more feldspar, lithic fragments and polycrystalline quartz at deposition compared to more mature sandstones. The zones D1 to D4 are characterized by immature sandstones in which the feldspars and lithic grains are typically altered to dickite or illite (as we can see later), which inhibits quartz cementation, as discussed above. In contrast, compositionally mature sandstones like D5 are dominated by monocrystalline quartz which promotes the formation of quartz overgrowth cements (Fig. 31). Grain size and sorting are the major controls on the abundance and distribution of quartz cement in the D5 drain. In zone D5 (Fig. 32), interactions of burrowing organisms with interlaminated fine- and coarse grained, well sorted sandstone result in complex pore-scale variations in grain size, sorting and clay content that control the abundance of quartz cement and, ultimately, reservoir quality.

Compared to coarse-grained domains, fine-grained domains have high surface areas and, therefore, more abundant nucleation sites for cement formation. For this reason, quartz cement will more readily form in fine-grained samples. In well-sorted sandstones, quartz cement abundance varies inversely with grain size. Because the initial pore and pore-throat sizes are smaller in fine-grained samples, the precipitation of cement will have a more significant impact on reservoir quality compared to coarser-grained samples with their larger pores and throats.

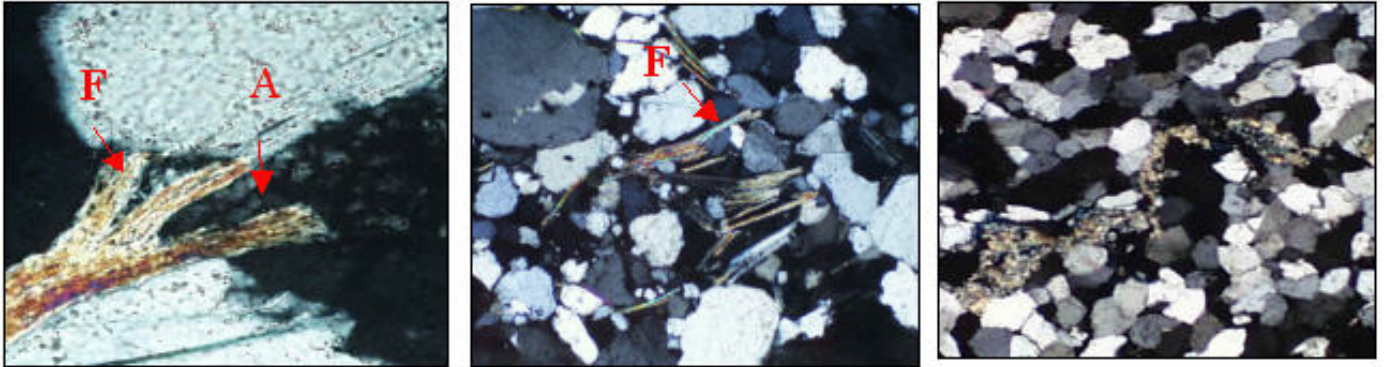


Figure 27 – Left handside and center : photomicrograph showing fresh (F) and highly altered muscovite (A), indicated at less two sources for the mica. Right abundant mica in mudstone drape. Left handside: highly kaolinitized Muscovite OMJ24, 3491.5 m, LP x 200, D3. Center: Fresh muscovite. OMJ24, 3474 m, LP x 40, D4. Right handside: Incipient formation of stylolithes OMJ24, 3476.5 m, LP x 40, D4.

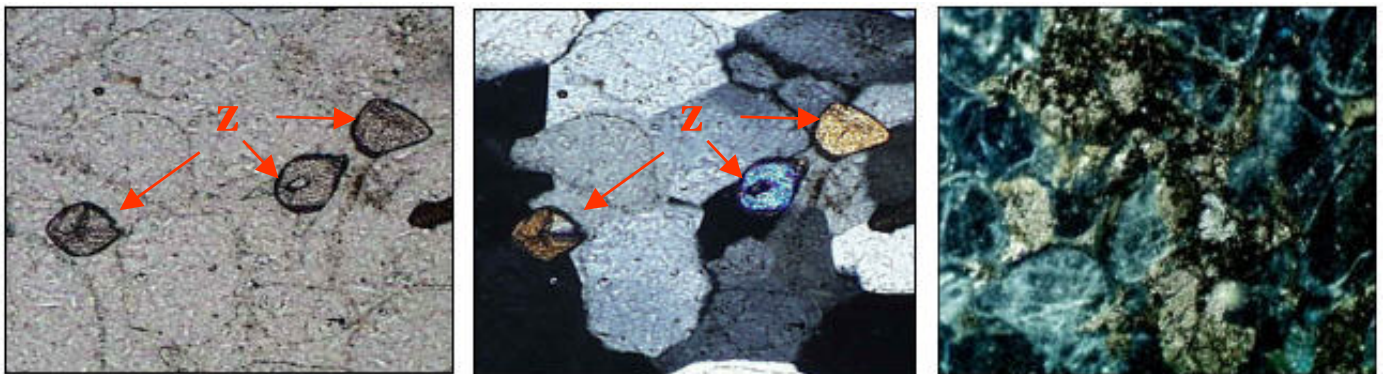


Figure 28 - Photomicrographs of heavy minerals in HMD samples . Left handside and center: Zircons (Z) are common. OMJ24, 3477.5 m, LN x 100, D4. Right handside: Pyrite probably replaced by less stable heavy minerals as amphiboles and pyroxenes. OMJ422, 3405.5 m, LRx100, D3.

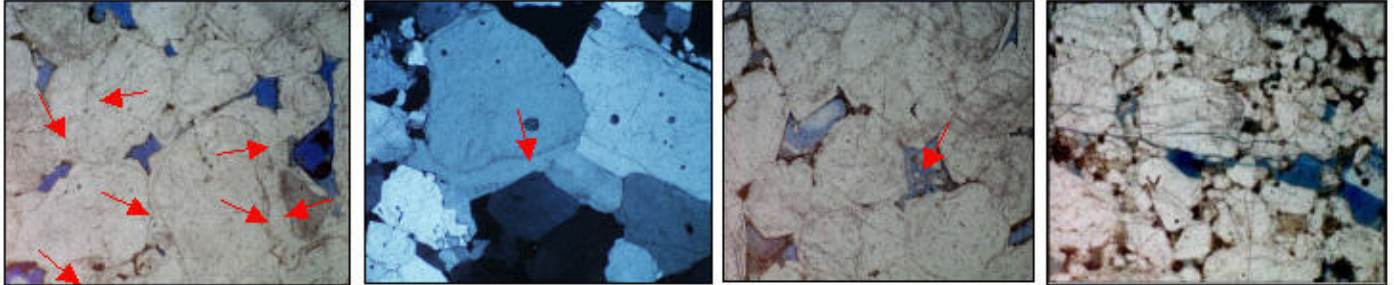


Figure 29 - Common modes of occurrence of quartz cement in HMD sandstones . Left handside:The micrograph illustrates syntaxial overgrowths (red arrows). Note well-developed dust rims (red arrows , far left micrograph). OMJ 822, 3382.50 m, LNx4, ID. Center left handside: Micrograph is same field of view as far left showing crystallographic continuity between host grain and cement micrograph. OMJ41, 3439.50 m, LNx40, ID. Center right handside show small euhedral prismatic quartz crystals projecting into moldic macroporosity created by the dissolution of an unstable framework grain. OMJ 822, 3424.50 m, LNx4, D1. Far right handside: micrograph illustrates quartz cement in partially healed fracture. OMJ422, 3413.5 m, LN x 40, D3 .

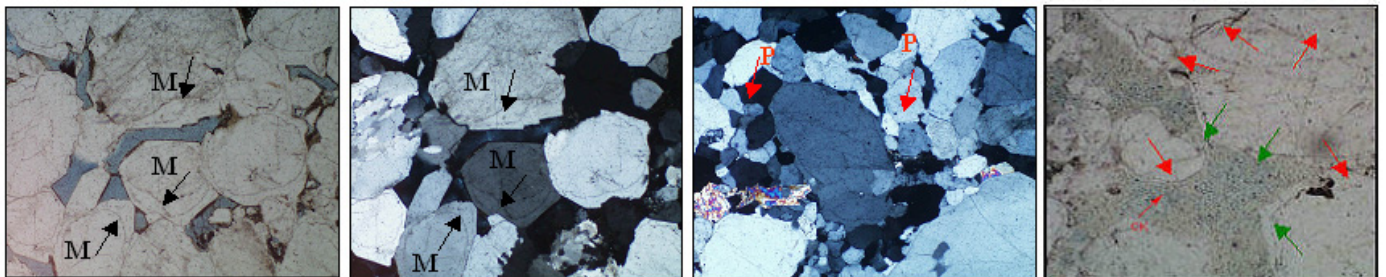


Figure 30 - At the pore level, quartz cement distribution and abundance is controlled by the nature of substrate grains and the presence of clays cement. Left handside pair: Monocrystalline quartz grains(M) have well developed overgrowths (black arrows). OMJ223, 3461.5 m, LP and LN x 40,D4, whereas polycrystalline quartz (P) , has complete poorly developed overgrowths center(pink arrows). OMJ41, 3421 m, LNx 40,D2. Right handside : In samples contain illite,kaolinite or dickite cements quartz overgrowths terminate when they reach the kaolin cement or illite (green arrows , whereas in clay free pores quartz cementation continued until the pores were completely occluded(red arrows). OMJ24, 3479 m, LN x 40, D4.

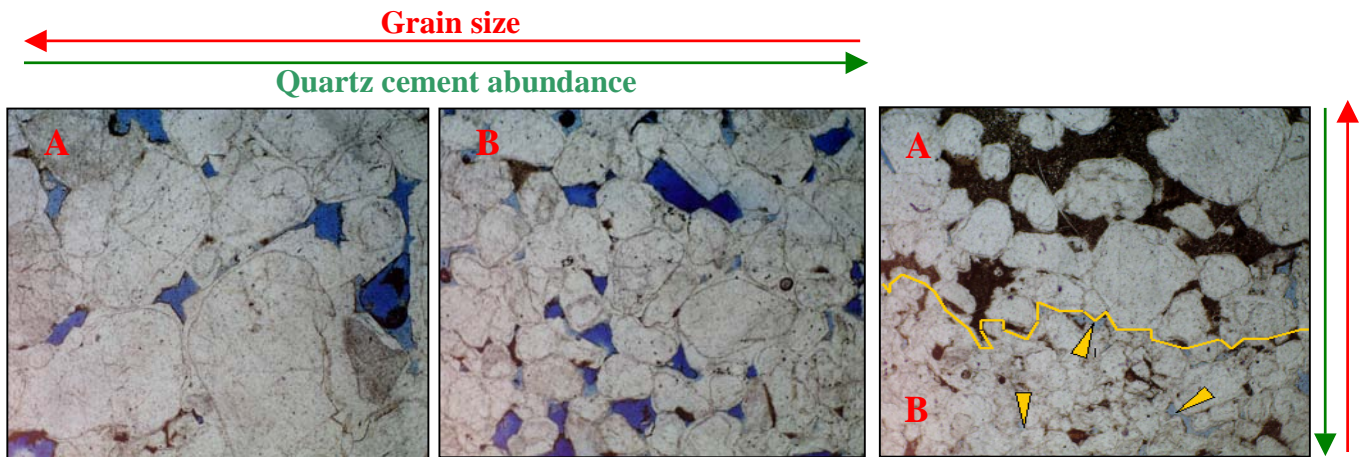


Figure 31 - In well-sorted sandstones, quartz cement abundance varies inversely with grain size. In coarse grained samples, there is an elevated porosity due to minor quartz cement and large pore size (A), whereas in fine grained samples more abundant quartz cement substantially decreases porosity (yellow arrows) and pore size (B). This intensifies the relation between grain size and reservoir quality. Yellow line indicates contact between diagenetically strongly silicified and non silicified material. Left handside: OMJ822, 3382.50 m, LN \times 4, ID. Center: OMJ822, 3385.50 m, LN \times 4, ID. Right handside: OMJ822, 3356.00 m, LN \times 4, D2.

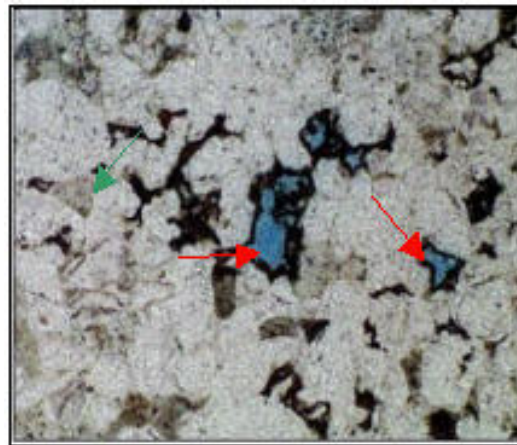


Figure 32 - In bioturbated sandstones, the abundance of quartz cement is controlled by the presence of minor amounts of detrital clay introduced by bioturbation. In clay bearing samples, quartz cementation is inhibited, so microporosity and minor interparticle macroporosity is preserved (red arrows). In clay-free bimodal sandstones, quartz cement occludes virtually all interparticle porosity (green arrows). OMJ422, 3344.5 m, LN \times 100, D5.

2.4.2. Carbonate (dolomite):

Dolomite occurs in trace to minor amounts (<5%). Because of dispersed distribution and low abundance, dolomite has no appreciable effect on reservoir quality nor petrophysical properties (Fig. 33).

2.4.3. Clays

Two principal clay minerals are defined by X-ray analysis of samples (kaolin and illite) (Fig. 34). Authigenic kaolins are, with illitic minerals, the most common clay minerals encountered within sandstone reservoirs. In this study, kaolins refer broadly to the different minerals of the kaolin group (kaolinite and dickite), as we can see later.

A. illite

Illite comprises up to 3% of the clay minerals in the HMD samples. In these samples, authigenic illite occurs as cement, as replacements of cements, and as detrital grains (probably altered feldspars and lithic fragments) (Fig. 35). Illite is present either as large plate or a very fine film around quartz grains and present sometimes the same facies as the kaolinite.

Kaolinite predominate in the good producing wells, and conversely illite is abundant in the non-producing wells.

B. kaolinite

Kaolinite is the most abundant clay mineral present in the HMD samples examined (7%). In these samples, authigenic kaolinite occurs as cement and as replacements of cements and detrital grains (Fig. 36). In places the recrystallization of the kaolinite in HMD samples is on dickite.

The authigenic kaolinite is partially replaced or illitized and/or dickitized in places. Kaolins are represented by two principal classical facies types :

- A well-crystallized vermiform type of kaolinite and irregular pore-fills between quartz grains (Fig. 37).
- Another form of kaolinite is derived from detrital mica, which first spreads as leafs, then separates to create large vermiform grains.

The very well-crystallized kaolinite has a pseudo-hexagonal form with 5 to 10 microns (Makhous, 1985)

C. Dickite

The dickite polymorph of kaolinite occurs as grain replacements and pore-filling cement in many zones of D1 to D4.

The distribution and abundance of dickite are apparently controlled by initial sandstone composition, temperature and local fluid chemistry. These relationships are shown further in Fig. 47. Few samples of examined sandstone from zone D5 typically contain traces, if any at all, of dickite. The paucity of dickite in these rocks probably results from the paucity of precursor feldspars. Dickite is common to abundant in compositionally immature sandstones D1 to D4, illite pseudomorphs after kaolinite increase in abundance at the expense of dickite (Fig. 38).

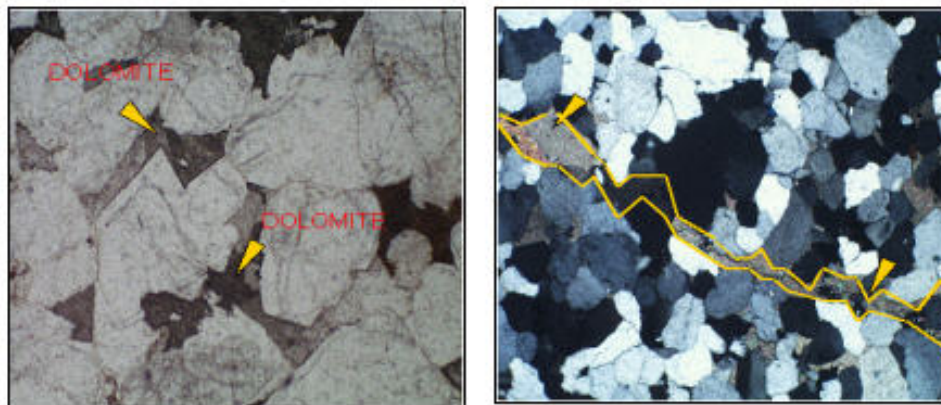


Figure 33 –Left handside: Dolomite (yellow arrows) occurs in trace to minor amounts as grain replacements or cement. OMO27, 3317.50 m, LN_x4, ID. Right handside: Micrograph illustrates dolomite cement in partially healed fracture (yellow arrows and lines). OMO27, 3312.50 m, LP_x40, ID.

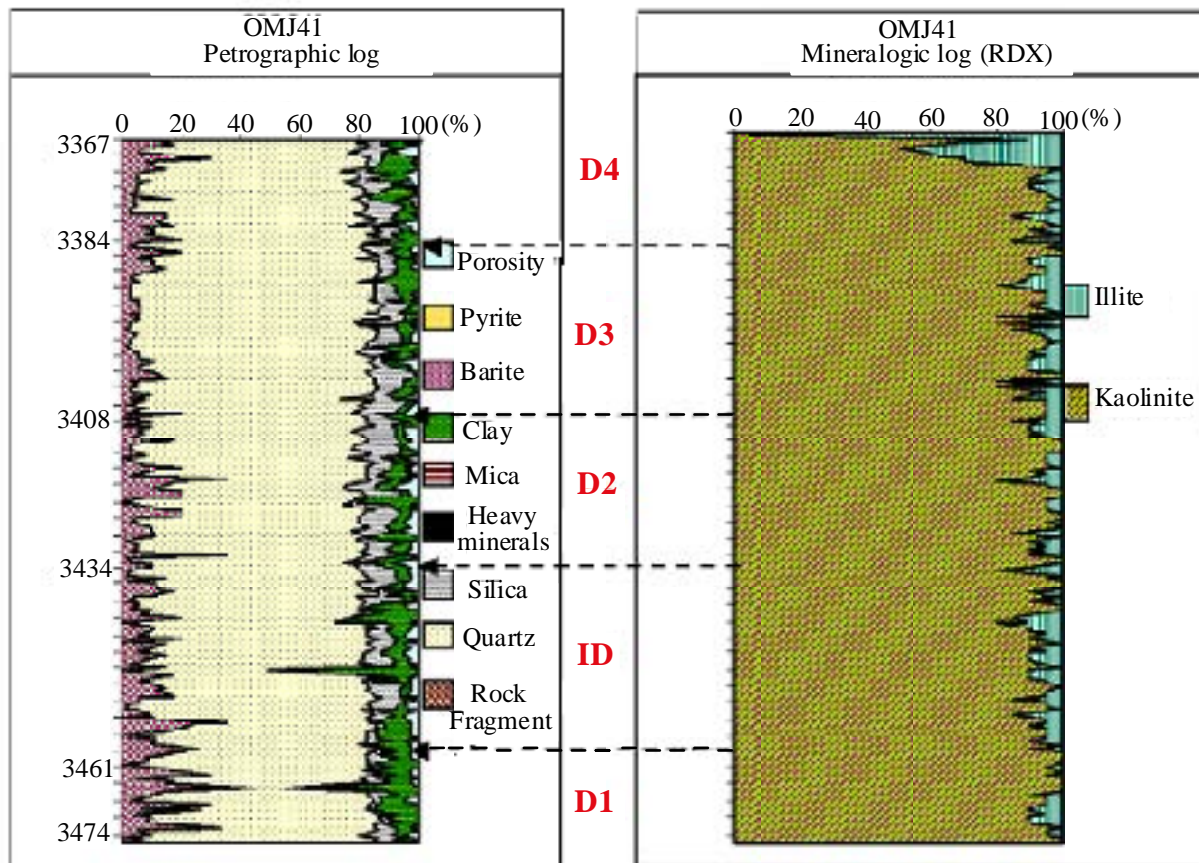


Figure 34 - An example showing the percentage of mineral components within the reservoir rocks of different reservoir zones. Left handside: Mineral content of the reservoir. Right handside results of XRD analysis in drill hole OMJ41 (see map Fig. 20 for geographic location). Kaolinite and illite are the common clays within the reservoir.

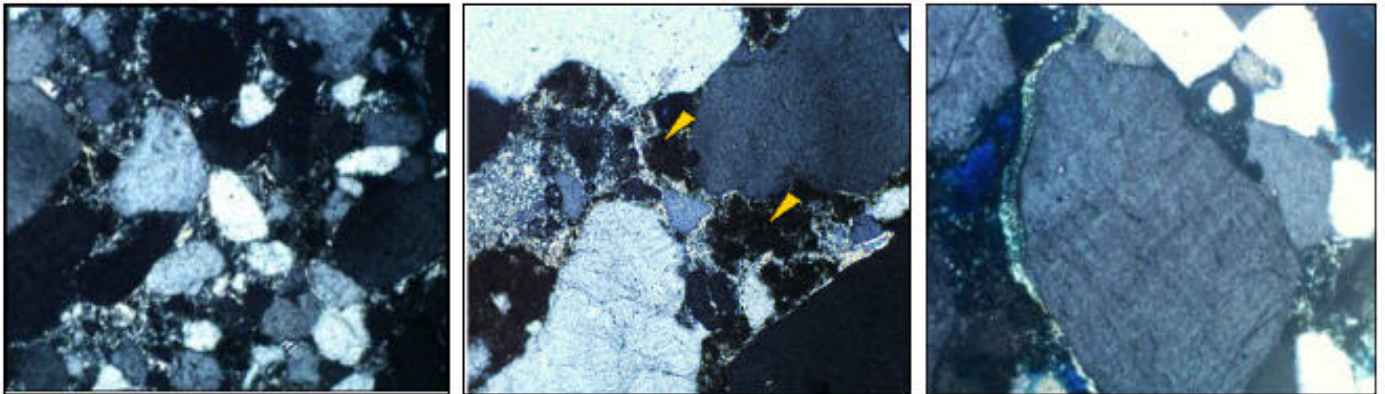


Figure 35 - Left handside: Illite cement OMJ422, 3342.5 m, LPx10, D5. Center: Mass of kaolinite surrounded by illite (yellow arrows) which probably results from an early illitization of kaolinite. OMK25, 3410 m, LPx10, D1. Right: Geopetal clay around quartz grain (illite) OMJ422, 3464.5 m, LPx100, ID.

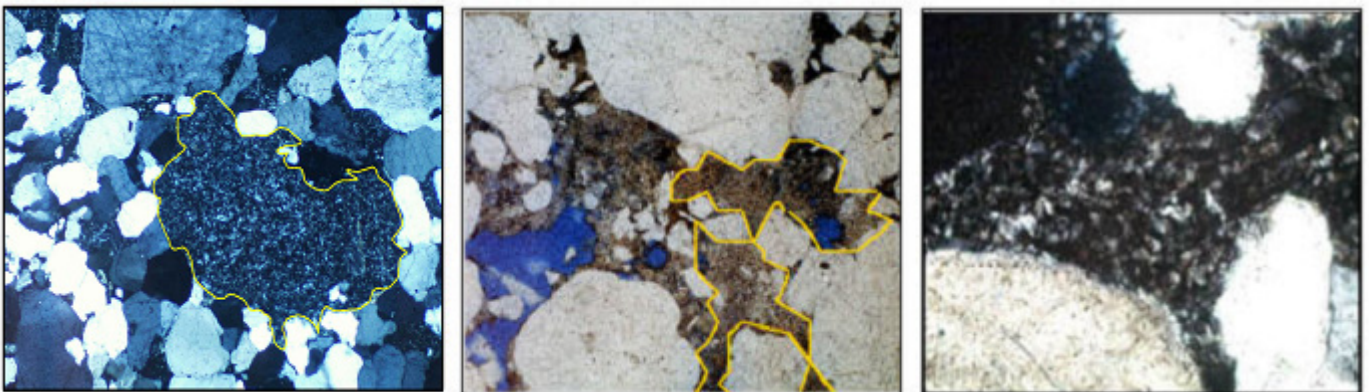


Figure 36 - Kaolinite grain replacement and pore filling cement. Right handside: A mass of kaolinite occurs as nodular aspect (yellow line). OMJ41, 3459 m, LNx40, ID. Center: Pervasive kaolinite pore-filling cement (yellow line). OMJ822, 3380.50 m, LNx4, ID. Right handside: Kaolinite cement. OMJ422, 3427 m, LNx200, D2.



Figure 37 - Photomicrographs showing highly kaolinitized mica . Left handside and center:Highly altered mica to kaolinite (red arrows). OMJ41, 3425.50 m, LP and LN \times 100, D2.Right handside: Authigenic kaolinite occurs as replacements of detrital grains(mica). OMJ24, 3491.5 m, LP \times 200,D3.

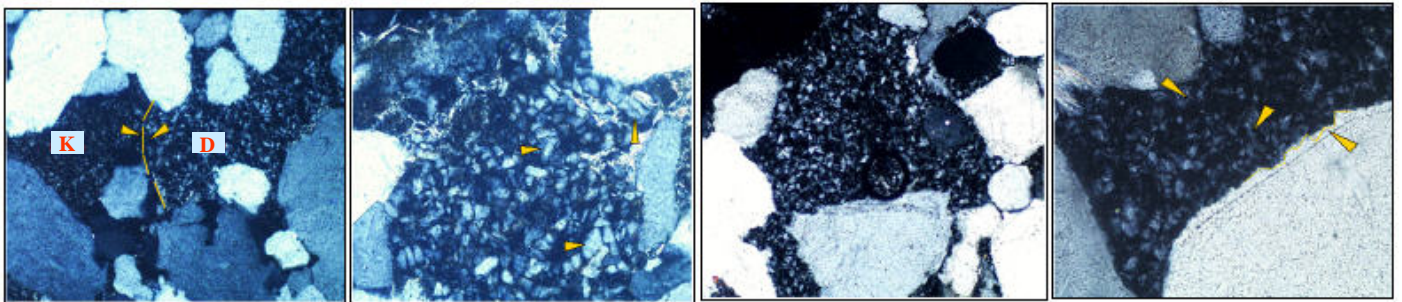


Figure 38 - Photomicrographs showing typical occurrences of dickite in HMD sandstones. Far left handside: Dickitization front (yellow line) appears when both kaolinite and dickite coexist. OMJ812, 3401 m, D1, LP \times 10 . Left-center: Dickite crystals (yellow arrows). OMJ812, 3401 m, LP \times 20, D1. Right – center and far-right: Kaolinite cement completely dickitized, yellow arrows show dickite crystals. OMO27, 3328.00 m, LP \times 20, D1, and OMJ822, 3396,50 m, LP \times 10, ID .

D. Chlorite

Chlorite is present as a minor clay mineral within the reservoir rocks. It has been observed as authigenic crystals only in two wells, and with low percentages in OMJ24 (in D5) and OMJ 422 in the upper part of the D4 (Fig. 39). Note that this mineral has no influence on reservoir filtration capacity.

2.5. Minor components:

Pyrite:

Pyrite occurs in trace amounts. It is most commonly scattered unevenly throughout the sandstone and often fills fractures (Fig. 40) with a variable frequency, it depends on geochemical conditions and diagenesis which are preceded. Therefore, we cannot maintain the sedimentary origin of this sulfur, which can penetrate into the rock by liquid seepage.

Barite and Anhydrite:

Trace amounts of barite were observed in only a few samples. Barite has no effect on HMD reservoir quality. Barite cements are present in two main forms: pore-filling and fracture-filling. Pore-filling barite forms large crystals that completely fill inter-particle pore space (Fig. 41-42). The pores that this cement fills formed after compaction and quartz cementation, indicating a relatively late time of formation. No porosity is associated with barite. Because of high grain density and lack of porosity, these barite nodules may cause local spikes in density logs. Trace amounts of anhydrite are generally associated with carbonate (dolomite) and /or barite (Fig. 43).

3. Diagenesis

3.1. Textural maturity of HMD sandstones

Compositionally mature sandstone

The diagenesis of compositionally mature sandstones at deposition, as is the case for D5, is dominated by quartz cementation, resulting in a depositional quartz arenite. Quartz cementation began soon after deposition, after some minor compaction at temperatures of less than 100°C. Continued quartz cementation during the sediment compaction filled most pores in places.

Compositionally immature sandstone

The diagenesis of compositionally immature sandstones (D1 to D4) is dominated by alteration and dissolution of unstable grains, resulting in a (diagenetic) quartz arenite, and displays complex diagenetic histories, which vary with temperature and initial sandstone composition. In zones D1 to D4, feldspars are completely altered to kaolinite/ dickite and rock fragments are illitized. The alteration and/or dissolution of feldspars and lithic grains shifts rock composition to “diagenetic quartz arenite”.

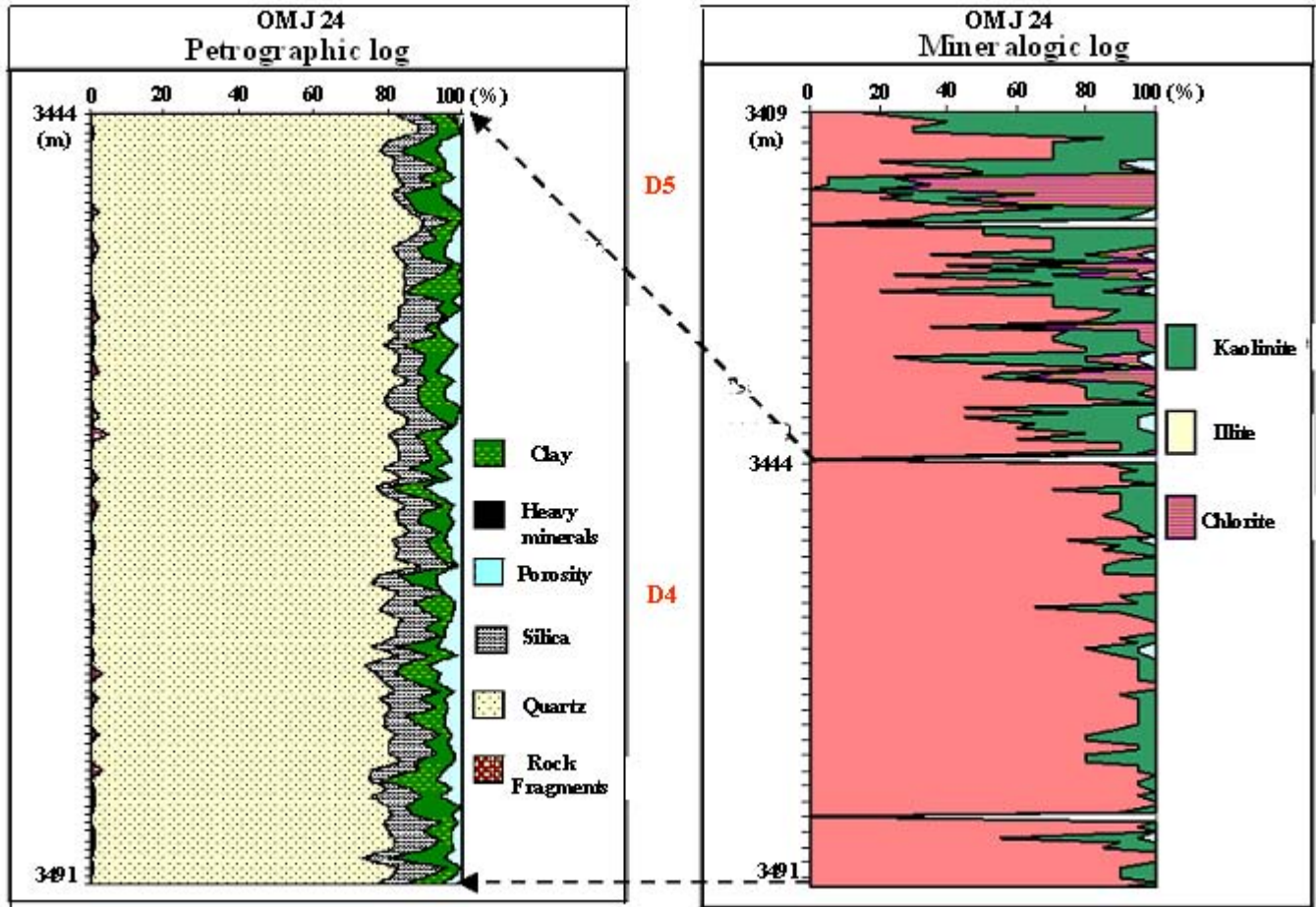


Figure 39 - An example showing mineral percentage components within the reservoir rocks of the different zones of the reservoir Ra. Left handside: The results are based on microscopic description. Right handside: Results of XDR analysis of the interval 3491- 3409 m in drill hole OMJ24 (see map Fig. 20 for geographic location). Note the increasing amount of kaolinite towards the top of the interval. Chlorite occurs above 3427 m.



Figure 40 - Trace amounts of pyrite occur in most samples as small framboids and cubes filling cements, it is more common in mud drapes. OMJ422, 3405.5 m, LPx100, D3.

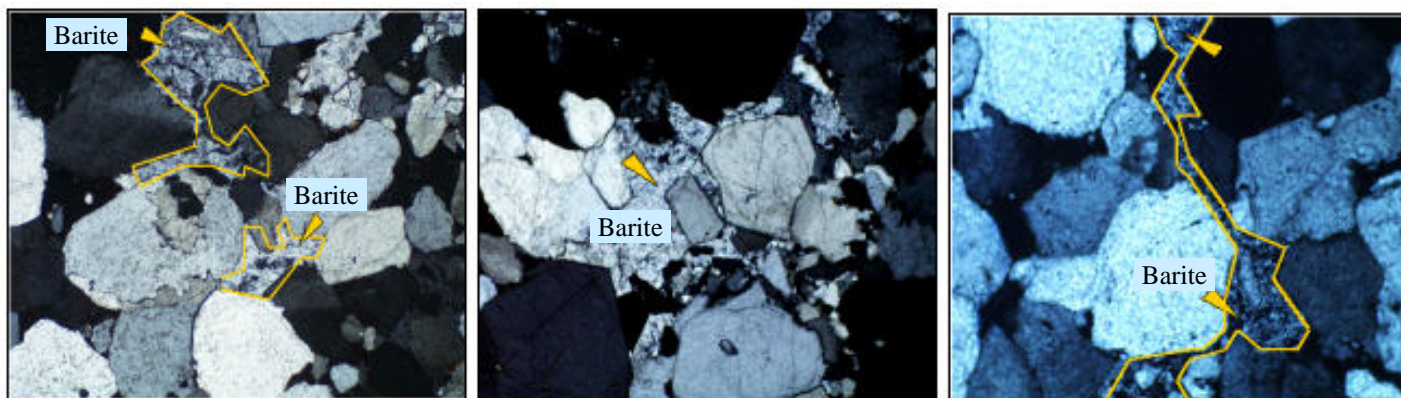


Figure 41 - Authigenic Barite cements. Left handside: Pore filling OMO27, 3346.50m, LPX4,D1 . Center OMJ822, 3356.50 m, LNx4, D2. Right handside: fracture filled by Barite. OMJ822, 3356.50 m, LNx10, D2.

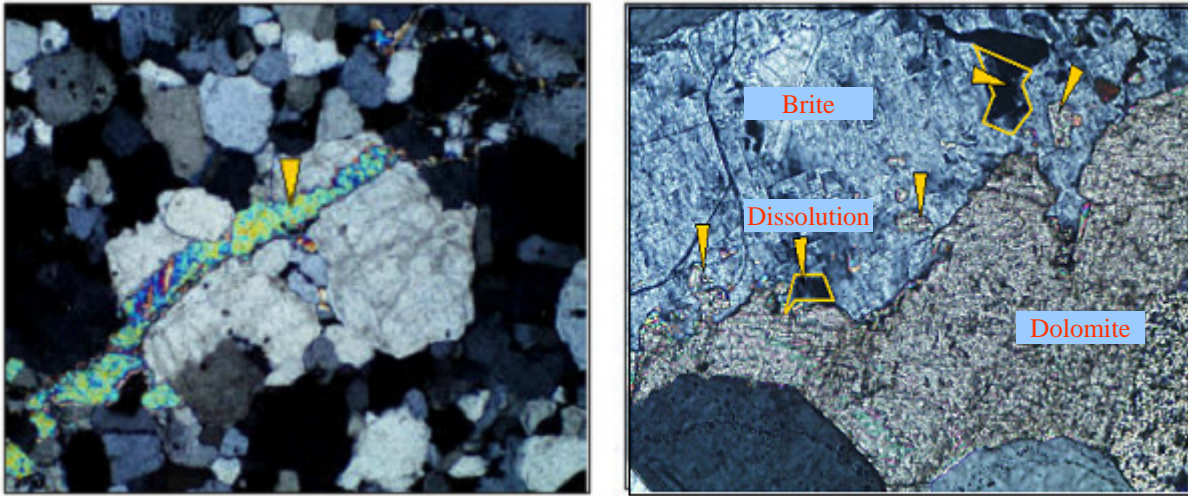


Figure 42 - Left handside: Fracture completely filled in by sulfate(yellow arrow). OMJ822, 3393.50 m, LPx4, ID. Right handside: An example of barite cement postdated the recrystallization of dolomite (yellow arrows), trace of dissolution are also present(yellow lines). OMO27, 3348.50 m, LPx4, D1.

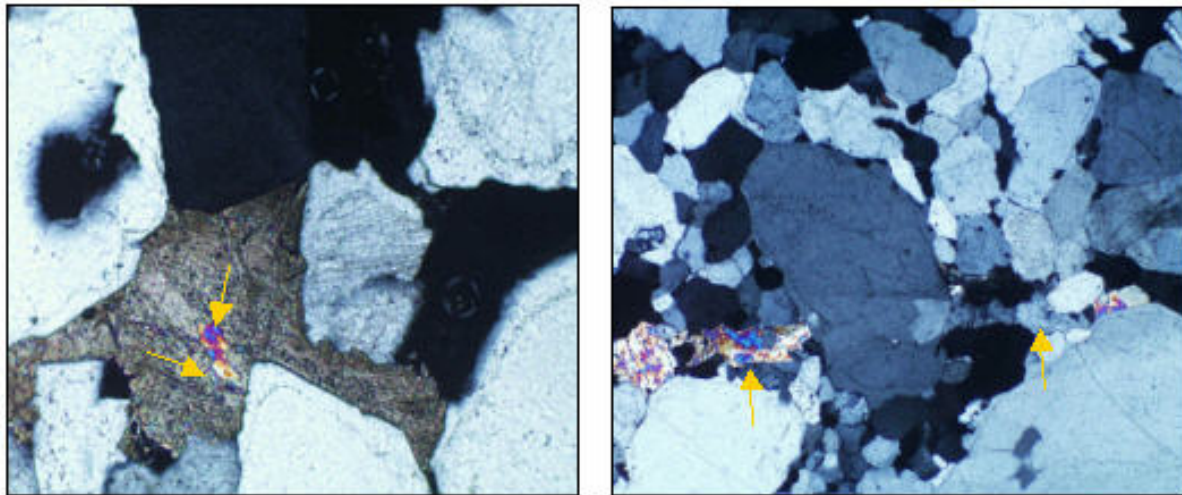


Figure 43 - Left handside: The presence of isolated anhydrite relics(yellow arrows) indicates that dolomite postdates anhydrite. OMK25, 3356.5 m, LP x10, D2. Right handside: Microfissures filled by sulfate minerals(barite and anhydrite, yellow arrows). OMJ41, 3421.00 m, LPx40, D2.

3.2. Authigenic kaolin and illitic minerals during burial diagenesis of sandstone

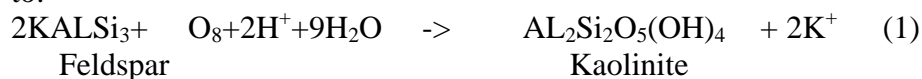
The occurrence of different kaolin polytypes (kaolinite and dickite), and the morphological and structural modifications of kaolin and illitic minerals, as function of the temperature and the burial depth, have been reported by Lanson, et al. 2002, and Beaufort, et al. 1998.

3.3. Kaolin in sandstones diagenesis

Descriptions of kaolinite and dickite structures can be found in Bailey (1980), Booking et al., (1989), and Drits and Tchoubar (1990), as recommended by Guggenheim et al., (1997). Recent works (Burley & MacQuaker, 1992; Ehrenberg et al., 1993; McAulay et al., 1993; Osborne et al., 1994; Lanson et al., 1995, 1996; Beaufort et al., 1998) indicate that the presence of both kaolinite and dickite in sandstones results from diagenetic evolution, the two polytypes coexisting over a depth interval until the onset of illitization.

In sandstones, three major types of diagenetic kaolin are recognized: kaolin replacing detrital mica, vermiform kaolin and blocky kaolin (Fig. 44-45).

Crystallization at the expense of detrital mica is obvious for the first kaolin type, due to petrographic relations between “expanded” mica flakes and authigenic kaolin growing in between (Nedkvitne & Bjorlykke, 1992; Ehrenberg et al., 1993; Macaulay et al., 1993; Osborne et al., 1994). In contrast, the crystallization conditions of the latter two morphological types are controversial. Two hypotheses have been suggested for the composition of fluids responsible for massive kaolin crystallization at the expense of both plagioclases and k-feldspars. According to the first hypothesis, kaolin crystallization is promoted at shallow burial depth by fluids of meteoric origin (Hancock, 1978; Hancock & Taylor, 1978; Sommer, 1978) that flush the formation either during early diagenesis or after structural inversion. As a consequence of feldspar dissolution, kaolin precipitates according to:



According to the second hypothesis, CO₂-rich or organic acid-rich fluids may be, together with meteoric fluids, responsible for feldspar alteration and subsequent precipitation of kaolinite according to reaction (1) (Rossel, 1982; Blackbourn, 1984; Goodchild & Whitaker, 1986; Pey & Krinsley, 1986; Ehrenberg, 1991; Gaupp et al., 1993; Platt, 1993). These fluids result from maturation of organic matter in shales and coal beds adjacent to sandstones.

3.4. Differential illitization of kaolin polytypes in sandstones:

Most studies of diagenetic sequences in sandstones point to the precipitation of illite during deep burial diagenesis (Fig. 46). In the North Sea area, illite generally forms at depths >3500 m at a temperature >120°C. Illite forms at the expense of kaolin (Ehrenberg & Nadeau, 1989; Bjorlykke & Aagaard, 1992; Bjorlykke et al., 1992). The relationship between illite and kaolin polytypes, however, is still ambiguous. It is usually admitted that this assumption is used to claim that blocky kaolin corresponds to a late diagenetic stage, which postdates the illitization event (Hurst & Irwin, 1982; Thomas, 1986; Lee et al., 1989; Giles et al., 1992; Haszeldine et al., 1992).

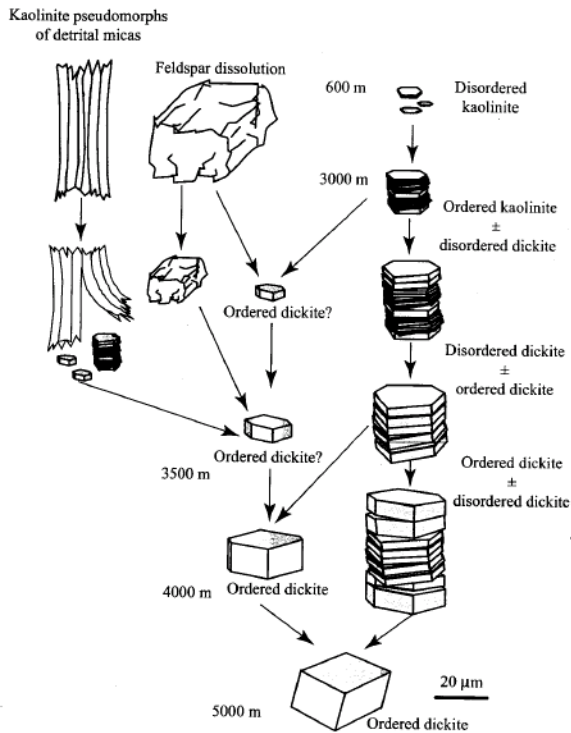


Figure 44 - Idealized scheme of the kaolinite to dickite conversion involving both morphological and structural changes as a result of interaction in sandstone reservoirs (modified from Beaufort et al., 1998., Cassagnabere, 1998).

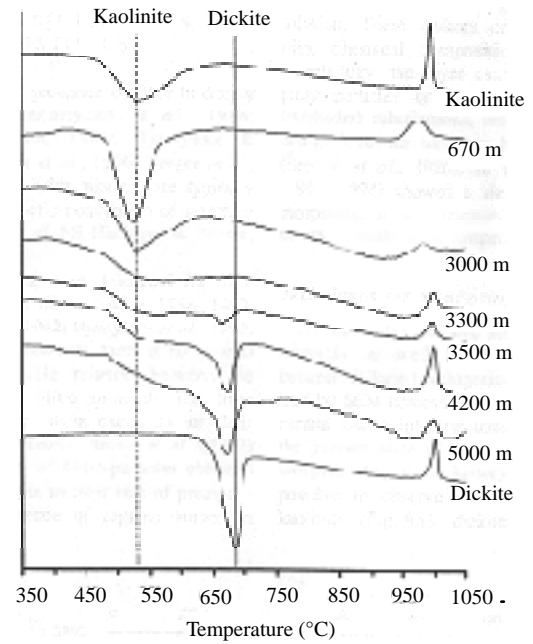


Figure 45 –DAT curves of kaolin group minerals as a function of their maximum burial depth (modified from Beaufort et al 1998.)

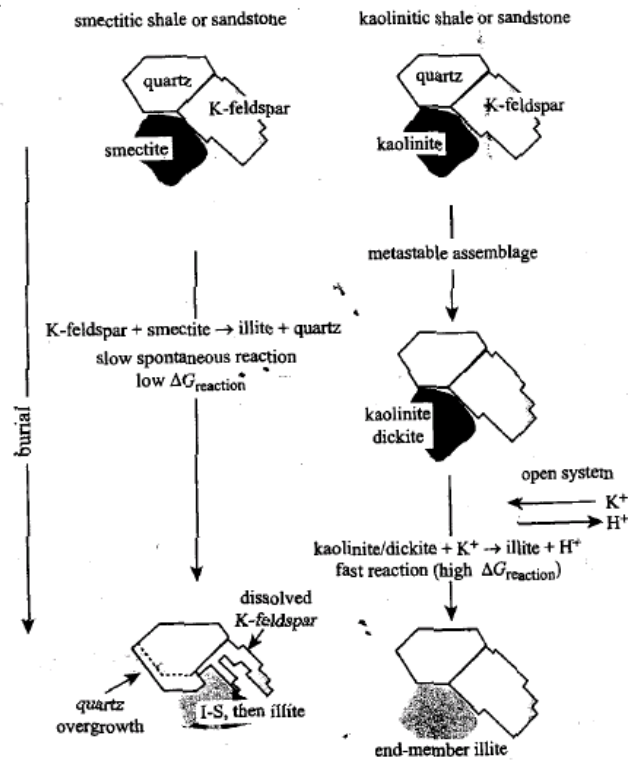


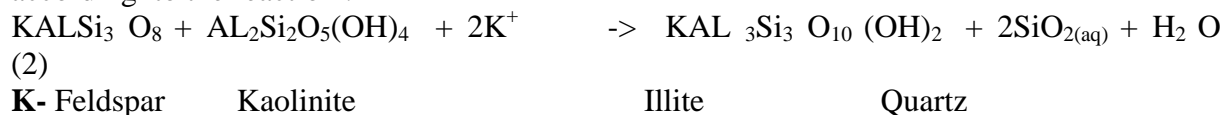
Figure 46 - Idealized schemes of the illitization process in sandstones as a function of the initial clay mineralogy (modified from Berger et al., 1997).

According to Beaufort et al., (1998) in the North Sea sandstones, illite replaces vermicular kaolinite at burial depths of ~3000m. The remaining kaolinite crystals show evidence of dissolution. From 3000-3500m, illitization develops at the expense of kaolin crystals consisting of blocky dickite crystals intercalated within vermicular stacks of kaolinite. Dickite crystals, however show evidence of small-scale dissolution and associated incipient illitization. At greater burial depth (~5000m), individual blocky crystals of dickite, which persist in the coarse-grained illite matrix, often show evidence of partial dissolution.

According to Lanson et al., 1996, this suggests that kaolinite dissolves faster than dickite during illitization.

Because dickite is thermodynamically more stable than kaolinite in the temperature range of burial diagenesis (Zotov et al., 1998), the chemical force which drives kaolin illitization is greater for kaolinite than for dickite. Therefore, kaolinite reacts at a higher rate than dickite at the same temperature and fluid composition.

According to Bjorlykke(1984), Bjokum & Gjelsvic(1988), Ehrenberg & Nadeau (1989), and Bjorlykke & Aagaard, 1992, this temperature threshold corresponds to the thermodynamical destabilization temperature of the kaolin +K- feldspar (+quartz) assemblage (Fig. 46) according to the reaction :



Kaolinite to dickite conversion is slower than dickite formation from K-feldspar decay (Beaufort et al., 1998).

3.5. The HMD diagenetic sequence reconstitution (Fig. 47A)

In sandstones, the occurrence, evolution and structure of clay minerals reflect the diagenetic history. The two groups of clay minerals most often encountered are kaolin and illitic minerals.

The observations described above, allow us to define the chronological successions of the diagenetic events as a function of the temperature and burial depth: (Fig. 47A) shows the diagenetic pathways which have been herein reconstructed.

The compositionally immature sandstones are stable and do not suffer any alteration down to a burial depth of 600 m at temperatures of around 100°C. Below this level, the first kaolinite appears. Feldspar is dissolved. This process promotes dickite formation. At greater depths, kaolinite is converted to dickite and kaolinite is illitized. At a burial depth of around 3500 m and temperatures of 700°C, dickite and illite coexist. At greater burial depths, dickite becomes illitized. Quartz cementation begins soon after deposition, following some minor compaction in sandstones at present-day temperatures less than 100°C. Quartz cementation continues during the sediment compaction and coexists with all diagenetic events.

Figures. 47B to 47F; reported on the diagenetic sequence correspond to the examples of the described diagenetic phenomena from the Hassi Messaoud study samples.

The importance of the varying diagenetic histories is that the major differences in initial composition and diagenesis are finally reflected in pore geometry, which controls reservoir properties, as we can further see.

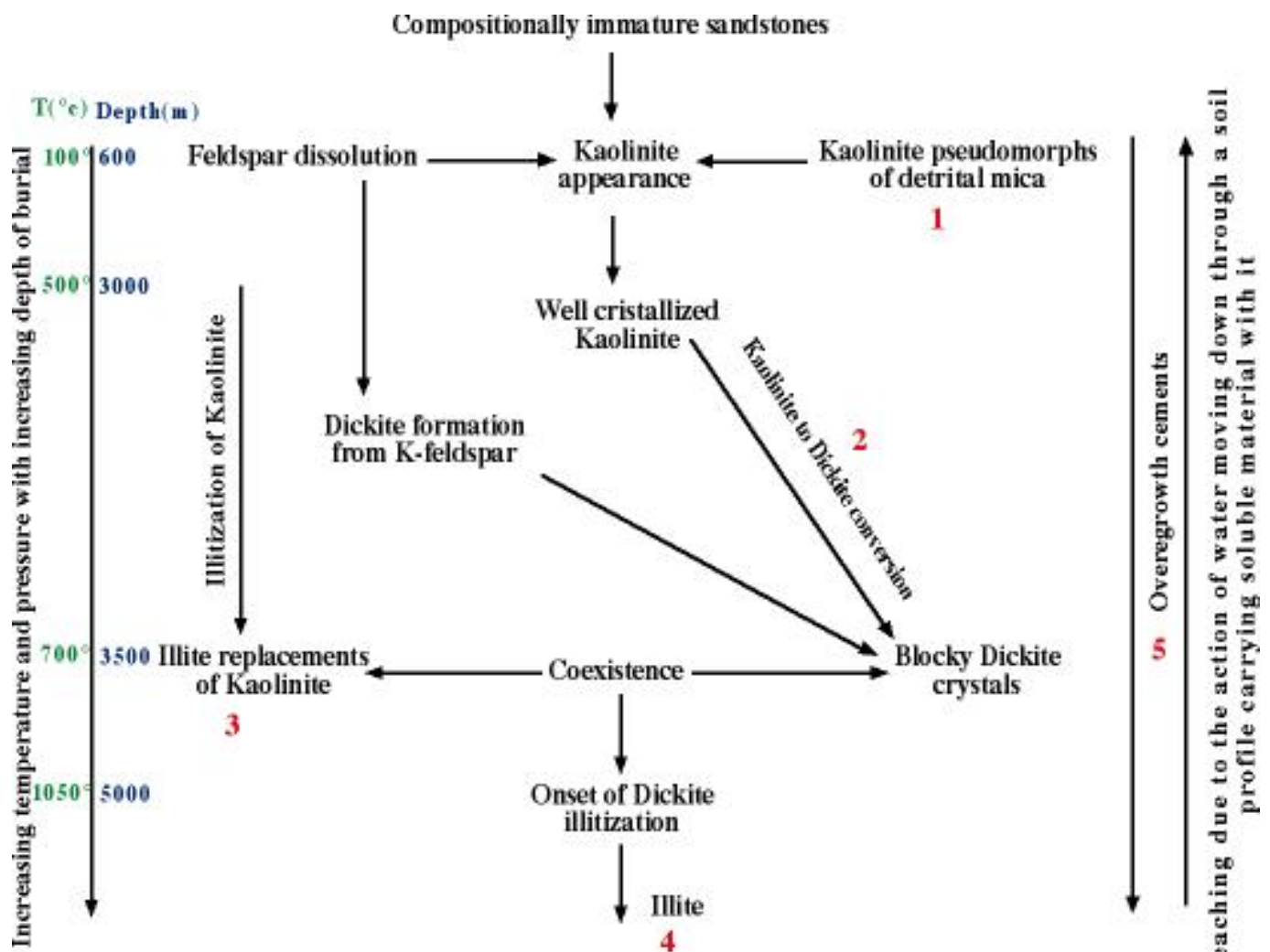


Figure 47A - Idealized scheme of the chronological diagenetic events in sandstone reservoirs as function of temperature, pressure and burial depths. The compositionally immature sandstones are stable and do not suffer any alteration down to a burial depth of 600 m at temperatures of around 100°. Below this level, the first kaolinite appears. Feldspar is dissolved. This process promotes dickite formation. At greater depths, kaolinite is converted to dickite and kaolinite is illitized. At a burial depth of around 3500 m and temperatures of 700°, dickite and illite coexist. At greater burial depths, dickite becomes illitized. The numbers (red colour) point to the photographs of different diagenetic transformations in the sandstone reservoir Ra of Hassi Messaoud (Figs. 47B -F). The maximum burial depth and temperature corresponding to the different diagenetic phenomena are obtained from Beaufort et al. (1998), Lanson et al.(2002) studies.

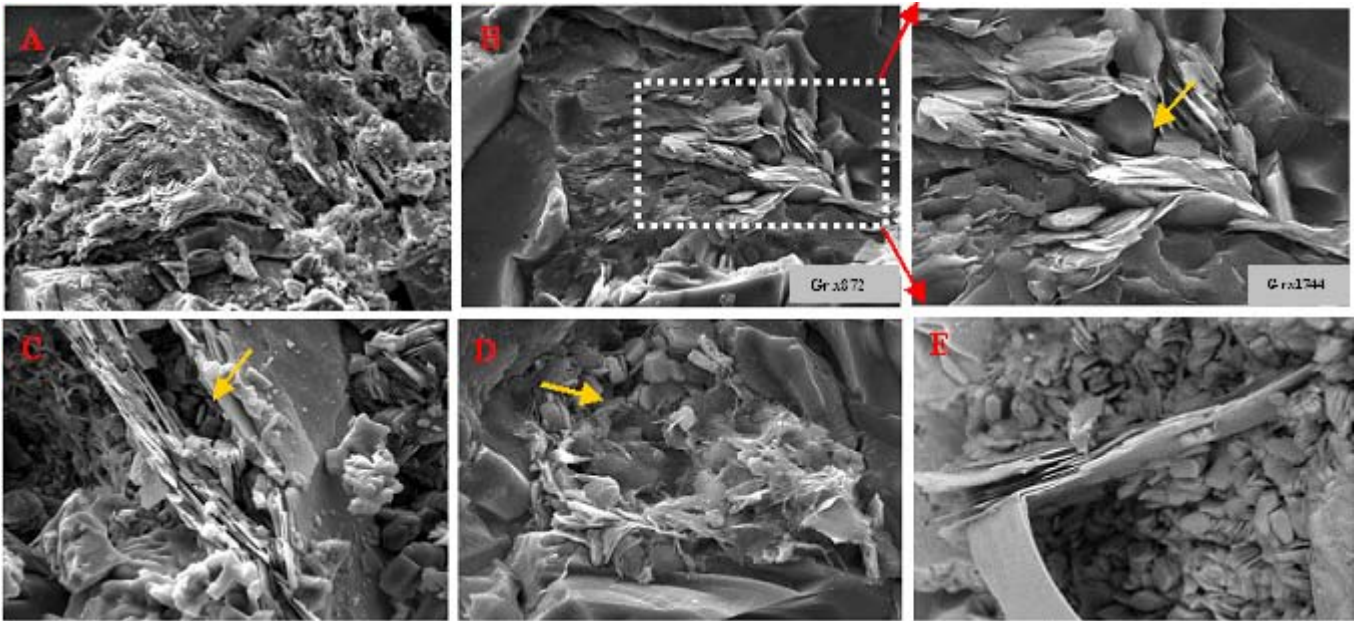


Figure 47B – 1: SEM micrographs of: (A) Incipient kaolinitization of mica. OMJ-812, 3343 m Gr x 494, D2. (B) and (C): kaolinite forming from detrital mica. Note formation of vermiform grains. OMJ-812, 3351.50 m, D2, Gr x 826 and OMJ-812, 3343.00 m, Gr x 826, D2. (D) and (E): Advanced stage of kaolinitization. Authigenic kaolinite forms from mica. OMJ-812, 3343.00 m, Gr x 1431, D2 and OMK-142, 3380.50 m, Gr.x625, ID.

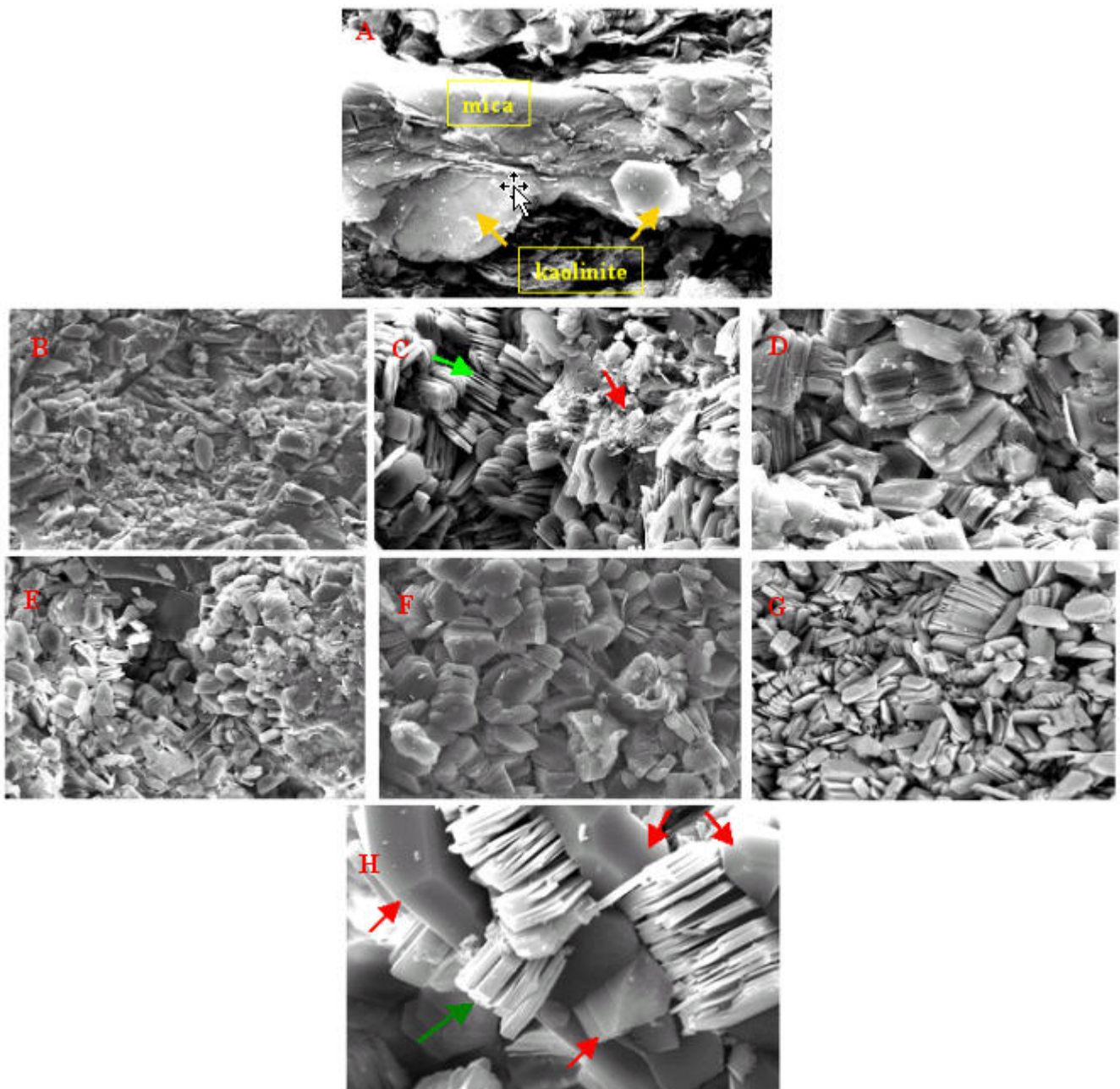


Figure 47C – 2: SEM micrographs of the evolution of the habit of kaolin as function of burial depth.

(A) Kaolinite occurs as replacement of mica in an advanced state. OMJ41, 3424.00 m, Gr.x1804, D2.

(B) Mixture of authigenic vermicular crystals and of anhedral crystals. OMJ812, 3369.00 m, Gr.x608, ID.

(C) Vermiform kaolinite green arrows and kaolinite partially dissolved (red arrows). OMK25, 3380.00 m, Gr x 1066, D1.

(E) Intercalation of blocky crystals between stacks of partially dissolved pseudo-hexagonal plates. OMK142, 3380.50 m, Gr.x1321, ID.

(F) and (G) Ordered dickite. OMJ812, 3400.50 m, Gr.x1280, D1, and OMK142, 3407.00 m, Gr.x630, D1.

(H) Blocky dickite (green arrows) whose spatial organization inherited from preexisting booklets. Cogenetic dickite and quartz crystals (red arrows showing mutual stopping of growth faces). OMJ223, 3443.00 m, Gr.x2571, D4.

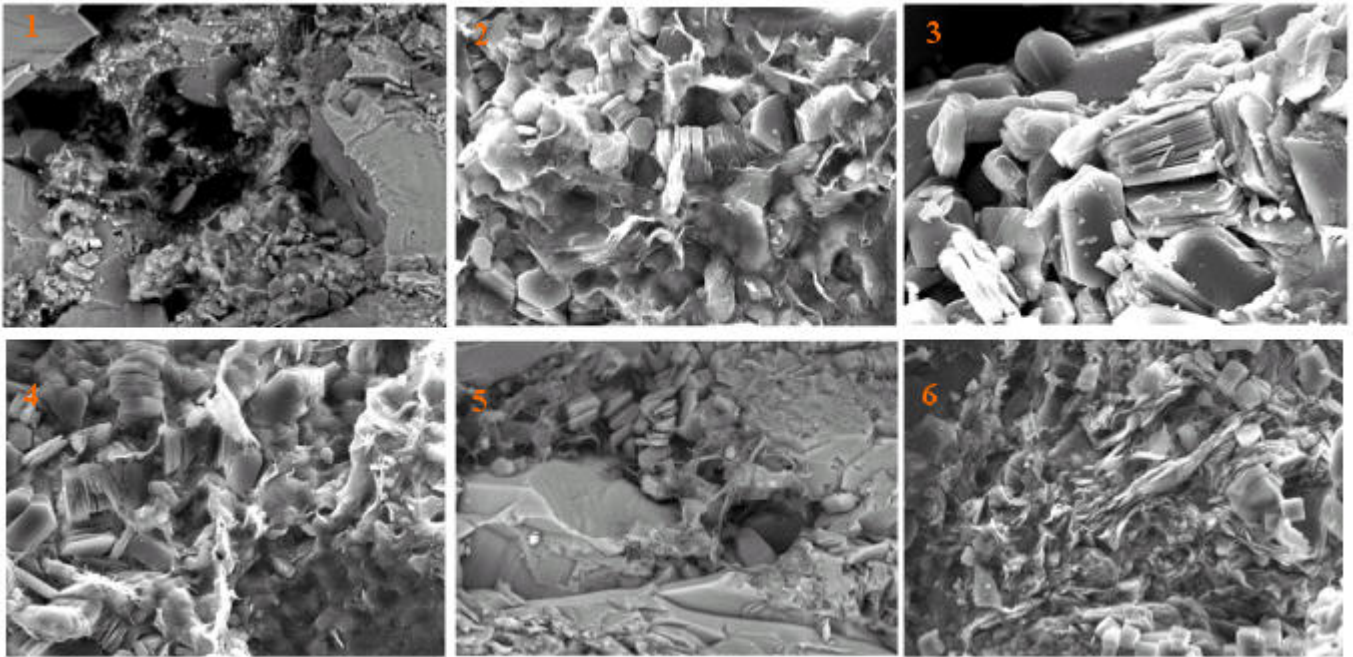


Figure 47D- 3: SEM micrographs showing the impact of illitization of the different habits of kaolin minerals.
(1) Illite replacing vermicular kaolinite. OMJ-41, 3457.75 m, Grx357, ID.
(2) Kaolinite crystals showing evidence of dissolution. OMJ-223, 3443.00 m, Gr.x1322, D4.
(3) and (4) Illite growing at the expense of blocky dickite crystals intercalated within vermicular stacks of kaolinite. OMJ223, 3461.50 m, Gr.1281, D4, and OMJ223, 3461.50 m, Gr.x1216, D4.
(6) Incipient illitization of blocky dickite crystals. OMJ812, 3381.00 m, Gr.x682, ID.
(5) Blocky dickite in a coarse grained illitic matrix. OMJ812, 3400.50 m, Gr.x640, D1.

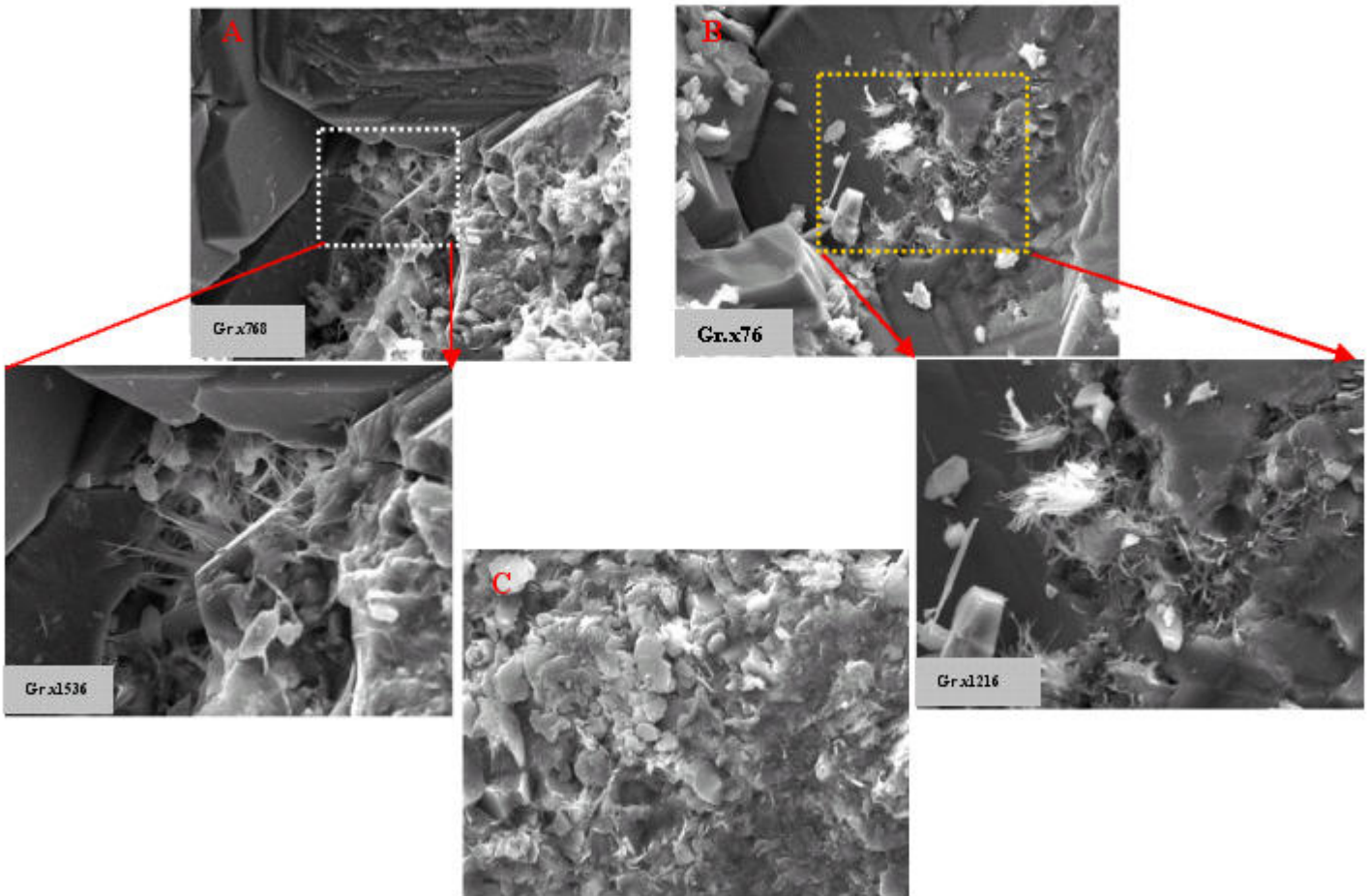


Figure 47E – 4: SEM micrographs of the evolution of illitic mineral habit as a function of burial depth.
(A) Lath-shaped illitic minerals. OMJ223, 3461.50 m, D4.
(B) Elongated, filamentous, almost one dimensional illitic crystals. OMK142, 3401.00 m, D2.
(C) Isometric pseudo-hexagonal-shaped illitic crystals probably inherited from partially dissolved kaolinite in an advanced stage of illitization of the kaolinite. OMJ41, 3424.00 m, Gr.x1381, D3.

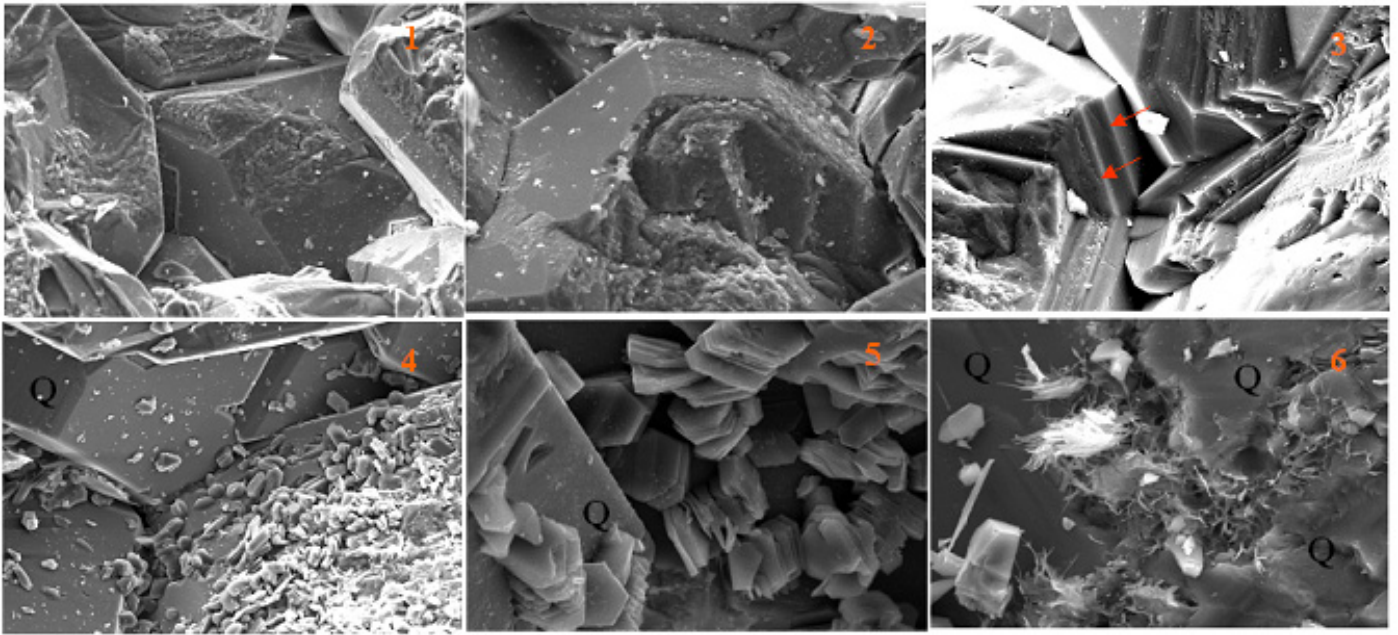


Figure 47F- 5: SEM micrographs of:

- (1) quartz overgrowths. OMJ812, 3354.00 m, Gr.x320, D2.
- (2) and (3) quartz overgrowths to show two generation of secondary silica (red arrows). OMJ812, 3369.00 m, Gr.x1051, ID and OMK25, 3380.00 m, Gr x 900, ID.
- (4) simultaneous growth of kaolinite books and quartz inducing intergrowth features OMJ223, 3443.00 m, Gr.x330, D4.
- (5) cogenetic? Dickite and quartz crystals showing mutual stopping of growth faces. OMJ812, 3351.50 m, Gr.x1349, D2.
- (6) apparent simultaneous growth of illite and quartz. OMK142, 3401.00 m, Gr.x1216, D1.

4. Pore Types

Hassi Messaoud samples contain a variety of pore types with a variety of origins, because petrophysical properties are controlled by the geometry and size of pores, rather than by their origin (primary versus secondary). Pore types are defined by geometry and size. Macropores are readily visible in core and thin section. Macropore types include intercrystalline, interparticle and moldic.

Micropores occur between clay particles and within altered rock fragments. Micropores are characterized by very narrow pore throats, leading to low permeability. Consequently, micropores contribute little to hydrocarbon production.

Intercrystalline macropores

Intercrystalline macropores are interparticle macropores that have been modified by the formation of quartz overgrowth cements. Because of these modifications, petrophysical properties of intercrystalline-dominated rocks differ significantly from those of interparticle – dominated rocks. Intercrystalline pores and their throats are bound by crystal faces of euhedral quartz overgrowths, which are extremely smooth and planar. These pores are locally well interconnected (Fig. 48).

Interparticle macropores

Because of the significant diagenetic overprint in the HMD Field, this is a minor pore type in most samples. Quartz overgrowths either occlude all interparticle macroporosity, or modify interparticle pores into intercrystalline macropores. Interparticle macropores only occur where clay rims or cements inhibited formation of quartz cements. If too much clay precipitates, interparticle macroporosity is filled by the microporous clay cement. Interparticle macropore walls are moderately rough, and pore throats are typically narrowed by clay rims and cements (Fig. 49).

Moldic macropores

Moldic macropores are large pores that formed by the complete dissolution of chemically unstable framework grains. The abundance and distribution of these pores are controlled by the initial abundance and distribution of unstable grains and the extent and character of leaching (Fig. 50). Bridged moldic macropores result where clay cements or residual material subdivides moldic macropores.

Interparticle micropores and Intercrystalline micropores

Interparticle micropores are small, very fine pores that occur between illitic clay particles (Fig51). Intercrystalline micropores are common to abundant between and within dickite booklets, and kaolinite particles (Fig. 52).

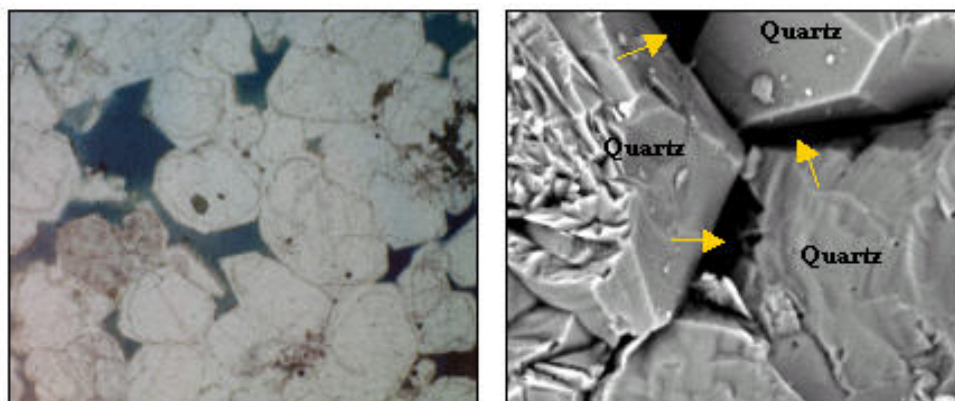


Figure 48 - Intercrystalline macropores represent interparticle macropores modified by quartz cementation. The pore walls are extremely smooth crystal faces, and throats are relatively large. Left handside: Micrograph of OMJ812, 3369 m, LN \times 40, ID. Right handside SEM micrograph of OMJ812, 3410 m, Gr \times 689, D1.

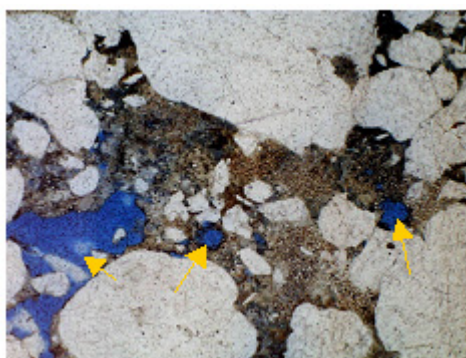


Figure 49 - Interparticle macropores (yellow arrows) are restricted to domains where clay rims or cements inhibited quartz cements. Pore walls are typically moderately rough and pore throats are reduced in size by clay rims and/or cements. OMJ822, 3380.50 m, LN \times 4, ID.

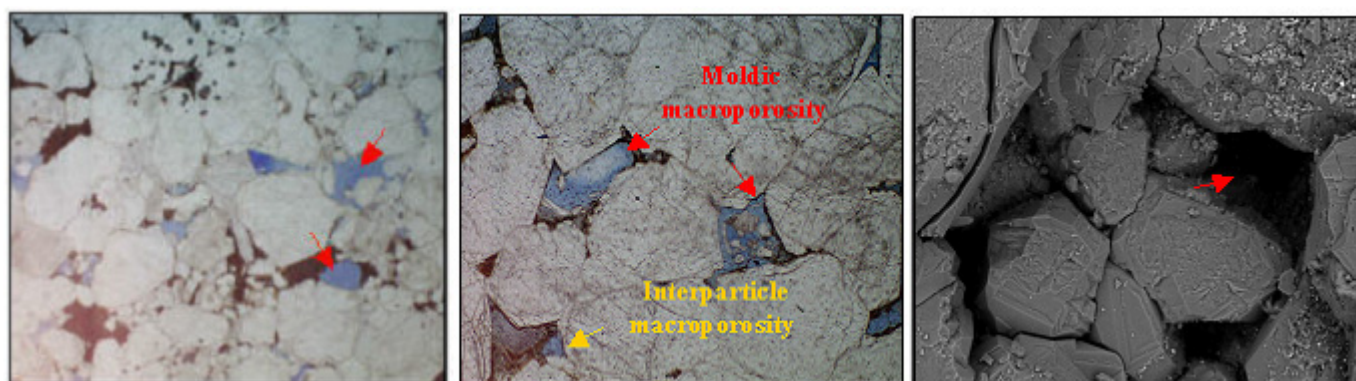


Figure 50 - Moldic pores are formed by the complete dissolution of chemically unstable framework grains (red arrows). Pore walls are typically very rough. Although pore bodies are large, pore throats are small and interconnectivity is poor. This pore type is common in compositionally immature sandstones. Right handside: OMJ822, 3424.50 m, LN \times 4, D1. Center: OMJ812, 3359 m, LN \times 2, ID. Left handside: SEM micrograph OMK142, 3407 m, Gr \times 165, D1.

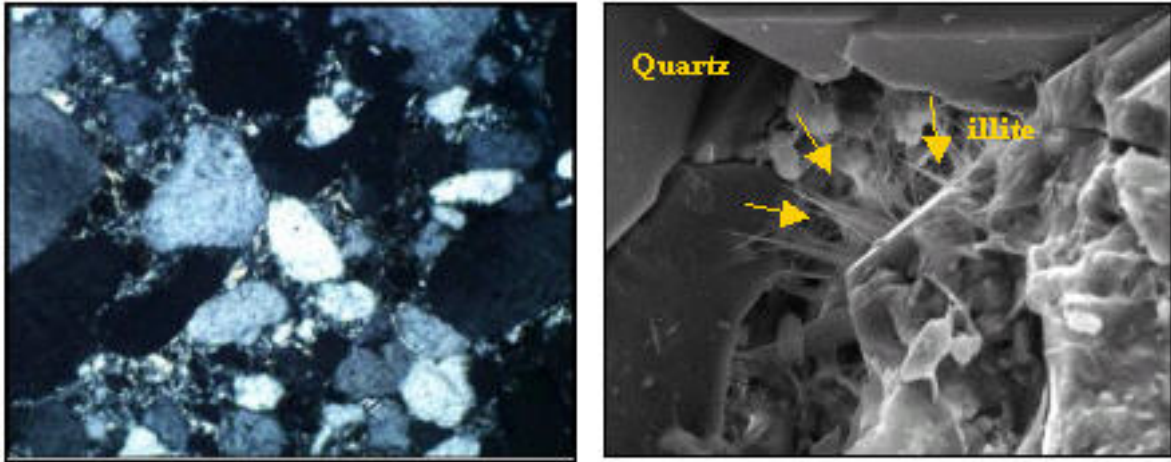


Figure 51 - Interparticle micropores within an illitized cement. Although porosity (yellow arrows) is high, surface is extreme and pore throats are very small, resulting in low permeability. Left handside: OMK25, 3342.5 m, LPx10,D2. Right handside: SEM micrograph OMK25, 3344 m, Gr x 988,D2.

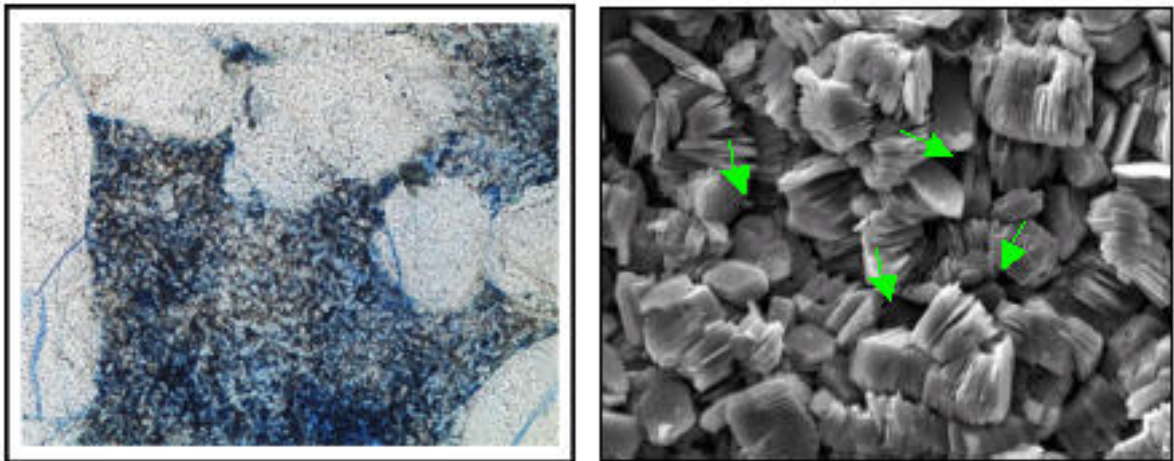


Figure 52 -Left handside: Intercrystalline microporosity is common between kaolinite and Dickite particles OMN56, 3399 m, LN x200, D1. Right handside: SEM micrograph of Kaolinite-dickite and intercrystalline micropores (green arrows) OMJ812, 3343 m, Gr x 988, D2.

5. Rock Types

The rock types are fundamental building blocks of the reservoir. Herein, a rock type is defined by its lithologic character (composition, texture, and diagenesis) and pore space properties (pore abundance, type, size and geometry). Four major rock types have been identified in the thin-sections examined from Ra zones:

Rock Type D: Dickite –rich microporous sandstones;

Rock Type M: Moldic macroporous quartzose sandstone;

Rock Type I: Intercrystalline macroporous quartz sandstone;

Rock Type B: Bioturbated sandstone.

The rocks were characterized according to the dominant characteristics.

5.1. Rock Type D

This rock type consisted of moderately sorted quartzose sandstone with common to abundant dickite cement and grain replacements (Fig. 53). Quartz cement is common, and rock may locally contain minor illite cement or grain replacements. Pore types include abundant intercrystalline microporosity associated with dickite and minor interparticle microporosity associated with illite cements and grain replacements. Helium porosity in the rock type typically ranges from 7 to 15 percent, and air permeability typically ranges from 1 to 100 mD. The relationship between porosity and permeability has a gentle slope.

5.2. Rock Type I

Rock Type I is dominated by well-sorted monocrystalline quartz grains cemented by syntaxial quartz cement (depositional quartz arenite) (Fig. 54). This rock type is extremely quartzose. Pore geometry consists of well-interconnected intercrystalline macropores. Traces of dickite cement with associated intercrystalline microporosity occur in some samples. Coarse-grained samples commonly contain trace amounts of illite. Porosity is somewhat limited by quartz cement, but permeability is excellent due to well-interconnected intercrystalline macropores. Helium porosity in the Rock Type I typically ranges from 7 to 14 percent, and permeability typically ranges from 1 to 1000 mD. Porosity is somewhat limited by quartz cement, but permeability is excellent due to well-interconnected intercrystalline macropores. The relationship between porosity and permeability has a steep slope.

5.3. Rock Type B

Rock Type B consists of well-sorted quartzose bioturbated sandstone. Quartz cement completely occludes all porosities, whereas in clay-bearing domains, quartz cement growth was inhibited and minor interparticle microporosity and trace interparticle macroporosity are preserved. Consequently, reservoir quality is poor (Fig. 55). Variations in reservoir quality in this kind of rocks are controlled by the distribution and abundance of clay which inhibited quartz cementation. Clay abundance and distribution were controlled by depositional processes and by bioturbation. Helium porosity typically ranges from 1 to 5 percent, and permeability from 0.01 to 0.1 mD. This rock has very poor reservoir properties.

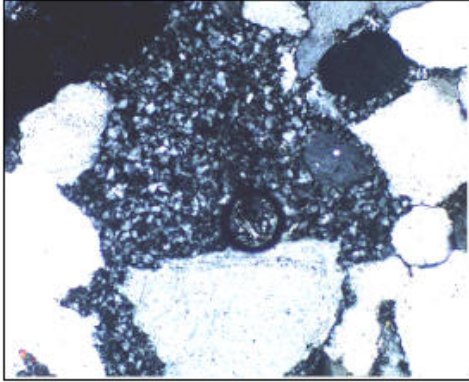
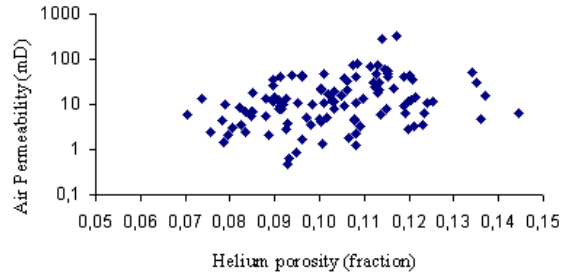


Figure 53 - Rock Type D: Dickite- rich microporous sandstone. OMJ822, 3396,50 m, LPX10, ID.



Porosity – permeability cross plot. Example of OMJ 812 all zones.

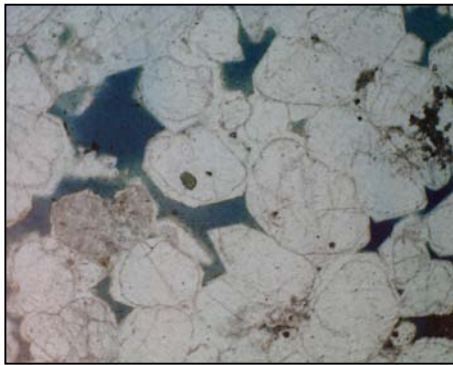
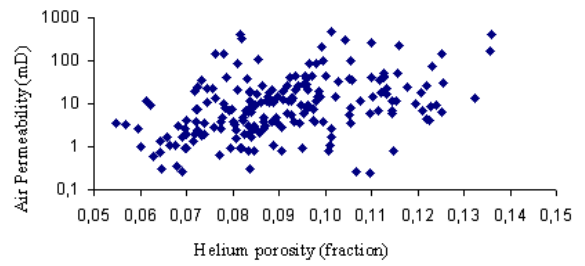


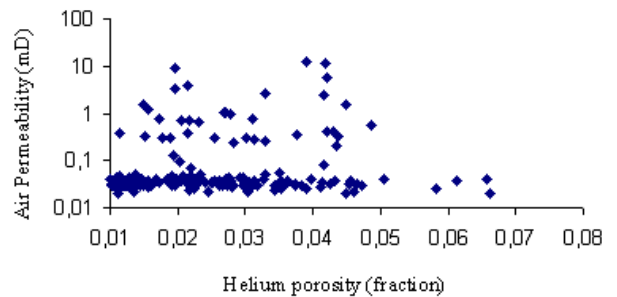
Figure 54 - Rock Type I: Inter-crystalline macroporous sandstone. OMJ812, 3369 m, LNx40, ID.



Porosity – permeability cross plot. Example of OMJ 812 all zones.



Figure 55- Rock Type B: Bioturbated sandstone. OMJ422, 3344.5 m, LNx100, D5.



Porosity – permeability cross plot. Example of OMJ223 zone D5.

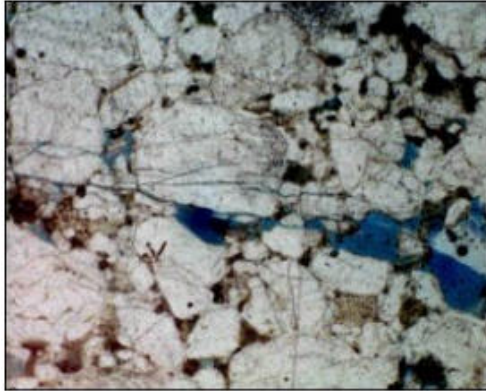
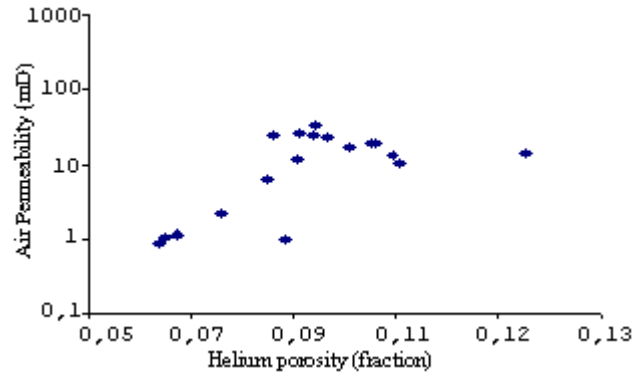


Figure 56 - Rock Type P: Pseudomatrix-rich sandstone. OMJ422, 3413.5 m, LN x100, D3.



Porosity – permeability cross plot.
Example of OMJ 812 zone D2.

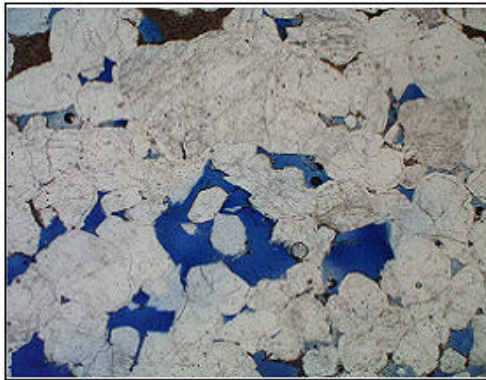
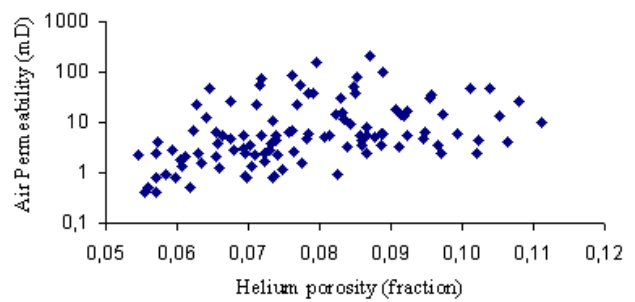
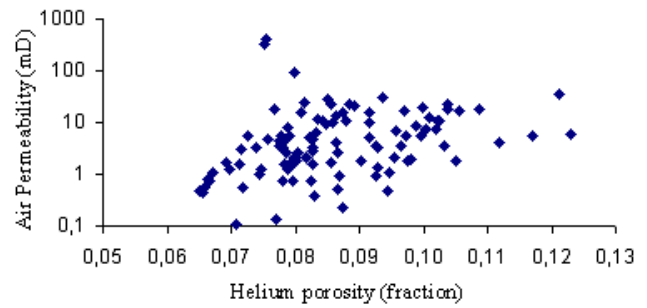


Figure 57 - Rock Type M: Moldic macroporous sandstone. OMN56, 3388.5 m, LN x20, D1.



Porosity – permeability cross plot.
Above: An example of OMJ 812 all zones.
Below: Another example of OMK 142 all zones.

5.4. Rock Type P: Pseudomatrix-rich sandstone

Rock Type P is characterized by compositionally and texturally immature sandstone composed of quartz grains, pseudomatrix (deformed rock fragments), and scattered moldic pores. Virtually all porosity is occluded by pseudomatrix and quartz cement. Because of the rarity of this rock type in the HMD samples (5 samples) examined, we described it briefly (Fig. 56). Helium porosity typically ranges from 7 to 11 percent, and permeability typically ranges from 1 to 10 mD. Porosity and permeability have an intermediate slope.

5.5. Rock Type M: Moldic macroporous quartzose sandstone

Rock Type M consists of a "diagenetic quartz arenite" dominated by quartz grains and moldic macropores formed by dissolution of unstable framework grains (Fig. 57). Quartz cement typically fills virtually all primary interparticle porosity. Quartz grains and cement make up about 80 percent of the rock framework. Rock fragments are dissolved or altered to illite. Pore types include a continuum between moldic macropores, bridged moldic pores (when there is a direct contact between the dissolved grains) and intraparticle micropores (illite cement). Helium porosity typically ranges from 7 to 12 percent, and permeability typically ranges from 1 to 10 mD. The relationship between porosity and permeability has a gentle slope.

6. Reservoir Quality and Heterogeneity

The distribution of the rock types is controlled by initial sediment composition and diagenetic overprint. The drains D1 to D5 are comprised mostly of medium to coarse sandstone. The interval studied records the complex interplay of depositional processes and sandstone composition in immature fluvial sandstones and more mature tidal sandstones. Coarser-grained sandstones are texturally and compositionally immature, and consist of rock types D and M. Finer-grained sandstones are more mature due to reworking in tidal environments and marine influences, where rock types I and B are most common. The interplay between fluvial and tidal influences resulted in significant variation in rock types.

Rock type I is interbedded and intermixed by burrowing with the rock type B (bioturbated sandstone) in zone D5. The intercrystalline macroporous sandstone rock type grades and interbeds with rock type D (dickite – rich sandstone) and rock type M (moldic macroporous quartzose sandstone) in zones D1 to D4. The upward transition from dickite rich sandstone and moldic macroporous sandstones to intercrystalline macroporous quartz sandstone reflects the progressive change in initial sediment composition from more litho-feldspathic sandstones (the precursor to dickite-rich and moldic macroporous sandstones) to quartzose (precursor to intercrystalline macroporous sandstone). The Cambrian reservoir Ra of the northwestern part of Hassi Messaoud field displays highly variable reservoir quality: helium porosity ranges up to 15 percent, whereas air permeability ranges up to 1000 mD in places. The Ra reservoir porosity–permeability cross plot displays a strongly bifurcating pattern due to variability among rock types (Fig. 58). The low porosity- low permeability cloud of data represents Rock type B ($\Phi = 1\% - 5\%$, $K = 0.01 - 0.1 \text{ mD}$), the medium permeability- medium porosity cloud of data represents Rock types M ($\Phi = 7\% - 12\%$, $K = 1 - 10 \text{ mD}$) and P ($\Phi = 7\% - 11\%$, $K = 1 - 10 \text{ mD}$), whereas the high permeability – high porosity cloud of data represents Rock type D ($\Phi = 7\% - 15\%$, $K = 1 - 100 \text{ mD}$) and I ($\Phi = 7\% - 14\%$, $K = 1 - 1000 \text{ mD}$). To classify the major rock types of the reservoir Ra according to their reservoir qualities, it is very clear that rock type I has better reservoir properties than those of rock type D; rock type D is petrophysically

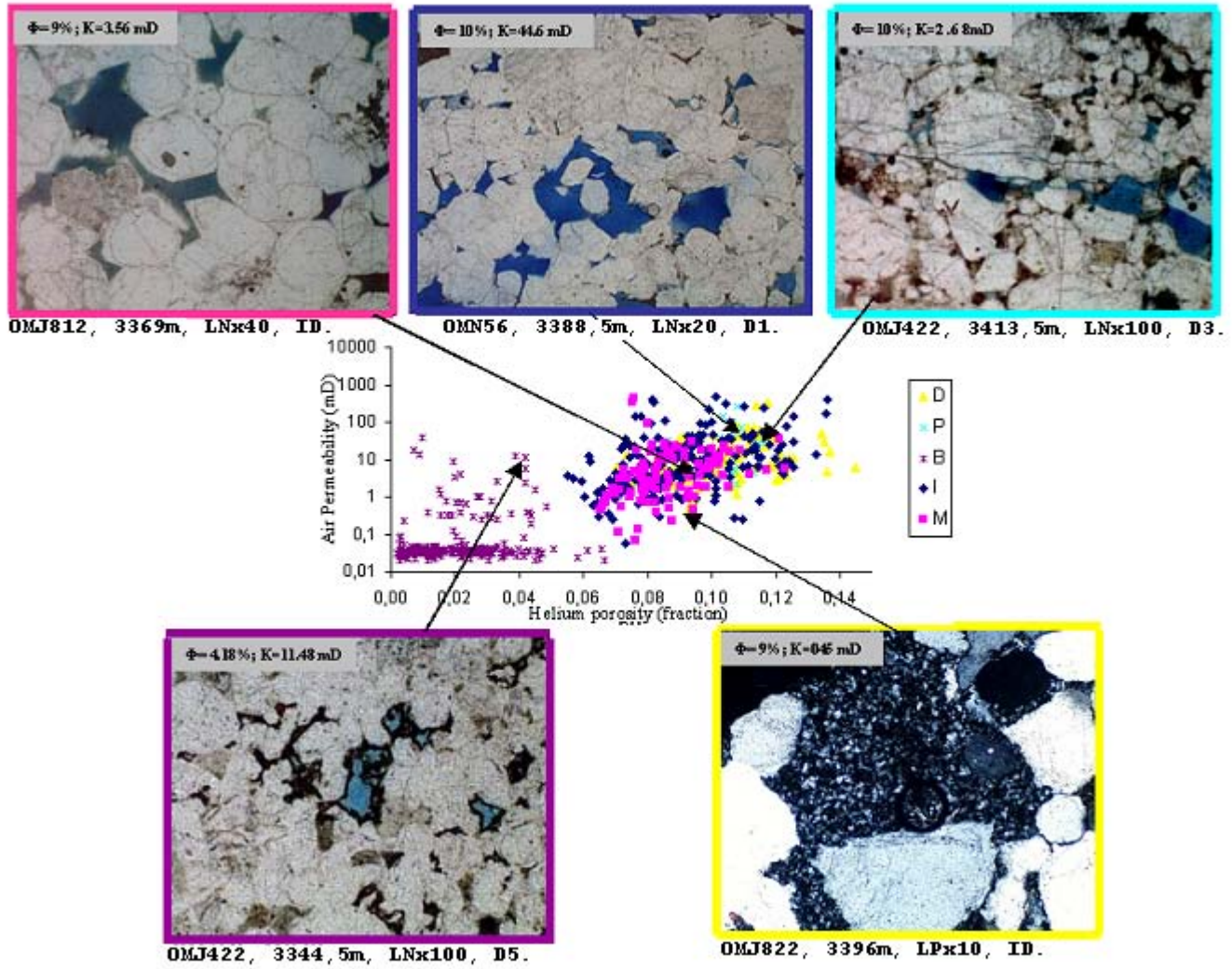


Figure 58 - Ra porosity –permeability plot of conventional core data of zones D1 to D5 from the five studied wells: OMK25, OMK142, OMJ812, OMJ41 and OMJ223, showing the relationship between both porosity and permeability and the texture of sandstone rocks. Color –coded by rock type .

more interesting than M. Rock type B presents the worst reservoir quality. The lower part of the reservoir (fluvial), where the rock types I and D dominate in the majority of the study wells, represents the best reservoir quality, compared to the upper part of the reservoir (tidal), where rock type M is generally mixed with rock types B and I (Fig. 59). Grain size, pores, cementation, microfissures and fractures have direct influences on reservoir characteristics: Coarse-grained little silicified sandstones, intercrystalline connected porosities, open microfissures and fractures present a positive influence on reservoir qualities (Fig. 60). In contrast, fine-grained highly-silicified sandstones, unconnected porosities, plugged microfissures and fractures by chert, sulphate, dolomite, barite or clay cement cause the deterioration of reservoir properties (Fig. 61).

7. Comparison among the wells

It is clear that the comparison between the wells may not be representative because of the long distance between the studied wells. The correlation, however, provides some information about the general lateral variation of the present reservoir composition and characteristics of the area of interest. The petrophysical properties of the reservoir Ra in all zones improve from the west towards east according to the rock type distribution (Fig. 62).

All cored zones in OMJ223 and OMJ 41 present low to medium quality of the reservoir.

OMJ 812, OMK142 and OMK 25 consist of the best quality of the reservoir represented by samples of D2, ID and D1. Vertically the lower part of the reservoir from D2 to D1 represents the best reservoir properties.

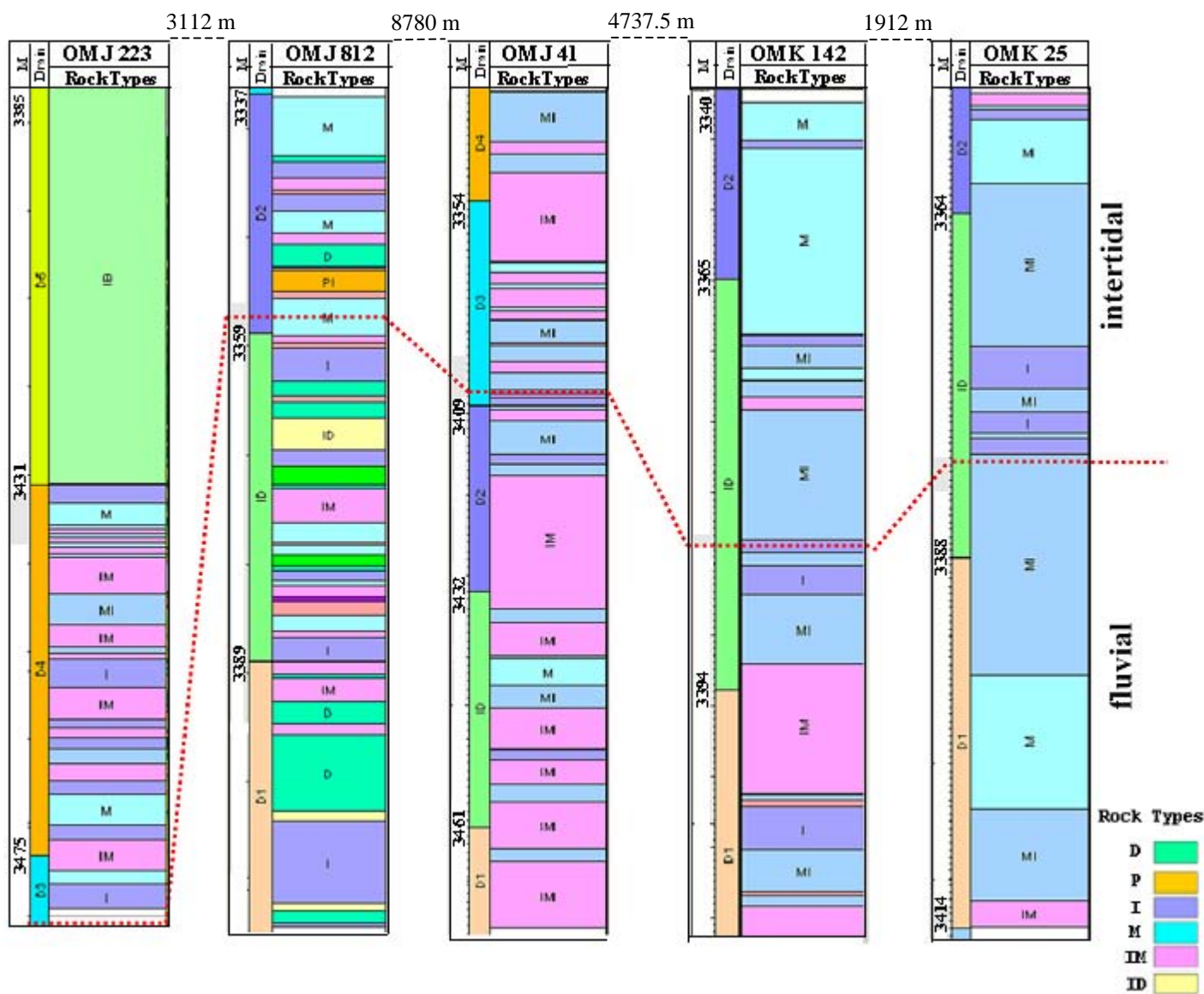
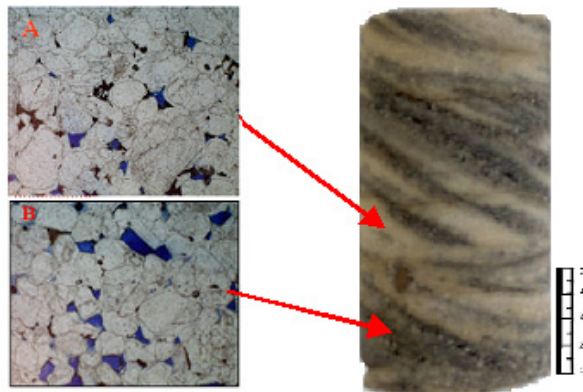
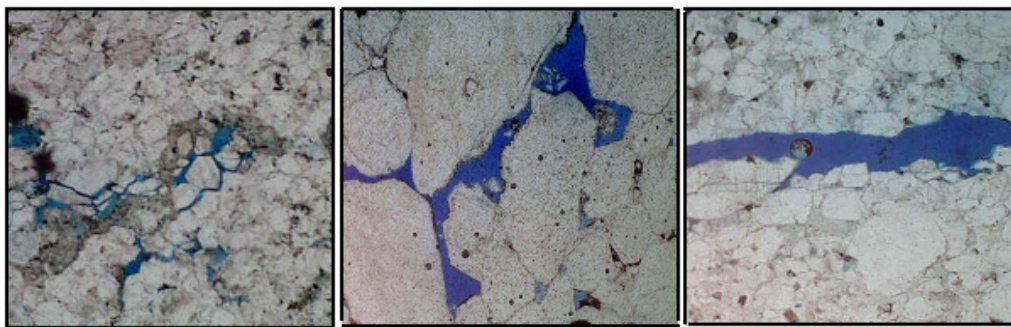


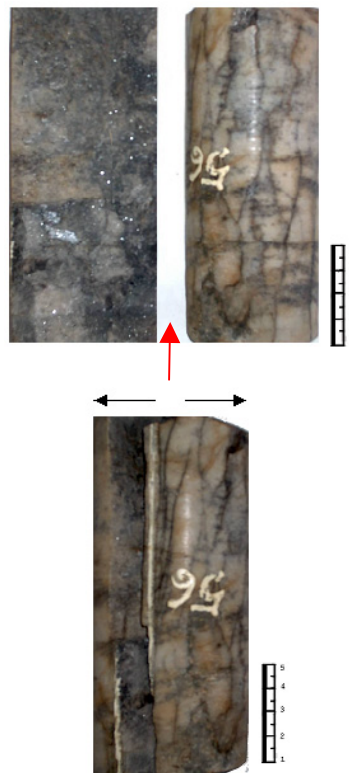
Figure 59 - Schematic stratigraphic columns of rock types in wells.
M: Moldic macroporous quartzose sandstone.
B: Bioturbated sandstone.
D: Dickite rich microporous sandstone.
I: Intercrystalline macroporous quartzose sandstone.
P: Pseudomatrix-rich sandstone.
IM: Intercrystalline and moldic with predominance of intercrystalline rock type.
MI: Intercrystalline and moldic with predominance of moldic rock type.
ID: Intercrystalline and Dickite-rich sandstone with predominance of intercrystalline rock type.
Red dotted line indicates the first apparition of Scolithos traces and it represents the supposed limit between fluvial and tidal environments in the area of interest.



Core photograph and thin –section photographs showing coarse grained highly silicified sandstone (A) and poorly silicified sandstone(B).



A porous rock is not necessarily permeable. These Photomicrographs showing the cases of the best reservoir rock types of the Hassi Messaoud Field: Left handside and center: connected intercrystalline macroporosity. Right handside: Open microfissure.

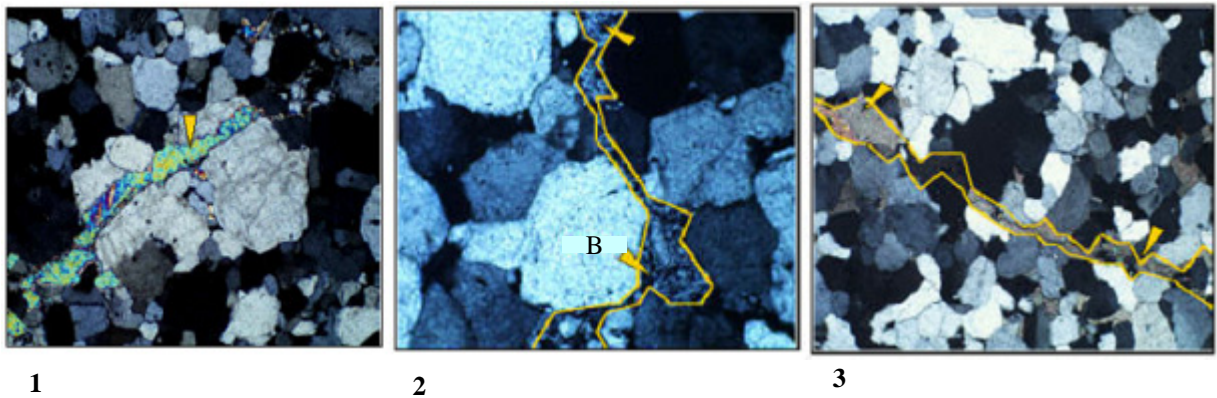


Example of open macrofracture.

Figure: 60



Fine grained, bioturbated, highly silicified sandstones with unconnected porosities



Microfissures and fractures plugged by chert, sulphate(1), barite (2), dolomite (3) or clay cement (4) cause the deterioration of reservoir properties.

Figure: 61

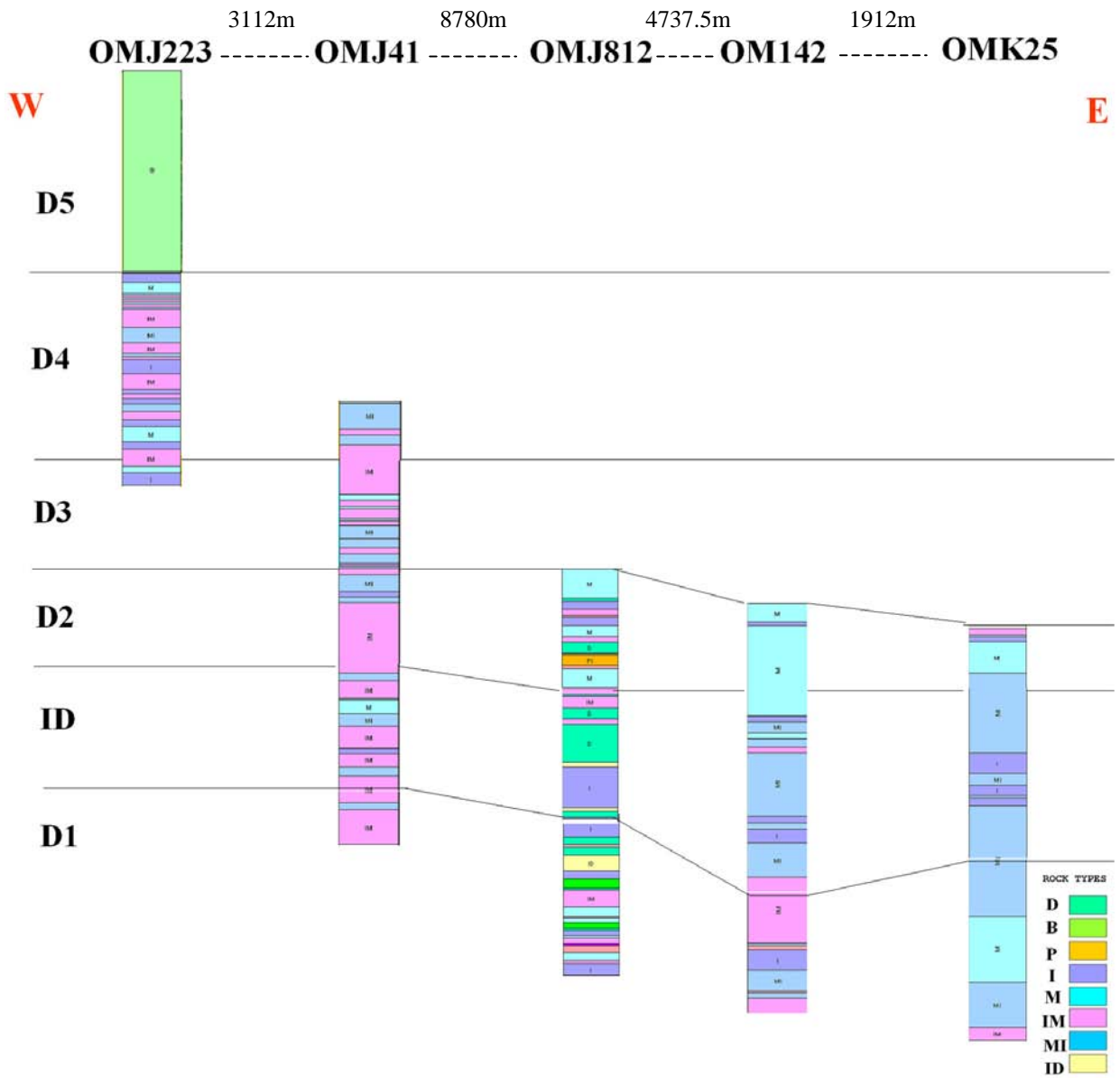


Figure 62 – Stratigraphic distribution scheme of major rock types by well and by drain. The layers represent heterogeneous samples composed of multiple rock types indicated by colors.

1. Concept of hydraulic units (HU)

Understanding complex variation in pore geometry within different lithofacies rock types is the key to improving reservoir description and exploitation. Core data provide information on various depositional and diagenetic controls on pore geometry.

Variation in pore geometrical attributes in turn defines the existence of distinct zones (hydraulic units) with similar fluid-flow characteristics. A hydraulic unit is defined as the representative volume of total reservoir rock within geological properties that control fluid flow; it is a reservoir zone that is laterally and vertically continuous and has similar flow and bedding characteristics. This chapter will focus on the evaluation of formation permeability for a sandstone reservoir in the northwestern part of HMD field.

2. Methodology

The concept of flow units has been the subject focus of many of studies and publications. The detailed method in SPE 30158 has been chosen for our study because it is actually the most usable by different petroleum companies. HU are obtained by combining Darcy's law for flow in tubes, a tortuosity factor and pore radius of Kozeny, (1927), and later Willie, and Gardner, (1956). The authors undertake technical methods which are detailed in SPE 30158 to define flow zone indicator (FZI), and reservoir quality index (RQI) as: $RQI = 0.0314 \frac{k}{\phi}$ and $RQI = \Phi_z FZI$.

The applicability of this permeability estimation technique has been proved in carbonate and sandstone reservoirs.

41 wells (Fig. 63) from the zone of interest have been the subject of permeability prediction by hydraulic flow units. The study wells are all cored and have conventionally petrophysical core data measured every 0.25 cm.

Both RQI and FZI have been calculated in the study zone by well and every 0.25cm. To be able to define the representative HU (flow units) of the study area, all FZI values calculated from all wells have been grouped and sorted increasingly to determine the ideal FZI range of each flow units (HU) which match properly with both permeability and porosity. Five flow units have been defined in the study area (see Tab. 1).

Flow Units	FZI Range
NRES Non Reservoir	0 – 0.4
HU2	0.6 – 2.8
HU3	2.8 – 5.8
HU4	5.8 – 12
HU5	>12

Tab. 1: Flow Units and their equivalent of FZI ranges of the Ra reservoir in the area of interest.

FZI Permeability matching plots, which were created using all available data in different zones of the Reservoir Ra (D5, D4, D3, D2, ID, D1), generally showed a good correlation coefficient of each flow unit by zone (Fig. 64). The composite logs confirm that the HU matched both porosity and permeability logs very well.

HU5 correspond to the higher permeability and porosity in reservoir sandstones Ra and NRES corresponds to silts or sandstone with poor petrophysical characteristics (Fig. 65-66).

3. Comparison between FZI and rock types

Rock types can be used to link depositional facies, diagenesis, reservoir properties and wireline log response. Hydraulic units are related to geological facies distributions but do not necessarily coincide with facies boundaries. Comparison between different rock types and defined flow units of the well OMJ 812 (which is composed by more efficient rock types variety) leads to confirm the previous results concerning the best rock type properties of the Ra reservoir.

Intercrystalline rock type represents higher petrophysical characteristics than rock type D. Rock type D has better reservoir properties than rock type M; all three rocks constitute the good quality of the reservoir Ra in the area of interest of Hassi Messaoud field (fig. 67).

4. Conclusion

The parameters that influence fluid flow are mainly pore throat geometrical attributes. The pore geometry is in turn controlled by mineralogy and texture. Various combinations of these geological properties can lead to distinct rock flow units that have similar fluid transport properties. Therefore, an HU can include several rock facies types, depending on their depositional texture and mineralogical content.

A new, practical and theoretically-based technique has been developed to identify and characterize units with similar pore throat geometrical attributes (hydraulic units).

This technique is applicable for both cored and uncored wells. It includes:

- Improved prediction of permeability and permeability distribution from cored intervals wells.
- Improved well-to-well rock properties correlations for refinement of petrophysical models.
- A unique parameter, the flow zone indicator (FZI) for delineating the number of layers (hydraulic units) required for assignment of geological and petrophysical parameters in reservoir modeling software.

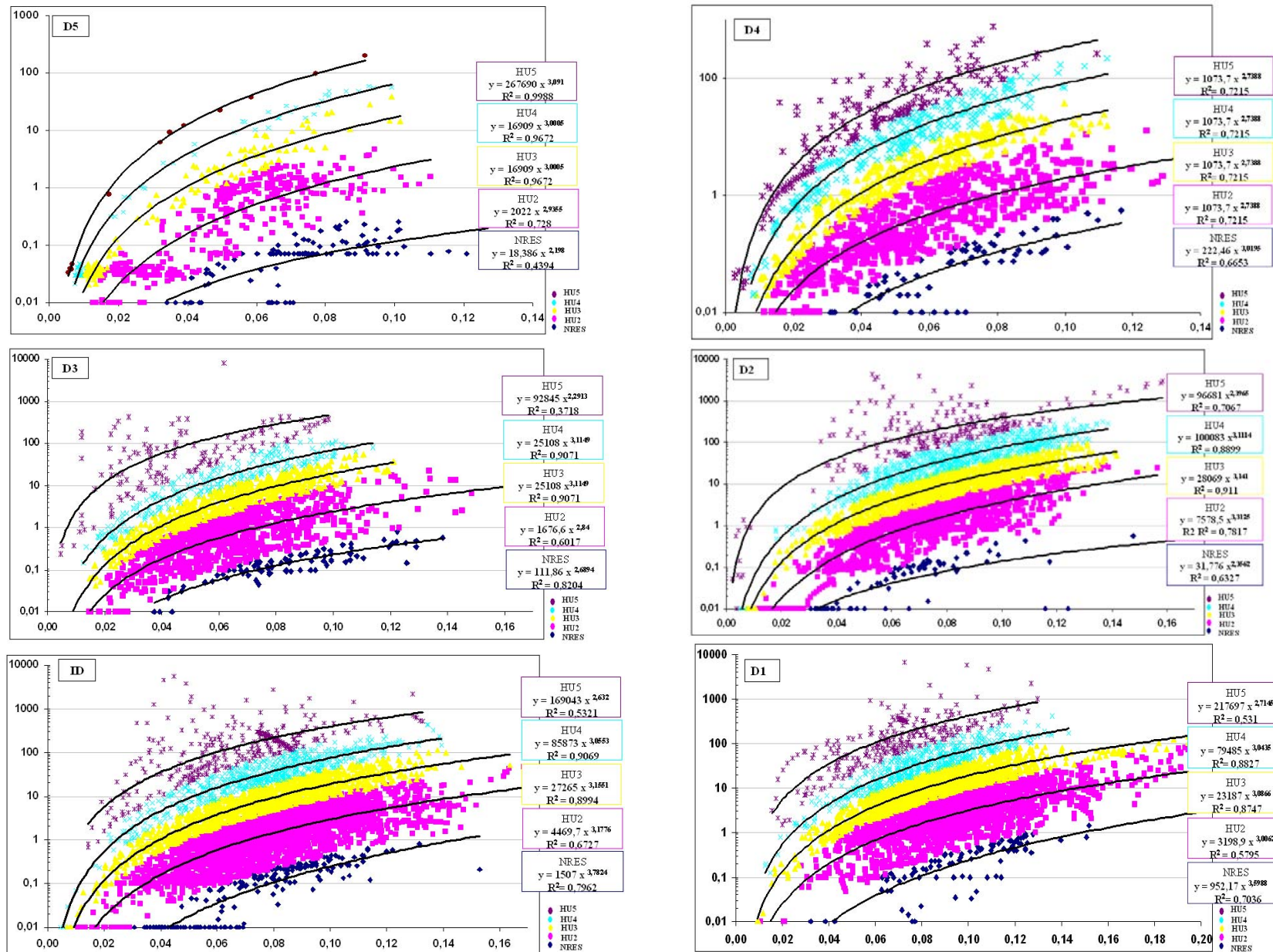


Figure 64 : FZI - Permeability matching from the core data of all study wells, by zone. The plots show different group of facies which correspond to flow units. The coefficients of correlations are generally high indicating a good relationship between both porosity and permeability of defined flow zones. Color-coded by flow unit.

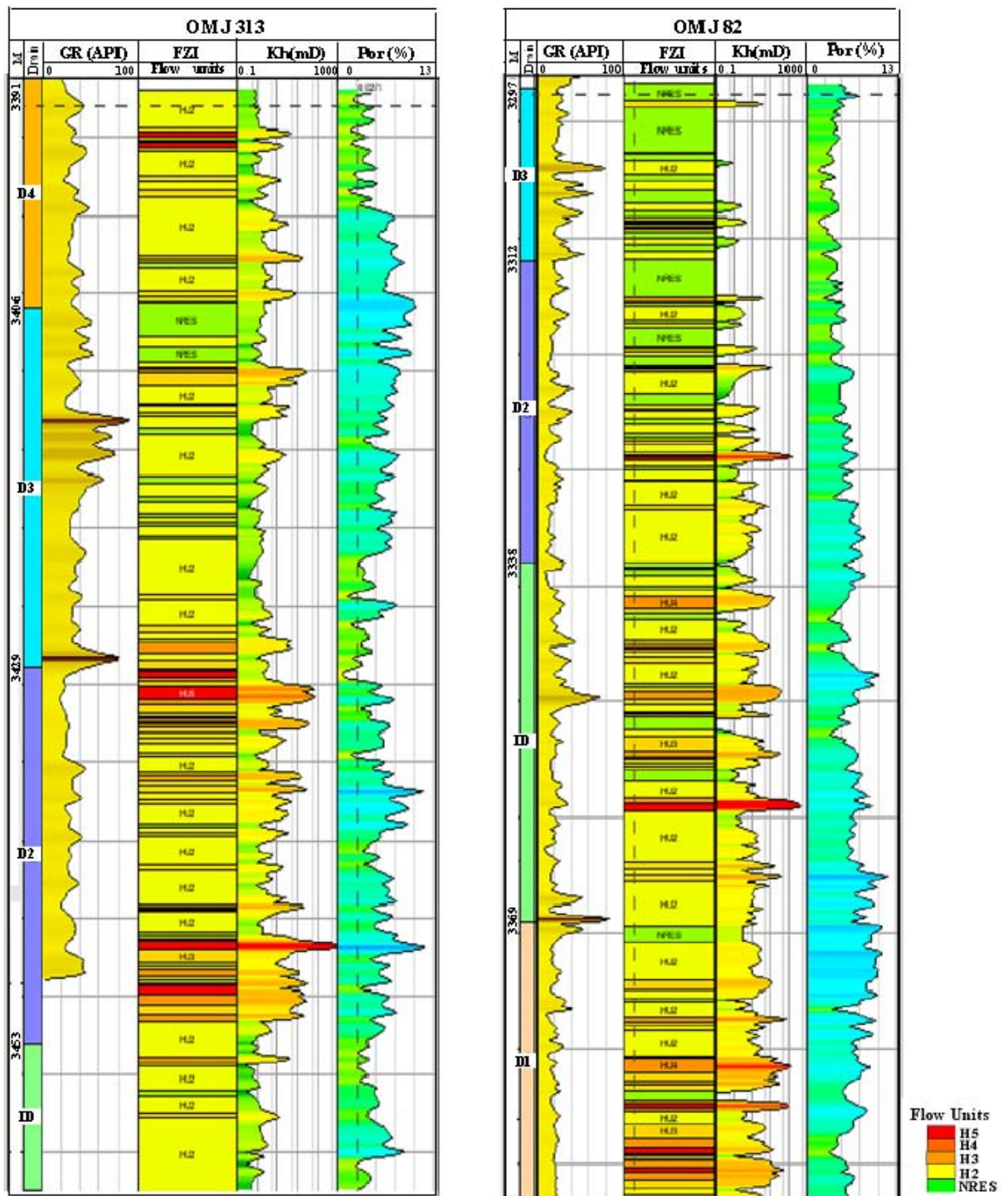


Figure 65 - Two examples of log composite of two wells, which have generally a mediocre reservoir quality. NRES(non reservoir) correspond to the silt drapes and /or to the sandstone with very low porosity and permeability. HU2 represents mediocre petrophysical characteristics. left handside:OMJ313. Right handside: OMJ82 (see map Fig. 20 for geographic location).

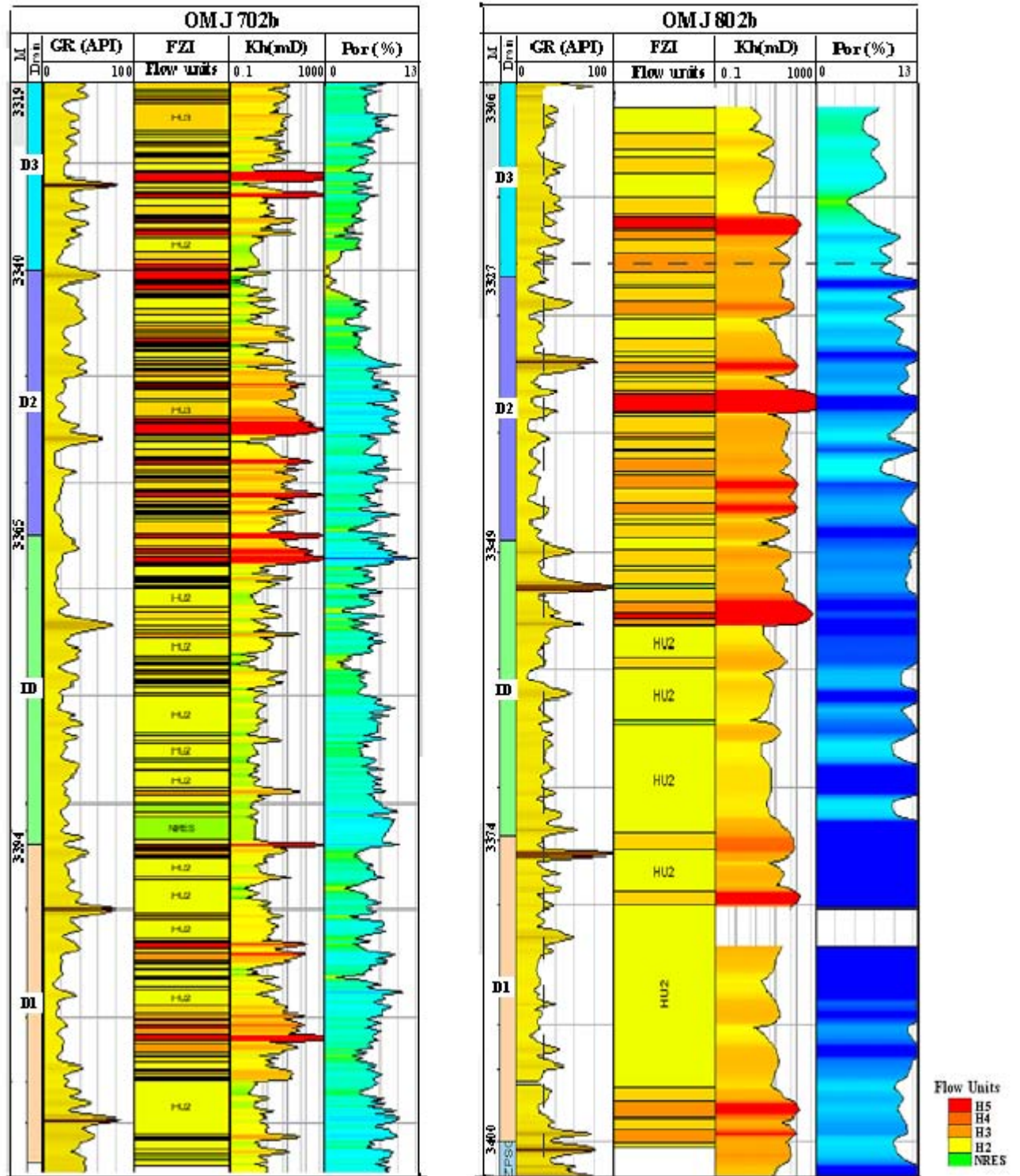


Figure 66 - Hydraulic units in the drill holes OMJ802b and OMJ702b (see map Fig. 20 for geographic location). Note that the best reservoir properties occur in the upper part of the reservoir. H3, HU4, HU5 are the flow units which represent high permeability and porosity in the wells.

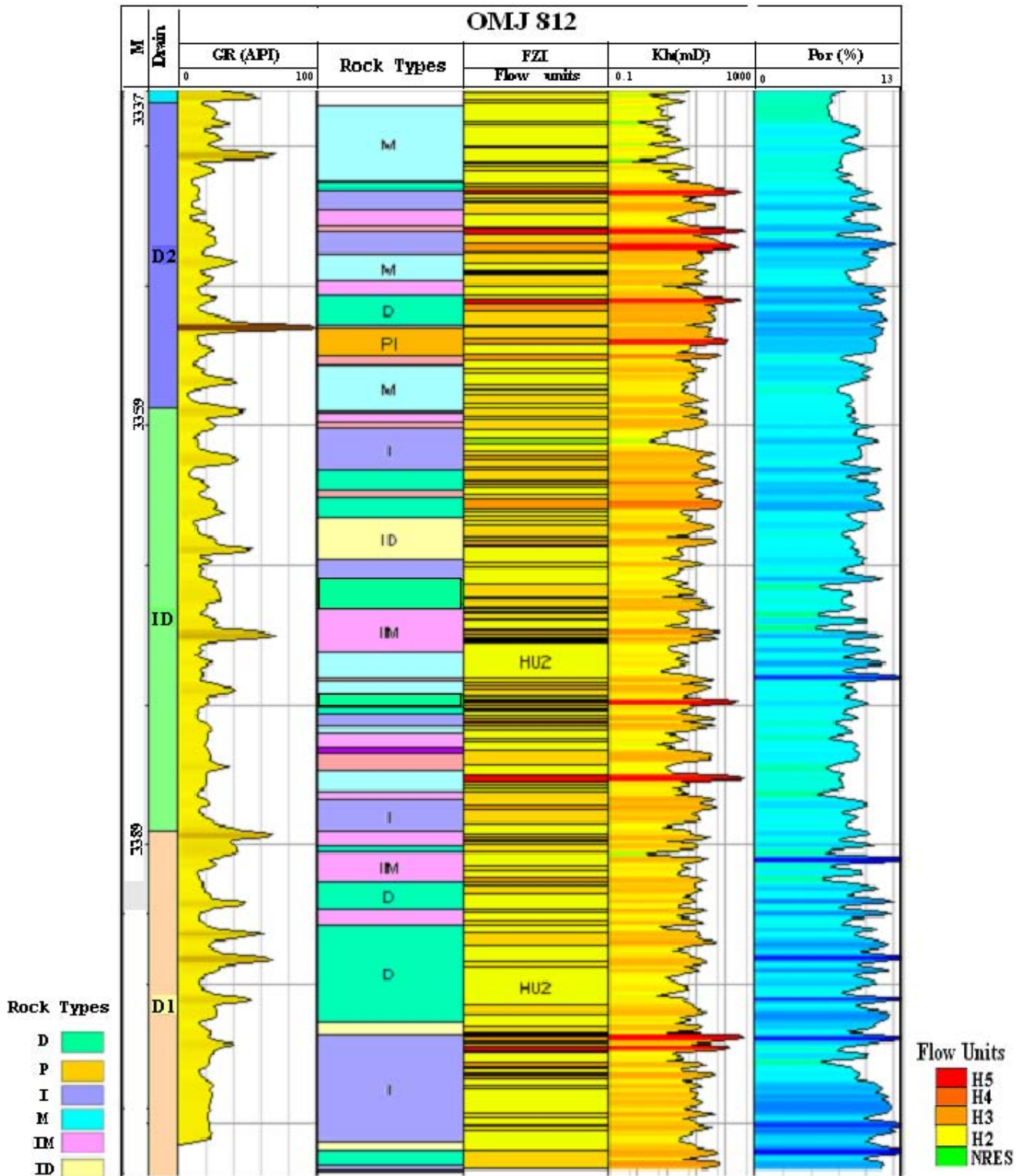


Figure 67 - Representative example of the area of interest in the drill well OMJ812 (see map Fig. 20 for geographic location). The log composite correspond to the correlation between the defined rock types, Flow units, and both permeability , porosity. This correlation confirm that Rock Type I has better reservoir characteristics than Rock Type D, and the reservoir properties of Rock type D are better than those of Rock Type M.

1. Procedure and methods

In order to present an inter-well correlation of the heterogenous reservoir of Hassi Messaoud, the intelligent software Petrel has been used.

In our approach, 4 types of modeling have been carried out according to the different results of study parameters of the reservoir Ra in previous chapters.

- Structural modeling
- Facies modeling
- Petrophysical modeling
- Fzi modeling

Modelling in petrel consists of the following steps:

Gridded surface: to create a gridded surface from seismic interpretations, structural maps and faults. The gridded surfaces in this study have been created on the tops of D5, D4, D3, D2, ID, D1, for petrophysical and FZI models and on the top of tidal and fluvial zones for the geological facies model (Fig. 68);

Zonation: this step creates the different zones of the reservoir D5, D4, D3, D2, ID, D1 from the surfaces (Fig. 69);

Layering: create interzone layering in the Ra reservoir. We used 0.5 cm as the layer scale for all models (Fig. 70 and Tab. 2).

Drains	Thickness (m)	Number of layers
D5	46	92
D4	42	84
D3	25	50
D2	26	52
ID	32	64
D1	30	60
Total	301	402

Tab. 2: Different Drains of the Ra reservoir and their equivalent of layers used in Reservoir Modeling.

Upscaling of facies: this is the formation of a body with the given facies in the model. The upscaling of porosity in petrel is performed using a simple average of

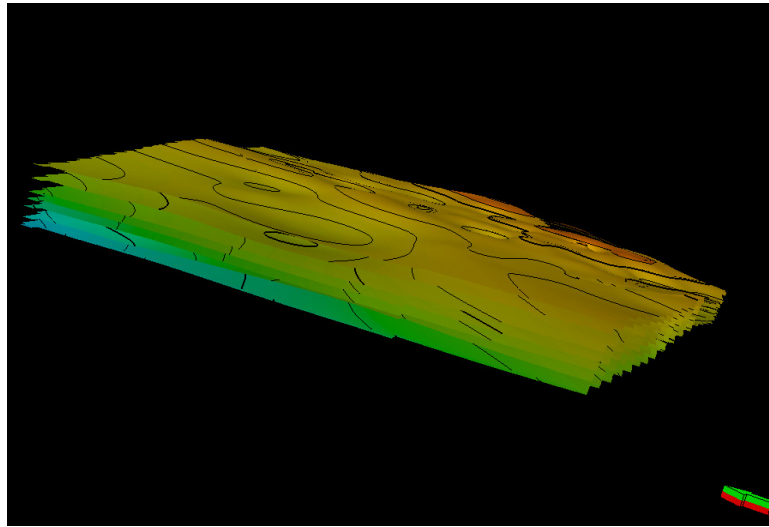


Figure. 68: Gridded surfaces of reservoir zones from the top to the bottom: D5, D4, D3, D2, ID, and D1.

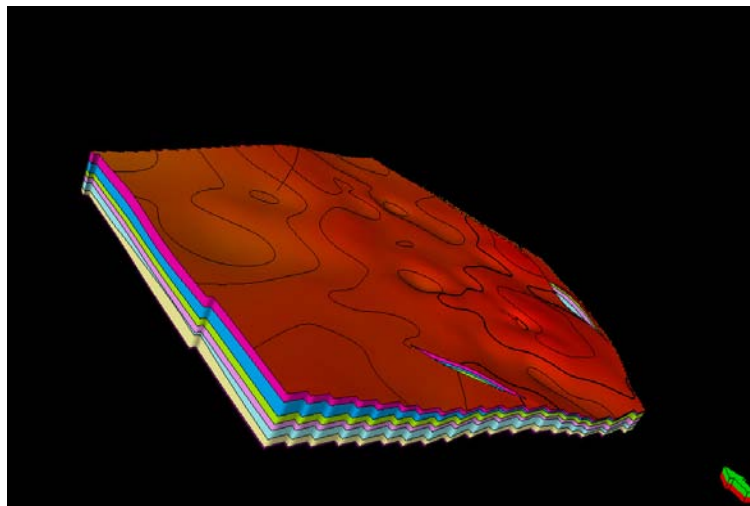


Figure. 69: Reservoir zones (Drains) from the top to the bottom D5,D4,D3,D2,ID,and D1.

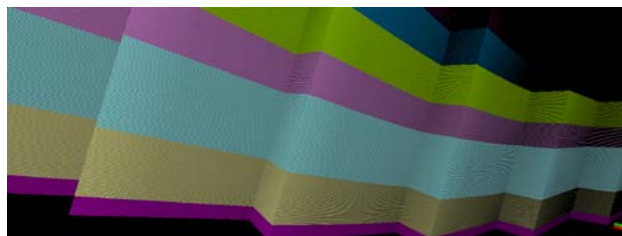


Figure. 70 - Reservoir layers and reservoir zones (Drains).

porosity by layer. Permeability is upscaled using the combination of arithmetic and harmonic average in Petrel.

2. Structural Modeling

Structural modelling is the first step in building 3D models and is subdivided into three processes:

Fault Modeling: Defining the faults in the geological model which will form the basis for generating the 3D grid. These faults are loaded from seismic interpretation into Zmap (landmark, software) (Fig. 71);

Pillar Gridding: Generating the grid represents the base of all modelization. The grid used in Hassi Messaoud reservoir Ra study is 100m X 100m X 0.5m (Fig. 72);

Making Horizons: Building the zones of the reservoir (D5, D4, D3, D2, ID, D1) in the model and then creating the layers in the zones; 0,5m represents the layer scale in our study.

Structural modeling consists of fault modeling, pillar gridding and vertical layering. All three operations are tied together into one single data model - a three dimensional grid. The structural model represents a skeleton of the study zone from which all other models will be built (Fig. 73 -74).

The structural cross sections (Fig. 75) made from the 3D structural model in many directions of the study sector, show the lateral extension of reservoir zones D5, D4, D3, D2, ID and D1 and their thickness variations including the faults. The reservoir zones are eroded by the Hercynian unconformity in the eastern part of the study area, a set of reservoir zones is quite full in the west part.

3. Facies and Petrophysical models

3.1. Introduction

Property modelling is the process of filling the cells of the grid with petrophysical properties. The layer geometry given to the grid during the layering process follows the geological layering in the model area. These processes are therefore dependent upon the geometry of the existing grid. When interpolating between data points, petrel will propagate property values along the grid layers.

Property modelling used for modelling in Petrel is split into 2 separate processes:

Facies Modeling : Interpolation of discrete data, e.g. facies.

Petrophysical modeling : Interpolation of continuous data, such as permeability for example.

The purpose of property modelling is to distribute properties between the wells such that it realistically preserves the reservoir heterogeneity and matches the well data.

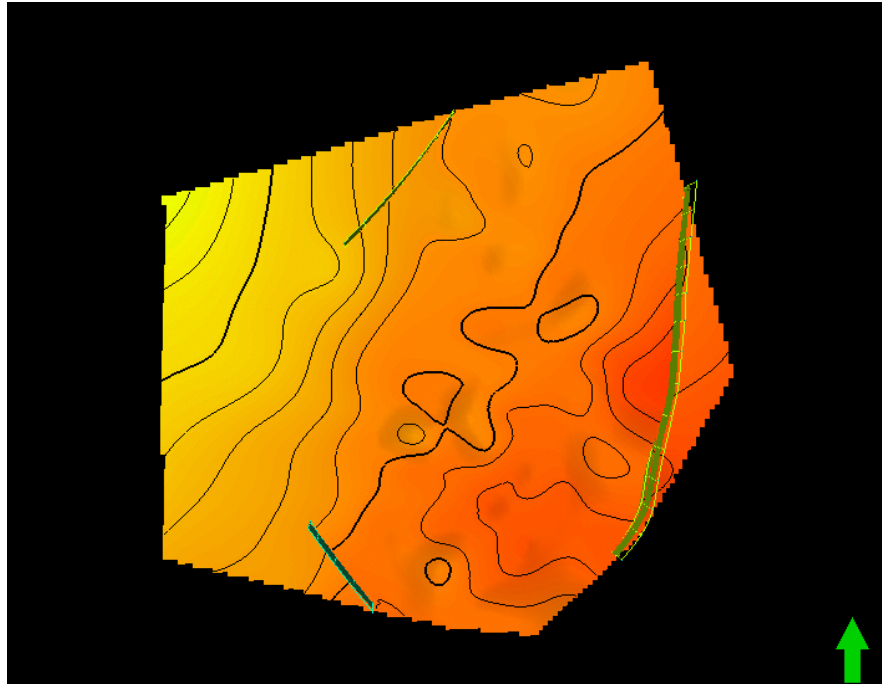


Figure. 71 - Structural gridded surface of the top of the reservoir Ra including the faults. Three major faults exist in this area of interest.

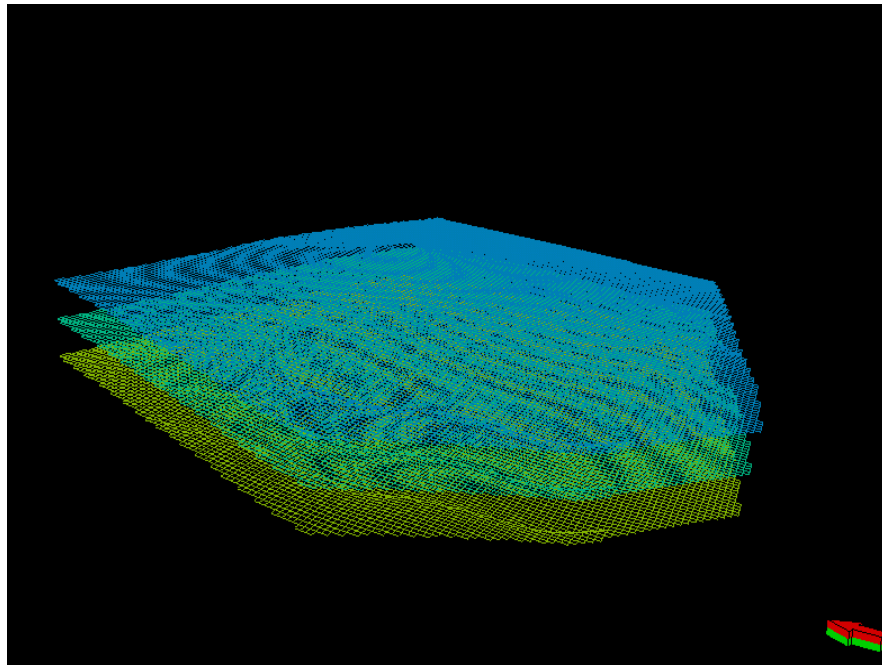


Figure. 72 - Picture from 3D model showing the cellular gridding used in the area of interest 100 x 100 x 0.5m.

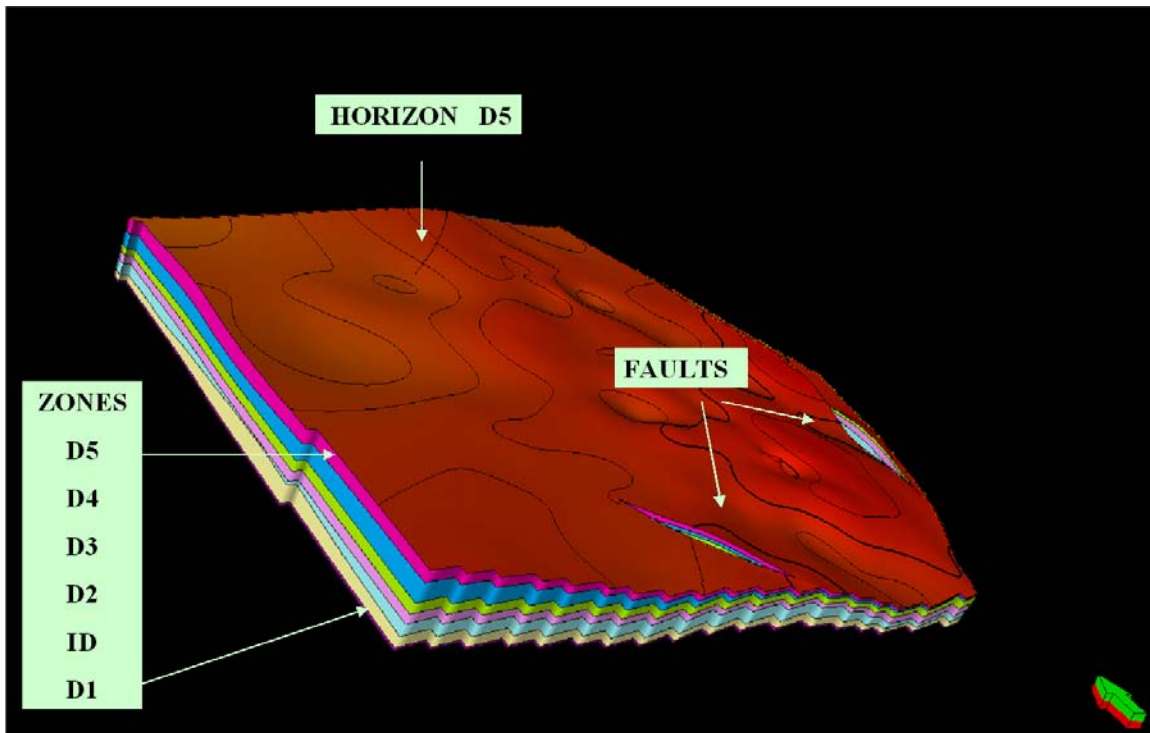
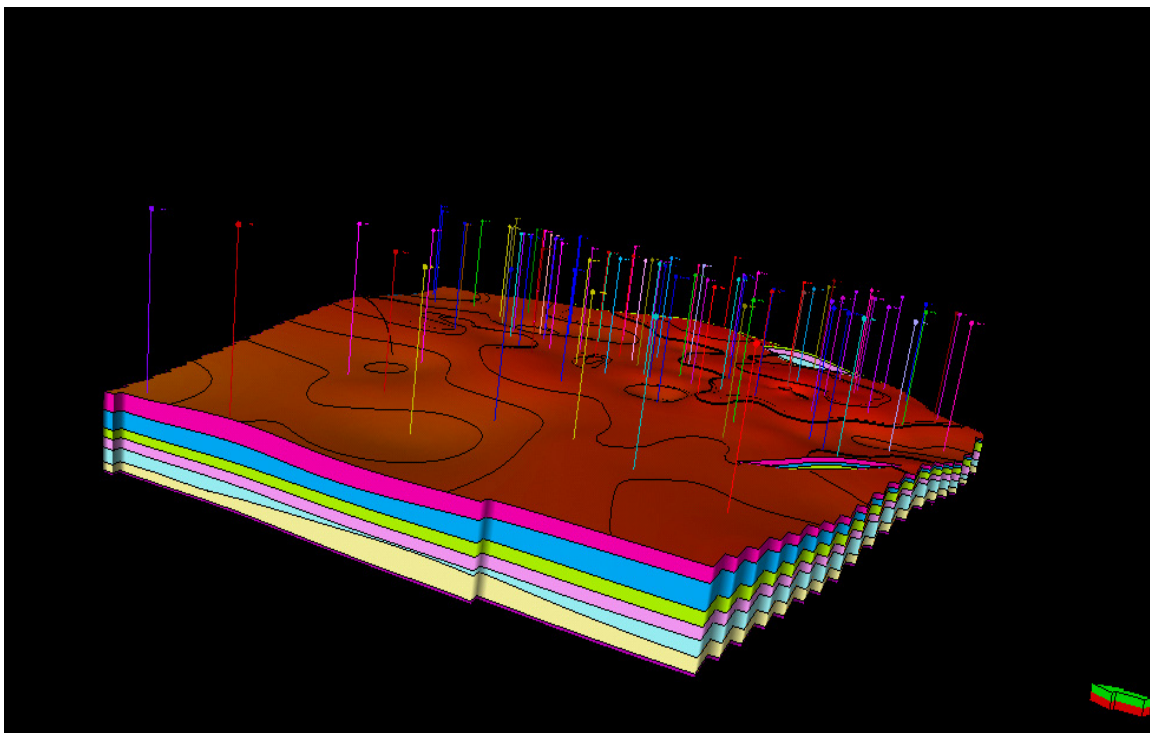


Figure. 73 – 74 - An example of the final structural model of the reservoir Ra of NW part of Hassi Messaoud Field above, and the same model below including the wells.



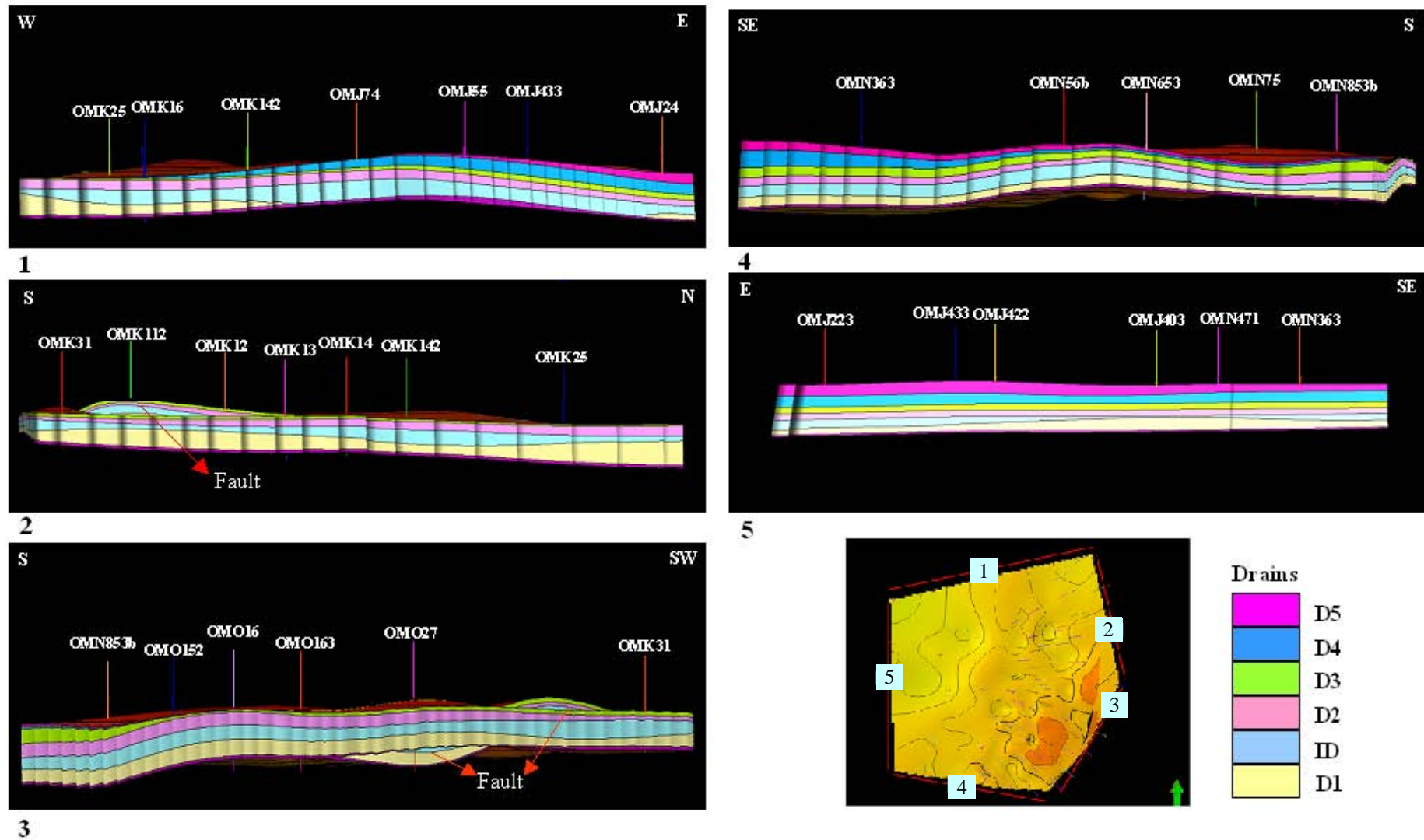


Figure 75 – Examples of structural cross sections in the area of interest.
 Cross section 1: Disappearance of zone D5 and D4 in the eastern part of the sector due to the Hercynian erosion.
 Cross section 2: In this direction only 3 drains of the reservoir appear: D2, ID, D.
 Cross section 3: This section is located near the fault (see picture right handside).
 Cross section 5: In the eastern part of the study zone all drains occur. Drain thicknesses are generally constant. This part is not affected by faults or the Hercynian unconformity.

3.2. Facies Modeling

Facies Modelling is a means of distributing discrete facies throughout the model grid. This step involves many different facies modelling approaches. The most-used methods are:

Object Modeling (used for facies modelling), which populates a discrete facies model with different bodies of various geometry, facies code and fraction.

Sequential Indicator (used for Fzi modelling) creates a stochastic distribution of the property, using the Directional settings as variograms and extensional trends.

3.2.1. Facies model of geological facies (Object Modelling)

3.2.1.1. Facies types

Two fundamental facies types are defined in the fluvial/tidal environments which characterize the depositional mode of the Cambrian reservoir Ra of NW part of Hassi Messaoud field (Fig. 76):

Siltstones: The impermeable part of the reservoir.

Channel Sand: The sand is considered to have the best reservoir quality due to the relatively high energy of deposition and consequent coarse grain size.

Two channel types are defined in the sandstone reservoir Ra: the fluvial channels characterize the lower part of the reservoir, while tidal channels constitute the upper part of the reservoir.

The described facies are coded and loaded in petrel to build a 3D facies model in the area of interest.

3.2.1.2. Cross sections

As already described in the sedimentology chapter, 6 N-S and 6 E-W cross sections have been realized in the study sector, including 32 wells, which were the focus of core description and paleoenvironment interpretation. The cross sections show the vertical and areal variation of tidal and fluvial facies, as well as the distribution of silts (Fig. 77 -78). Figs. 16-17 show that reservoir zone subdivision does not follow primary sedimentary features such as the first appearance level of the scolithos traces. The N-S section shown in Fig. 77 illustrates the thickness variations of the tidal sequences, which thickens towards the N.

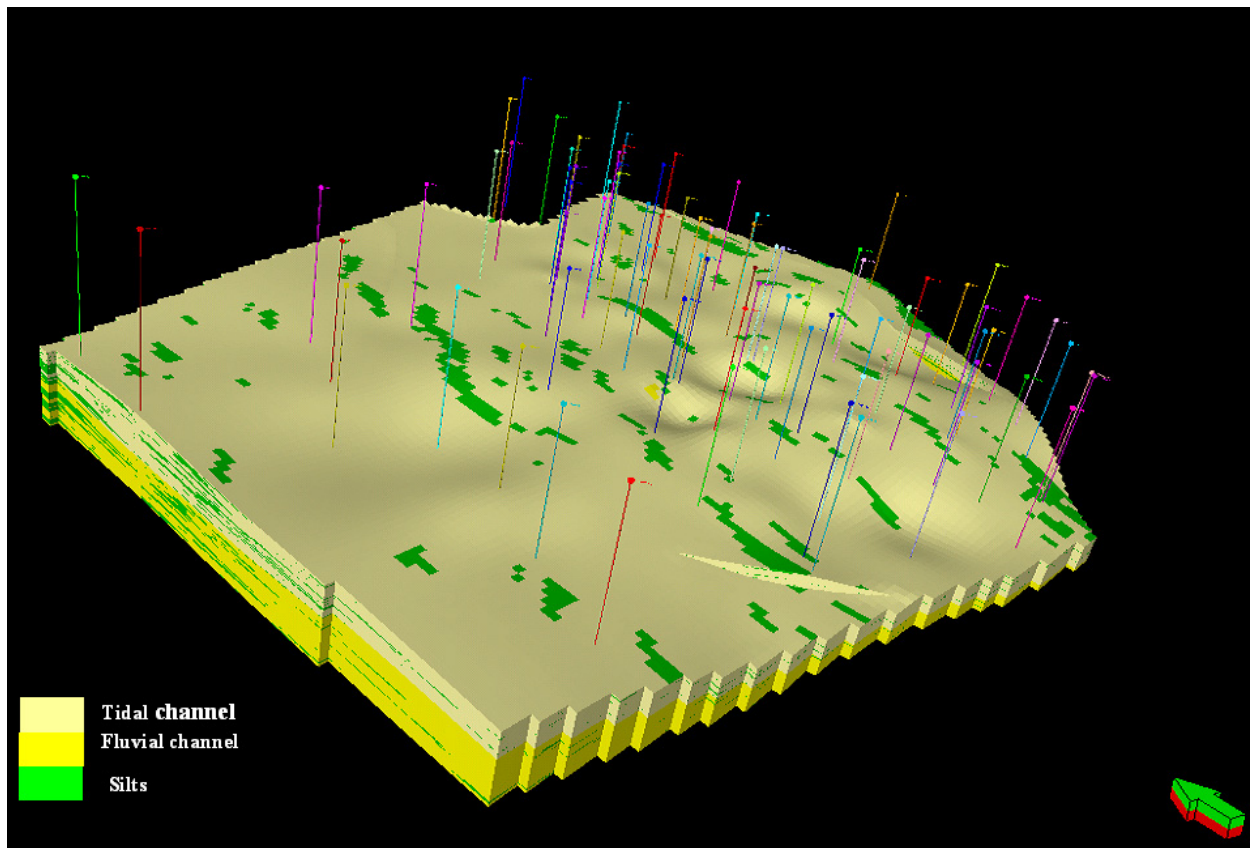


Figure. 76: 3D dimensional facies model of the NW part of Hassi Messaoud Field (reservoir Ra). Facies types are colour coded .

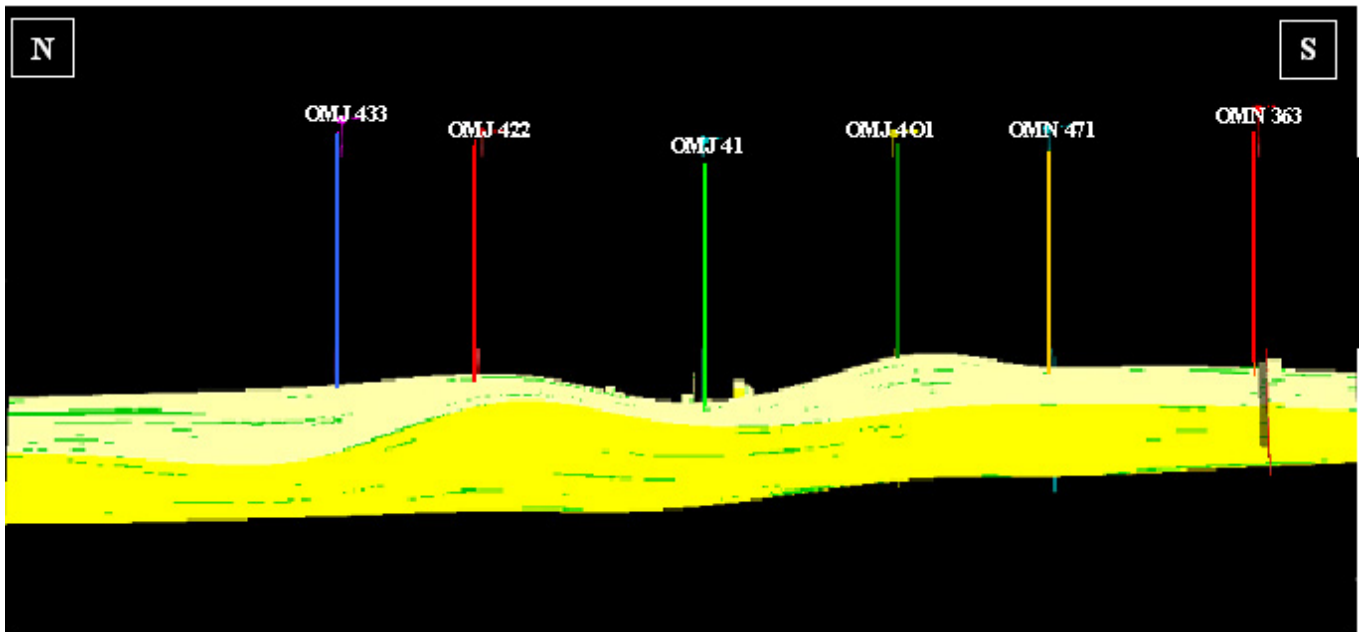


Figure. 77: N-S cross section from the geological model showing the interwell facies distribution.

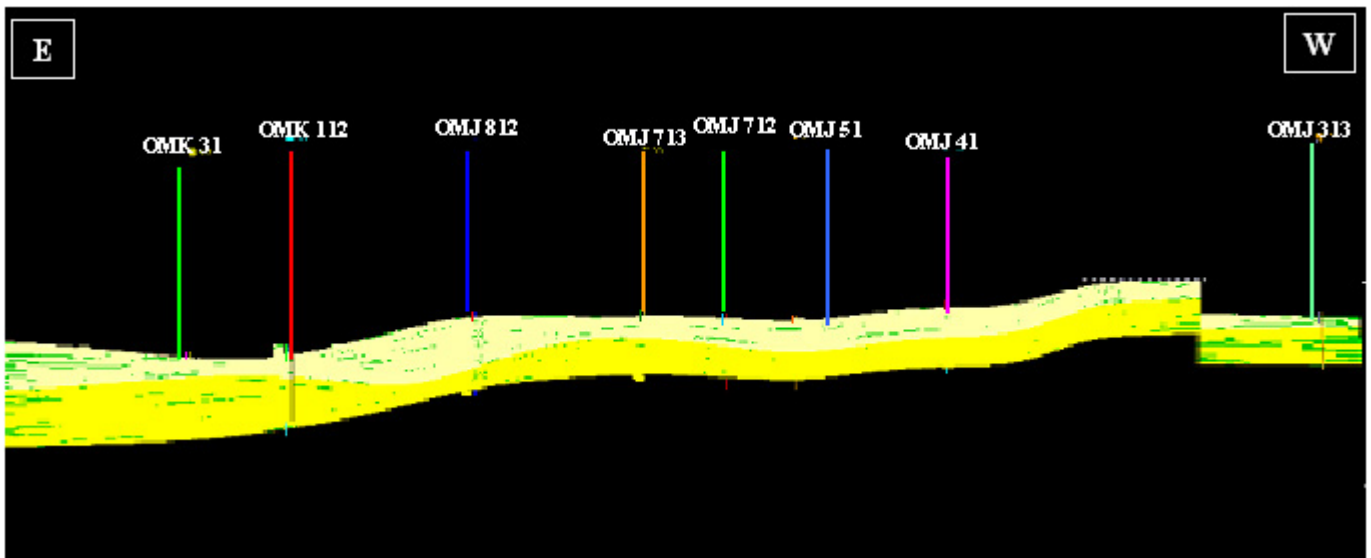


Figure. 78: E-W cross section from the geological model showing the interwell facies distribution.

3.2.2. Facies model of FZI of flow units (Sequential Indicator)

Five flow units have been defined in the area of interest. These flow units have been loaded in petrel as petrophysical facies. Because petrophysical data need a special interpretation in comparison with geological facies, we used a sequential indicator method for FZI modelling (Fig.79).

3.2.2.1. Using variograms in modeling

It is important to remember that the property modeling is used to describe the natural variation in a property. The variogram should therefore describe this natural variation, rather than broad scale trends. Before beginning the variogram analysis, it is necessary to have a knowledge of regional trends in data analysis. The most important data in variogram analysis are the orientation of channels, the distribution of wells in the area of interest, and the facies distribution and the spacing between wells in different directions. A variogram is a description of the variation in a property, based on the principle that two points close together are more likely to have similar values than points far from each other. The range of a variogram could be different in different directions and will of course often vary in the vertical direction. The Data Analysis module therefore allows us to analyse our data in two directions horizontally (these will be perpendicular to each other) and also vertically. Major, minor and vertical ranges specify the variogram function range in the major, minor and vertical direction. Because the spacing between wells varies in many directions (generally ≥ 2 km), 14 models of FZI as a function of variogram have been built in the study area, and 3 cases (minimum case, maximum case and most likely case) from the 14 models have been chosen to explain approximately the different areal cases of reservoir characteristics distribution (Tab. 3). Horizontally, it is relatively rare that we have enough sample points to generate an ideal variogram. Instead we should use our conceptual knowledge to estimate what kind of lateral variation we may expect.

FZI model cases	Azimuth	Vertical range	Minor range	Major range
Minimum case	30	0.5 m	500 m	500 m
Maximum case	30	0.5 m	1000 m	1000 m
Most likely case	30	0.5 m	500 m	1000 m

Tab. 3: Different cases of FZI modeling in the study area.

The lateral and vertical distribution of FZI facies through the area of interest can be shown clearly in models saved on video format (video models).

3.2.2.2. Cross sections

Two examples of the major cross sections N-S and E-W throughout the study area from the FZI most likely case model showed the flow units distribution in these directions (Figs. 80-81).

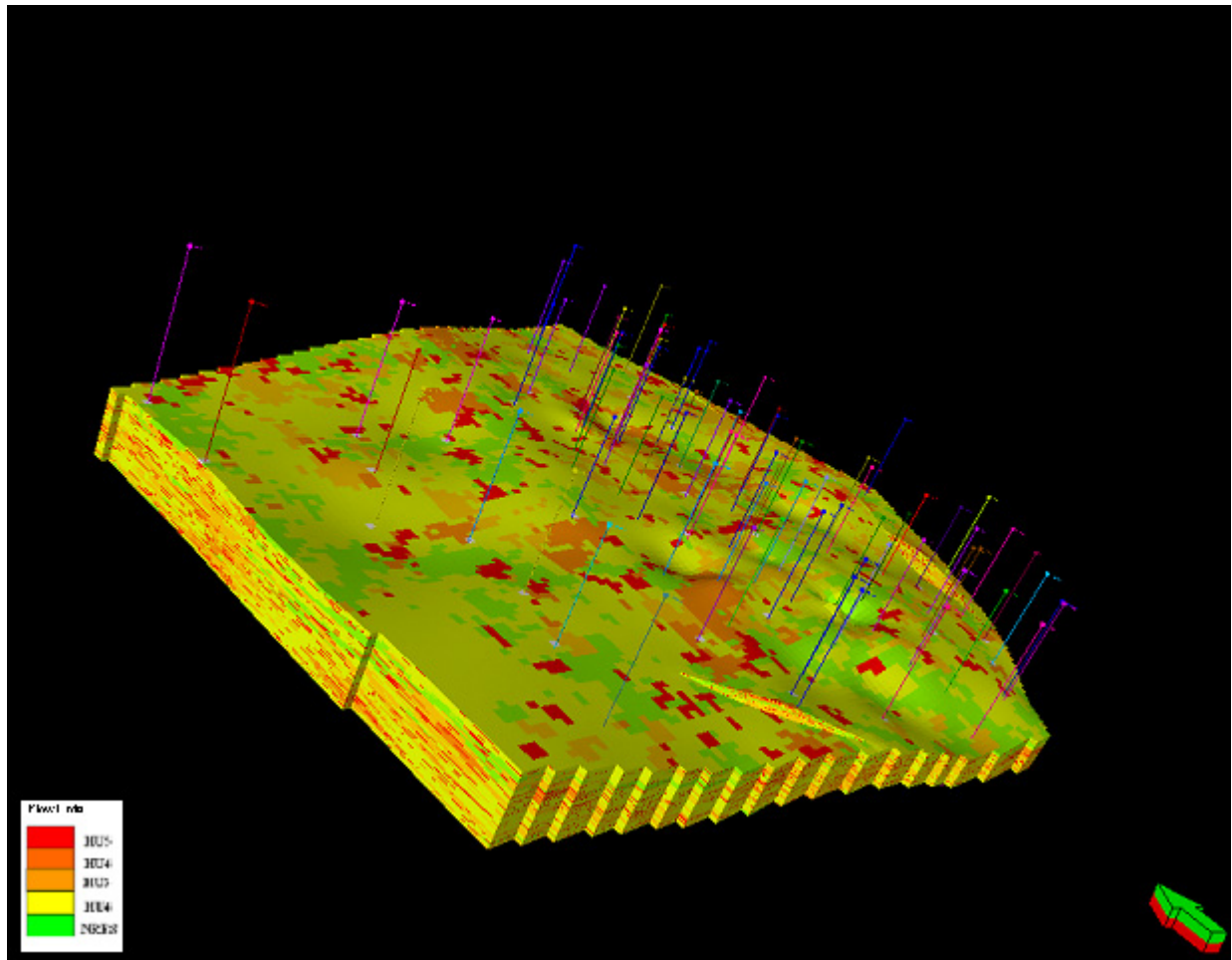


Figure. 79: 3D dimensional FZI model of the NW part of Hassi Messaoud Field (reservoir Ra). Flow unit types are colour coded .

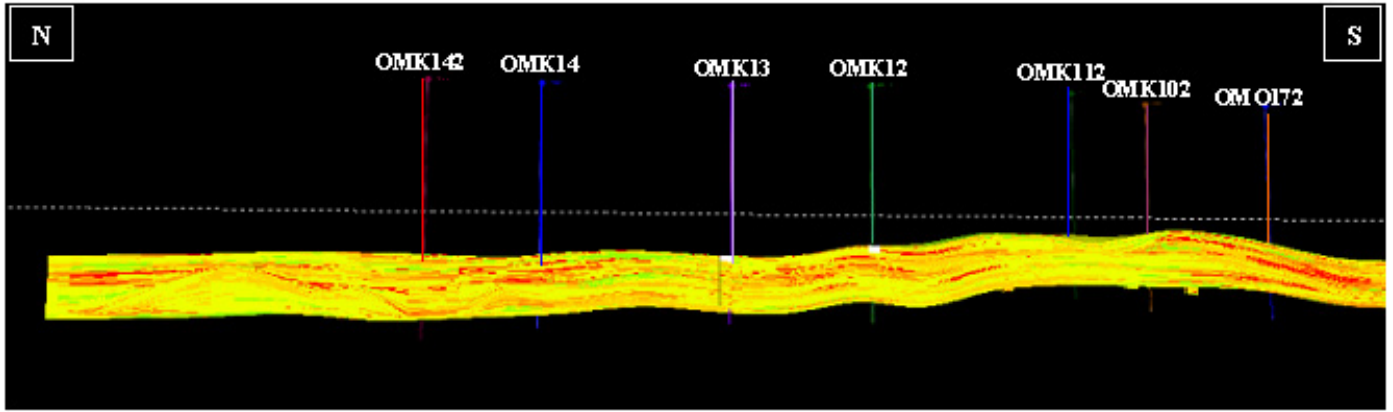


Figure. 80: N-S cross section showing the most likely case of the FZI model.

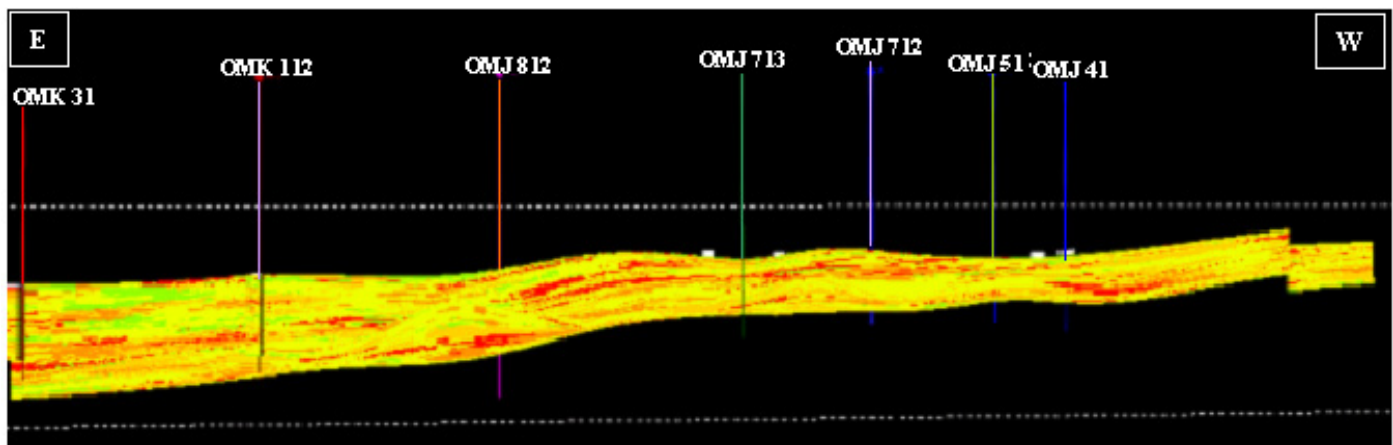
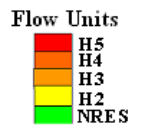


Figure. 81: E-W cross section showing the most likely case of the FZI model.

3.3. Petrophysical Modeling process

The most-used method for permeability modelling is sequential gaussian simulation. In our study, only the permeability parameter has been a focus of petrophysical modelling, because the porosity is generally constant in a study area and varies between 8 and 13 %. Sequential Gaussian Simulation honors well data, input parameter distributions, variograms and trends. The variogram and distribution are used to create local variations, even away from input data. The simulation is most appropriate for use, for cases where the shape of particular facies bodies is uncertain. Information related to the stochastic simulation options can be found in the GSLIB manual (Deutsch and Journel, 1998).

Sequential indicator simulation is a stochastic modelling technique, whereby the result is dependant above all upon:

- Upscaled well log data
- Defined variogram
- Frequency distribution of upscaled data points.

It should be noted that for all geostatistical models, the upscaling of porosity is performed using simple average. Permeability is upscaled using the combination of arithmetic and harmonic average. This is the case of petrel properties modelling.

In permeability modeling (Fig. 82), 3 cases (minimum case, maximum case and most likely case) have been carried out to explain the areal distribution of reservoir characteristics (Tab. 4).

KH model cases	Azimuth	Vertical range	Minor range	Major range
Minimum case	30	0.5 m	500 m	500 m
Maximum case	30	0.5 m	1000 m	1000 m
Most likely case	30	0.5 m	500 m	1000 m

Tab. 4: Different cases of KH modeling in the study area.

Two examples of the major cross sections NS and EW through the study area from the KH most likely case model showed the permeability distribution in these directions. (Fig. 83- 84).

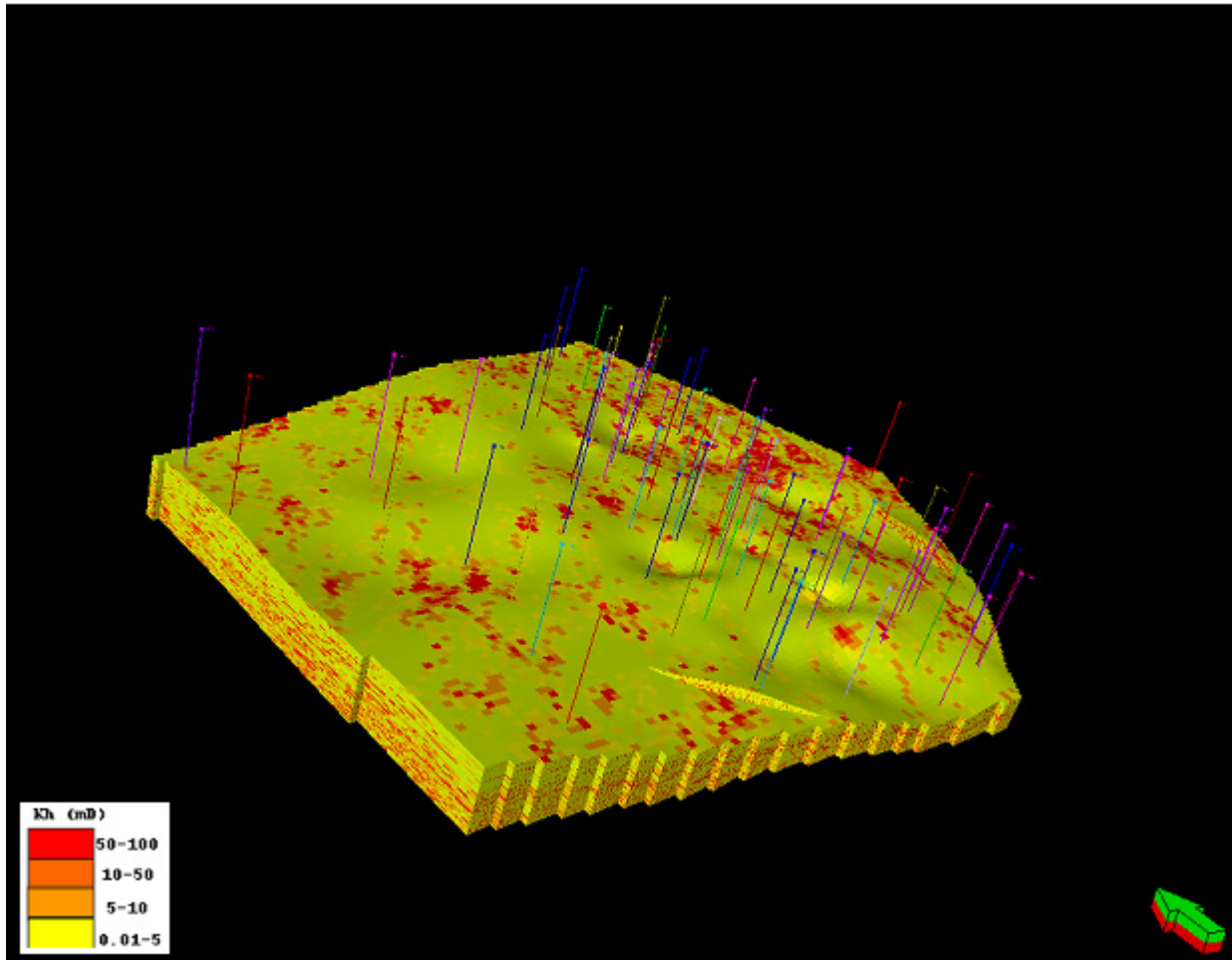


Figure. 82: 3D dimensional KH model of the NW part of Hassi Messaoud Field (reservoir Ra). K(Permeability) ranges are colour coded .

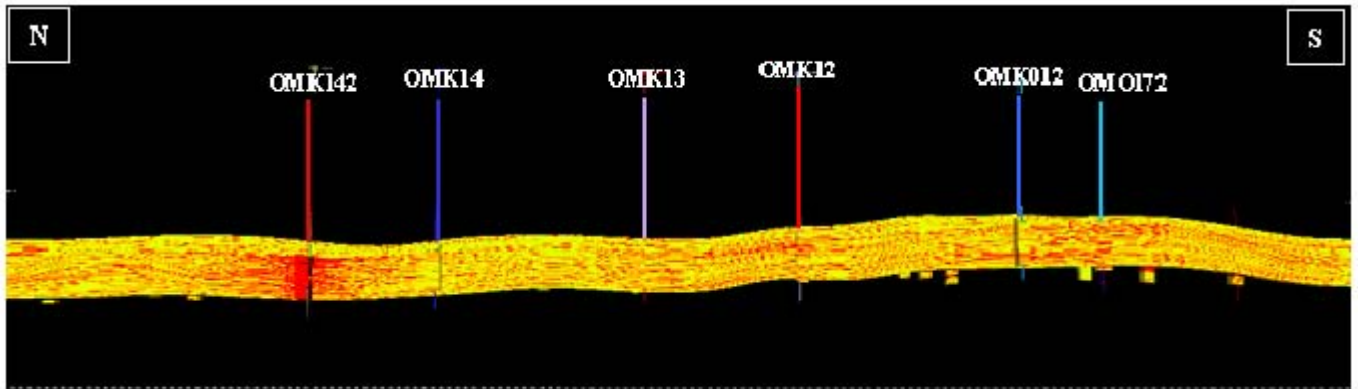


Figure. 83: N-S cross section showing the most likely case of KH model.

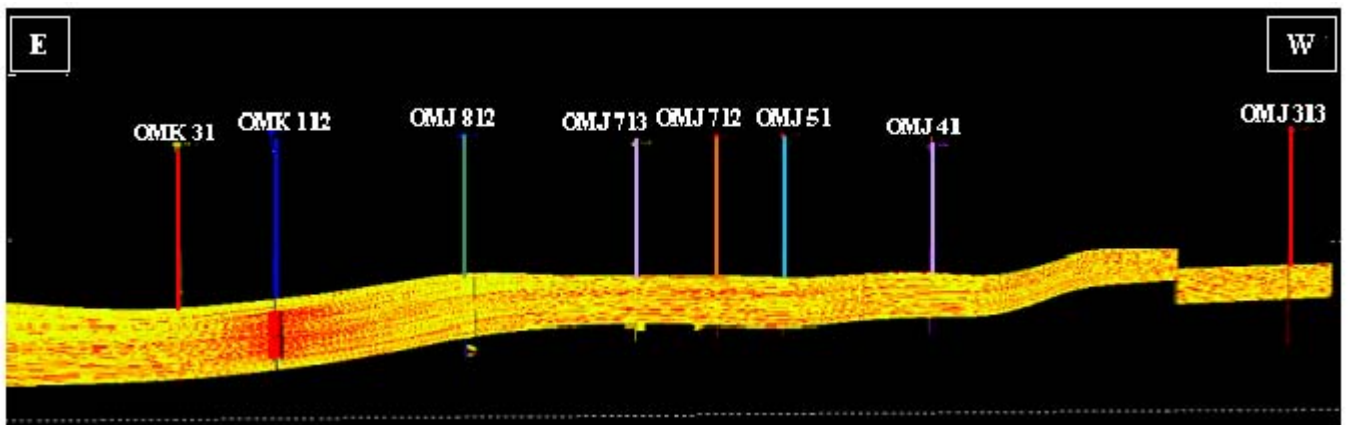
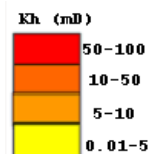


Figure. 84: E-W Cross section showing the most likely case of KH model.

Conclusions

The focus of this study is the characterization of the Cambrian reservoir of the northwestern part of the Hassi Messaoud field, based on the geological and petrophysical characterization of the reservoir. Ra is an anisometric quartzose sandstone, beige in color when it is not impregnated. Grain size is generally medium to coarse in the lower part of the succession and becomes finer-grained upward. This trend begins in D4. Clay cement is common in the lower part of the reservoir. Quartz cement evolves inversely.

In the reservoir Ra, two parts are distinguished significantly based on their different reservoir qualities. The upper Ra consists of fine- to medium-grained sandstones with a high percentage of quartz cement; in this part the reservoir is mediocre. The lower Ra is a medium to coarse grained sandstone which can present the best reservoir qualities.

Description of cores and sequence analysis allow for the following conclusions:

1. The lower part of the Ra represents fluvial braided channels, the upper part is composed by tidal channels.
2. The fluvial part is characterized by fining-upwards stacked sequences of coarse- to medium-grained sandstone, the tidal- nearshore part consists of coarsening upwards sequences, the grain size is medium to fine.
3. Onsets of tidal sedimentation coincide with the appearance of marine trace fossils (Scolithos).
4. Applying the sequence stratigraphic model of Zaitlin et al. (1994), the fluvial deposits are assigned to a lowstand systems tract, the tidal deposits represents the early transgressive systems tract.

The principal goals of petrographic interpretation were to:

- 1) Examine all Ra zone thin sections from the 18 wells in the area of interest.
- 2) Assign them to rock types based on composition, texture, diagenesis, pore geometry and reservoir quality.
- 3) Compare the results of five wells (OMK25, OMK142, OMJ812, OMJ41, OMJ223) to understand the lateral and vertical rock types distribution.

The interplay of initial composition, depositional environment and diagenesis determine reservoir quality.

Four major rock types have been recognized in Zones D5, D4, D3, D2, ID, D1 based on pore-level properties: Sandstones rich-dickite (D), Intercrystalline macroporous quartz sandstone (I), Moldic macroporous quartzose sandstone (M), Bioturbated sandstone (B).

Coarser- grained sandstones are texturally and compositionally immature, and consist of rock types D and M. Finer grained sandstones are more mature due to reworking in tidal environment where rock types I and B are most common.

The lower part of the reservoir (fluvial), where the rock type I and D dominate in the majority of the study wells, represents the best reservoir qualities. In the upper part of the reservoir (tidal deposits-nearshore), rock type M occurs bedded with rock type B and I.

Understanding complex variation in pore geometry within different lithofacies of petrofacies Rock types is the key to improved reservoir description and exploitation. Core data provide information on various depositional and diagenetic controls on pore geometry. Variation in pore geometrical attributes, in turn, define the existence of distinct zones (hydraulic units) with similar fluid-flow characteristics.

41 wells from the zone of interest have been the subject of permeability prediction by hydraulic flow units to understand complex variation in pore geometry within different lithofacies of petrofacies rock types. 5 flow units have been defined corresponding to typical ranges of FZI by well. Hydraulic units are related to geological facies distributions but do not necessarily coincide with facies boundaries. The comparison between flow units, permeability, porosity and rock types confirm that the HU (hydraulic units) are related to petro- facies distributions and match the petrophysical data very well.

To summarize and visualize the previous results, 4 types of 3D models have been realized.

1. Structural modeling: the structural model consists of a skeleton of the study area, including fault modeling, pillar gridding, and vertical layering.
2. Facies modeling: The facies model is a means of distributing described facies throughout the model grid in the area of interest.
3. Petrophysical modeling: It consists of the areal distribution of the permeability as function of variogram parameters, like orientation of channels, major range and minor range.
4. FZI modeling: FZI model is a distribution of defined flow units in the study area using a variogram and our conceptual knowledge of regional trend in data analysis.

To build these models we have used an intelligent software Petrel, which is at present the most usable software for most petroleum companies.

The anisotropy of the Ra (D1-D4) reservoir and the isotropy of the Ri (D5) reflect the variations in the initial sediment composition. The compositionally mature sandstones D5 is dominated by monocrystalline quartz which promotes the formation of quartz overgrowth cements, this induces the isotropy of D5. In contrast, compositionally less mature sandstones initially contain more feldspar, lithic fragment and polycrystalline quartz. This composition promotes the alteration and dissolution of unstable grains during diagenesis resulting in a variety of the present rock types. This induces the anisotropy of the Ra reservoir (D1-D4).

Rock types are defined by their lithologic character (composition, texture, and diagenesis) and pore space properties (pore abundance, type, size and geometry). These parameters, especially pore throat geometrical attributes, lead to distinct rock flow units that have similar fluid transport properties, calculated from core data of wells (porosity and permeability).

In the area of interest, D1-D2 have the best reservoir quality as result of rock types and flow units. D3 and D4 have a mediocre quality. D5 has the poorest quality of the reservoir.

Key References

- Aliouche, H., Ayed, M., 1999, Fracturation au niveau du reservoir cambroordovicien du champ de Hassi Messaoud, Sonatrach, IAP.
- Bacheller, W.D., and Peterson, R.M., 1991, Hassi Messaoud Field, Algeria, Triassic Basin, Eastern Sahara Desert, in Foster, N.H., and Beaumont, E.A., eds., Structural Traps V: AAPG Treatise of Petroleum Geology, Atlas of Oil and Gas Fields, p. 211-225.
- Balducci, A., and Pommier, G., 1970, Cambrian oil field of Hassi Messaoud, Algeria, in Halbouty, M.T., ed., Geology of Giant Petroleum Fields: AAPG Memoir No. 14, p. 477-488.
- Baumann, T., 1983, Application of Sedimentological Studies in the Reservoir and Geological Modeling of the Al t-luwaisah Field, Oman, SPE 11452.
- Bardon, C., Longeron, D.G., Baudouin, F., Delhomme, A., and Naili, N., 1994, Gas/oil relative permeabilities and residual oil saturations in a field case of a very light oil, in the near-miscibility conditions: SPE 69th Annual Technical Conference & Exhibition, New Orleans, SPE 28625, p. 175-188.
- Bedjaoui, A., 2001, The feasibility study of underbalanced drilling in Algeria, Hassi Messaoud Field., Norman, Oklahoma.
- Bernard Biju-Duval, IFP, 1999, Géologie sédimentaire. Bassins, environnement de dépôts, formation du pétrole.
- Beaufort, D., Cassagnade, A., Petit, S., Lanson, B., Berger, G., Lacharpagne, J. C., Johansen, H., 1998, Kaolinite to dickite reaction in sandstone reservoirs, Clay Mineral, V.33, p.297-316.
- Beicip Franlab, 1995, Révision du modèle géologique du champ de Hassi Messaoud.
- Beicip Franlab, 1995, Caractérisation pétrophysique du réservoir Cambrien du champ de Hassi Messaoud.
- Beicip Franlab, 2002, Interprétation sismique du secteur NW du champ de Hassi Messaoud.
- Benrabah, B., 1984, Etude sédimentologique du Cambrien de la région d'El Gassi.
- Beuf, S., Biju-Duval, B., de Charpal, O., Rognon, P., Gariel, O. et Bennacef, A., 1971. IFP, 1971, Les grès du paleozoïque inférieur du sahara sédimentation et discontinuités évolution structurale d'un craton.
- Bhp Billiton Petroleum, 1996-2003, London, Petrographic and sedimentological studies and reports of the Cambro-Ordovician and triassic reservoirs of Rod field, Berkine Basin, Algeria.
- Bourbih said, 2000, Etude de l'échec de stimulation par acidification sur la zone 4 champ de Hassi Messaoud field., IAP, Sonatrach.
- Bostone Melbourne, 1986, Sedimentary environments and facies. Edited by Hgr eading (departement earth sciences university of oxford). Blackwell scientific publication. Oxford London Edinburgh.
- Boudjemaa, F., and Lakhchakhech, A., 2000, Approche géostatistique à la géométrisation du réservoir Ra des zones 20A et 2S du champ de Hassi Messaoud, Algeria.
- British Petroleum, internal reports, 2000, characterisation and modelling of natural fractures rhoud el baguel field, Algeria.
- Clayton Deutsch, V., André Journel, G., GSLIB Geostatistical Software Library and User's Guide, 2nd Edition, 1998 .
- Collinson, J. D., and Thompson, D. B., 1984, Sedimentary structures.
- Delhomme, A. El K., and Giannesini, J.F., 1979, New reservoir description techniques improve simulation results in Hassi-Messaoud Field, Algeria: SPE 54th Annual Fall Technical Conference & Exhibition, Las Vegas, SPE 8435, p. 1-11.

- Djamel Boutoutao, and Steve Larter, 2000, Understanding the regional migration routes and charging of the Hassi Messaoud oil field, Algeria.
- Dorsey, J. B., Litherland, J. G., Ait Saadi, A., and Boutalbi, A., 1975, Past and Predicted Future Performance of Hassi Messaoud Field, Algeria - Under Gas and Water Injection: SPE 50th Annual Fall Meeting, SPE 5537, p. 1-16.
- Dyes, A. B., Bensimina, A., Ait Saadi, A. M., and Khelil, C., 1972, Alternate Injection of HPG and Water - A two Well Pilot: SPE 47th Annual Fall Meeting, SPE 4082, p. 1-16.
- Djebbar Tiab, and Eric Donaldson, C., 1998, Petrphysics theory and practice of measuring reservoir rock and fluid transport properties.
- Diederik van Batenburg, Bachir Ben Amor, Rafik Belhaouas, 2000, New Techniques for Hydraulic Fracturing in the Hassi Messaoud Field, SPE 63104.
- Edward, H. I., Mohan, R. S., 1989, An introduction to applied geostatistics, FFS International vanconver, British Columbia, Newyork oxford, Oxford University Press.
- Evans, R. B., Lathon, M., Senaip, Connally, T.C., 1991, Stratigraphy of the Wajid Sandstone of Southwestern Saudi Arabia, SPE 21449.
- Frank, G. Ethridge, Romeo, Flores, M., and Michael Harvey, D., 1987, Recent developments in fluvial sedimentology. contributions from the third international fluvial sedimentology conference. edited by Society of rconomic paleontologists and mineralogists.
- Galeazzi S., Haddadi N., Blanpied C., Rubino J. L., Ousset E., 2000, Lower Paleozoic depositional cycles of the Berkine and Illizi basins of the Algerian Saharan Platform: their development in the paleo-Tethys Gondwana continental margin.
- Gringarten, E., Deutsch, C.V., Methodology for variogram interpretation and modeling for improved reservoir characterization), SPE 56654.
- Hassini, I., 1993, étude du maintien de préssion par l'injection d'eau sur la zone 4 du champ de Hassi Messaoud., IAP.
- Hassing, J., Parsons, T., Huang X. H., Baranowski, J., Pande, K., 2000, Approach to Geological and Reservoir Simulation Modeling Yields New Insights, SPE 64791.
- Henniche, D., chabouni, A., Benbakir, A., 1994, Synthèse des études de macrofacies du réservoir cambrien de la zone 4 du champ de Hassi Messaoud.
- Hearn, C.L., Ebanks, W.J., Tye, R.S., and Ranganathan, V., 1984, Geological factors influencing reservoir performance of the Hartzog draw field, Wyoming, JPT, 1335-1344.
- Henriquez, A., Kelly j., and Hurst, A., 1990, Characterization of fluvial sedimentology for reservoir simulation modeling, SPE 18323.
- Hurst, A., lovell M.A., and Morton, A.C., 1993, Geological applications of wirline logs. geological society special publication classics.
- Jorge Pizarro, Olinto Souza, Jr., Luiz Freitas, Liliana Gomez, Juan. Comas, 2001, Three-Dimensional Modeling of Structurally Complex Reservoirs, The Revancha Field Case, SPE 71636.
- Karim Aissaoui , Djebbar Tiab, 2001, Contribution of horizontal well log and pressure data in stochastic modeling., University.of Oklahoma, SPE70012.
- Kozeny, J., 1927, Uber kapillar leitung des wassers im boden, Stizurgsberichte, Royal Academy of Science, Vienna, V. 136, 271-306.
- King, G. R., Costa, R., Minck, R., Leggett, E., Carleton, B., Laidlaw, C., and Domingos, F., 1998, Reservoir characterization , Geological Modeling, and reservoir simulation of the N'Sano field, Upper Pinda reservoir, SPE39760.
- Koceir, M., Tiab, D., 2001, Influence of Stress and Lithology on Hydraulic Fracturing in Hassi Messaoud Reservoir, Algeria., University.of Oklahoma, SPE 62608.

- Lanson, B., Beaufort, D., Cassagnade, A., Berger, G., Cassagnabère, A., Meunier, A., 2002, Authigenic kaolin and illitic minerals during burial diagenesis of sandstones, *Clay Mineral*, V.37, p.1-2.
- Malcoln Rider, 1996, The geological interpretation of well logs, Second edition, Petroleum exploration consultant, Rider –French consulting LTD, Aberdeen and Sutherland.
- Mackey, SD., 1995, *Journal of Sedimentary Research*, 65B, p.7-31.
- Maghsoon Abbaszadeh, Japan Natl.oil corp., Hikari Fujii, Arabian oil co.Ltd., Fujio Fujimoto, Japan Natl.oil corp., Permeability prediction by hydraulic flow units –theory and applications, SPE 30158.
- Maamar el Djabri, 2001, Gas lift optimization and design in zone 7 Hassi Messaoud Field., Norman, University.of Oklahoma.
- Malenfer, J., and Tillous, A., 1963, Study of the Hassi Messaoud field stratigraphy, structural aspect, study of detail of the reservoir: *IFP Review*, v.18, p. 851-867 (in French).
- Massa, D., Ruhland, M., and Thouvenin, J., 1972a, Structure and fracturing in the Hassi Messaoud field (Algeria) , Part 1 - Observations of tectonic phenomena in the Tassili N Ajjer: *IFP Review*, No. 27/4, p.489-534 (in French).
- Massa, D., Ruhland, M., and Thouvenin, J., 1972b, Structure and fracturing in the Hassi Messaoud field (Algeria) , Part 2 - Application to the Cambrian reservoir of North Hassi Messaoud. New tectonic interpretation: *IFP Review*, No. 27/5, p. 665-713 (in French).
- McGowen, J.M., Benani, A., and Ziada, A., 1996, Increasing oil production by hydraulic fracturing in the Hassi Messaoud Cambrian Formation, Algeria: *SPE European Petroleum Conference*, SPE 36904, p. 303-320.
- Miesch, E.P., and Khelil, C., 1973, Application of material balance techniques in matching and predicting performance of the heterogeneous multilayer Hassi Messaoud Field: *SPE 48th Annual Fall Meeting, Las Vegas*, SPE 4431, p. 1-13.
- Miall, A.D., 2000, The geology of fluvial deposits, sedimentary facies, Basin analysis, and Petroleum geology.
- Michael, B. M., Diederik van Batenburg, Rafik Belhaouas, 2000, Production Gains from Re-Fracturing Treatments in Hassi Messaoud, Algeria, SPE 65186.
- Millot, G., 1964, *Géologie des argiles*.
- Nabil Drid, 2001, The performance of water alternating gas (wag) in stratified reservoirs in Hassi Messaoud field, Algeria., Norman, University.of Oklahoma.
- Norris, R. J., and Lewis, J.J.M., 1991, The Geological Modeling of effective Permeability in Complex Heterolithic Facies, Imperial College., SPE 22692.
- Nordine Sabaou, 2003, Sedimentology geometry and depositional environments of the Triassic reservoirs of the Saharan platform, Algeria., PhD thesis, University of Birmingham.
- Nourddine Benourkhou, 2001, Assesement of hydraulic fracturing in Hassi Messaoud, Algeria., Norman, University.of Oklahoma.
- OGCI oil and gas international consultant, 1998, Geostatistics for reservoir description.
- Petit, J., Potter, P.E., 1964, Atlas and glossary of primary sedimentary structures.
- Petit, J., 1954, Classification of sandstone.
- Petit, J., 1957, Sedimentary rocks.
- Potter, P.E., and Pryor, 1961, Dispersal centers of paleozoic and later clastics of the upper mississippi valley and adjacent areas.
- Quilling, R. Mc., Bacon, M., Barclay, W., Scheriff, R. E., Evoy, R. MC., Steel, R., 1984, An introduction to seismic interpretation (reflexion seismics in petroleum exploration).
- Reading, H. G. Departement of earth sciences, university of oxford., 2002, Sedimentary environments processes, facies and stratigraphy.

- Rachid Amokrane, 2001, Evaluation of re-entry wells in Hassi Messaoud Field, Algeria., Thesis, Norman, University of Oklahoma.
- Richard, C.Selly., London, Charpan, and hall, 1985, Ancient sedimentary environments and their subsurface diagnosis.
- Richard, C. Selly, 1988, Applied sedimentary, Departement of geology, Royal school of mines , Imperial college of Science and Technology, University of London.
- Robertson, 2000, Geological characterisation of reservoirs, Oil and Gas International Consultant, Training Center.
- Robertson, 2002, étude sédimentologique, pétrographique et diagénèse du Réservoir Cambro-Ordovicien du champ d'El Gassi, Algerie., Oil and Gas International Consultant.
- Robertson, 2000, Model Geologique du Basin d' Illizi , Oil and Gas International Consultant.
- Sonatrach internal reports, C and C Reservoirs, 1998, Reservoir evaluation report, Hassi R'mel field Triassic Basin, Algeria.
- Sonatrach internal reports, C and C Reservoirs, 1998, Reservoir evaluation report, Hassi Messaoud field Triassic basin, Algeria.
- Sonatrach internal reports, C and C Reservoirs, 1998, Reservoir evaluation report, El Borma field ghadames basin, Algeria/Tunisia.
- Sonatrach, internal report, WEC, 1995.
- SPE 21457, Lithology Determination of Clastic Reservoir Facies From Well Logs, Saudi Arabia.
- SPE 39760, Reservoir Characterization, Geological Modeling, and Reservoir Simulation of the N'Sano Field, Upper Pinda Reservoir.
- Triplehorn, D.M., 1967, Occurrence of pure, well cristallized 1M illite in Cambro-Ordovician sandstone from Rhourde El Baguel Field, Algeria: Jour. Sed Petrology, v.37 pp. 879-884.
- Turner, P., pilling, D., walker, D., exton, J., bennie, J., sabaou, N., 2000, Sequence and stratigraphy of the late Triassic TAGI(Blocks 401/402,Berkine Basin,Algeria), Marine and petroleum geology (Elsevier)18(2001)959-981.
- Vavra, C. L., 2002, Pore-level characterization of Rhourde el baguel field, Algeria, ARCO Exploration and Production Technology, Plano, Texas.
- Vavra, C.L., Kaldi, J.G., and Sneider, R.M., 1992, Geological applicationsof capillary pressure: A review: AAPG Bulletin, v76, p.840-850.
- Willie, M.R.J., and Gardner, G.H.F., 1958, The generalized Kozeny-Carmen equation, World Oil.
- WILLIS, B.J., 1994. Jounal of Sedimentary Reseach, 64B,p.60-67.
- Yuanchang, Qi., and Richard Jolly., British Petroleum, internal report, 2000, Fractured Cambrian sandstone reservoir of El Baguel field., Algeria.